Supporting Information

New Journal of Chemistry

1-Hydroxypyrene-based micelle-forming sensors for the visual detection of RDX/TNG/PETN-based bomb plots in water

Igor S. Kovalev,[a] Olga S. Taniya,[a] Dmitry S. Kopchuk,[ab] Kousik Giri,[c] Anindita Mukherjee,[a] Sougata Santra,*[a] Adinath Majee,*[d] Matiur Rahman,[a] Grigory V. Zyryanov,*[ab] Vasily A. Bakulev[a] and Oleg N. Chupakhin[ab]

[a]Department of Organic and Biomolecular Chemistry, Chemical Engineering Institute, Ural Federal University, 19 Mira Str., Yekaterinburg, K-2, 620002, Russian Federation.

[b]I. Ya. Postovskiy Institute of Organic Synthesis, Ural Division of the Russian Academy of Sciences; 22 S. Kovalevskoy Str., Yekaterinburg, 620219, Russian Federation

[c]Department of Computational Sciences, Central University of Punjab; City Campus, Mansa Road, Bathinda-151001, India

[d]Department of Chemistry, Visva-Bharati (A Central University) Santiniketan-731235, India

Contents

1. Structures of sensors 1-5

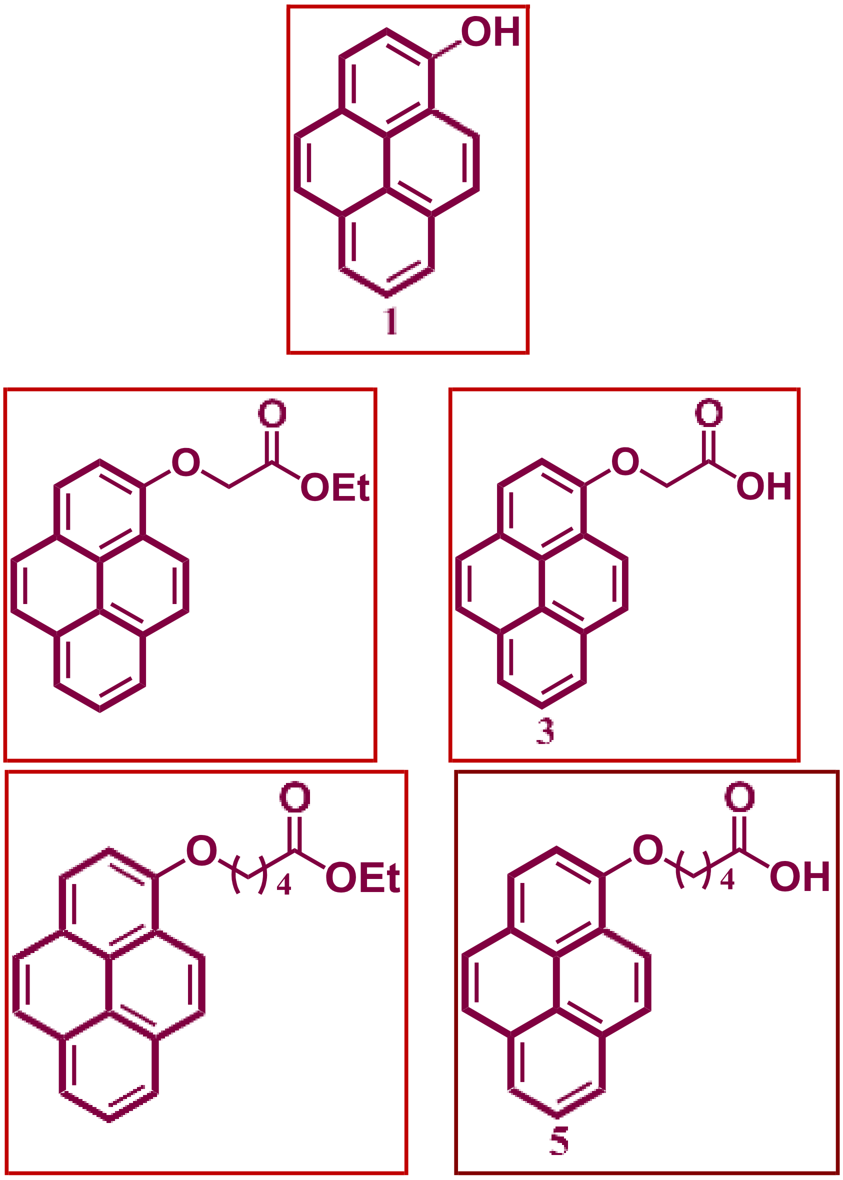

Fig.S1 Chemical structures of sensors based on 1-pyrenol: 1- 1-pyrenol, 2 - ethyl 2-(pyren-1-yloxy) acetate; 3- 2-(pyren-1-yloxy) acetic acid; 4- ethyl 5-(pyren-1-yloxy)pentanoate; 5-5-(pyren-1-yloxy)pentanoic acid

2. Chemical structures of the tested electron deficient compounds included in composition of explosives

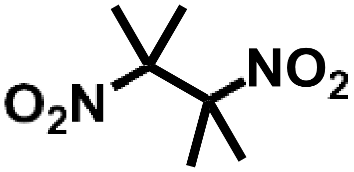

DMNB

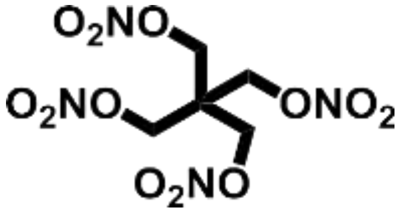

PETN

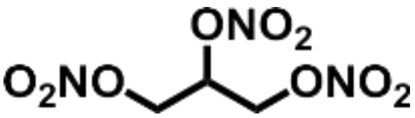

TNG

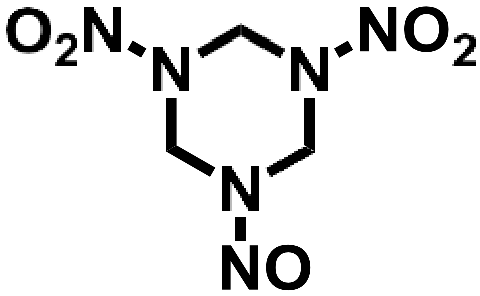

RDX

Fig.S2 Chemical structures of 2,3-dimethyl-2,3-dinitrobutane (DMNB), pentaerythritol tetranitrate (PETN), trinitroglycerin (TNG), 1,3,5-trinitro-1,3,5-triazinane (RDX)

Table S1 Data of explosives properties

Compound	P_{vap} 25^0 C, Torr (1)	Vapor concentration, ppb	Water solubilityat 20°C, mg/L	Soil organic carbon-water coefficient (Log Koc)	Octanol-water partition coefficient (Log Kow)
TNT	$1{,}8\text{x}10^{-3}$	10,6	130,0	300	2,00
RDX	$3{,}3\text{x}10^{-9}$	$5{,}39\text{x}10^{-3}$	59,7	1,80	0,87
PETN	$1{,}16\text{x}10^{-8}$	$7{,}17\text{x}10^{-3}$	43,0	3,24[a]	2,04[b]

[a] Quinn et al.

[b] HSDB

[c] Explosive standards reference guide ISO GUID 34 17025 9001

3. Materials and equipment

1-Pyrenol was prepared as described in literature [(2)]. Starting materials are commercially available. Fluorescence titration experiments were carried out by using the Horiba-Fluoromax-4 spectrofluorometer. Emission and excitation spectra were measured on the Horiba FluoroMax-4. UV-Vis absorption spectra were recorded on the spectrophotometer Perkin-Elmer (Lambda 35). Absolut quantum yields for fluorophores were by using the Integrating Sphere of the Horiba-Fluoromax-4. Sensors Lifetime measurement were performed on the Horiba FluoroMax-4 with using TCSPC method. ^{1}H NMR and ^{13}C NMR spectra were recorded on the Bruker Avance-400. DLS analysis was performed on a Malvern Zetasizer Nano.

4. Experimental methods

4.1 Fluorescence titration experiment

The fluorescence titration experiment started with preparation of fluorophore solution for measurement of absorption and emission spectra. For acids based on 1-pyrenol **2** and **4** there were potassium salts of aqua solution. As for esters based on 1-pyrenol **1**, **3** were used THF solutions. When we have known wavelength of emission and excitation for sensor it was possible to perform procedure of fluorescence quenching using method of Single Point. The solution of sensor by volume of 3 ml was placed in quartz cell 10^{-6}M with following by adding to it of 10-15 aliquots of each analyte in acetonitrile ($2 \times 10^{-4} \div 2 \times 10^{-5}$ M). Analysis of fluorescence emission intensity was performed on the base of a Stern-Volmer equation

$$\frac{I_0}{I}=1+K_{sv}[Q])$$

The binding constant (K_{sv}) was calculated as the slope of the graph intensity ((I_0/I)-1) versus the concentration of the quencher ([Q]).

Analysis of sensors sensitivity was performed on base on static quenching Perrin's model. It is described by the following equations:

$$\frac{I_0}{I}=\exp\ (K_p[Q])$$

$$K_p=V_pN_A[Q]=\frac{4}{3}\pi R^3N_A,$$

where N_A is Avogadro number, I is the fluorescence intensity in the presence of quencher, I_0 is the fluorescence intensity when [Q]=0, R_s is the radius of the quenching sphere. The Perrin radii were obtained from the slope of ln (I_0/I) versus [Q] plots.

4.2 Time-resolved fluorescence emission and lifetime titration experiment

For sensor **5** was measured of absorption spectrum so that the concentration of solution was less 0,1 of absorption intensity at selected wavelength. Time-resolved fluorescence measurements were carried out using time-correlated single-photon counting (TCSPC) with a nanosecond LED (370 nm). The lifetime titration experiment for **5** was carried out as usual procedure describing above for evidence of quenching character of sensors.

4.3 Photoluminescence Absolute quantum yield (PLQY) measurement

For each sensor the absorption spectrum was measured in order to select the excitation wavelength, and the optical density needs to be less than 0,1 at this wavelength in order to minimize the inner-filter effect. For the blank (naked solvent) and the sensor solution the emission and Rayleigh scattering spectra were recorded of by using the HORIBA FluoroMax-4. PLQY Integrating Sphere and the absolute photoluminescence quantum yield value was calculated by using the following equation:

$\varphi = \frac{Ec-Ea}{La-Lc}$, where *Ec* and *Lc* are the integrated luminescence of the sensor and blank, *Ea* and *La* are the integrated excitation profile of the sensor and blank.

5. Synthesis of fluorophores 1-5

5.1 Synthesis of 1-pyrenol 1(2)

Pyren-1sulfonic acid (12 g, 39.4 mmol) was taken as a starting material for synthesis of 1-pyrenol **1**. Pyren-1sulfonic acid was received by according the method describing previous our article (3). The reaction of alkaline melting of pyren-1sulfonic acid was carried out in accordance with method described in literature. The best ratio of potassium hydroxide to sodium hydroxide was selected and it was amounted to 56:40 (mass.) The pale green crystallizes were received with yield of 58 %.

^{1}H NMR (400 MHz, DMSO-d_6) δ ppm 7.54 (d, *J*=8.28 Hz, 1 H) 7.80 (d, *J*=8.78 Hz, 1 H) 7.86 - 7.94 (m, 2H) 7.97 - 8.07 (m, 3 H) 8.33 (d, *J*=9.29 Hz, 1 H) 10.26 (br. s., 1 H); ^{13}C NMR (101 MHz, DMSO-d_6) δ ppm 113.22, 118.07, 121.40, 123.56,123.60, 123.76, 123.86, 124.45, 125.42, 125.47, 126.08, 126.15, 127.38, 131.31, 131.35, 152.15 .

5.1 Synthesis of ethyl 2-(pyren-1-yloxy) acetate 2

The mixture of dry 1-pyrenol **1** (1 g, 4.5 mmol), ethyl chloroacetate (1.66 g, 13.5 mmol) and potassium carbonate (10 g, 72.36 mmol) were suspended in 60 ml of dry acetonitrile, the mixture was stirred at 60 ° C for 48 hours under argon. Water added to reaction mixture and the resulting product extracted by methylene. The solution was evaporated under reduced pressure, the residue re-crystallized from ethanol. The yield was 66 %.

^{1}H NMR (400 MHz, CHLOROFORM-*d*) δ ppm 1.28 - 1.36 (m, 3 H) 4.27 - 4.36 (m, 2 H) 4.98 (s, 2 H) 7.44 (d, *J*=8.28 Hz, 1 H) 7.89 - 8.00 (m, 3 H) 8.05 - 8.16 (m, 4 H) 8.55 (d, *J*=9.03 Hz, 1 H); ^{13}C NMR (101 MHz, CHLOROFORM-*d*) δ ppm 14.16, 61.40, 66.58, 77.20, 109.34, 120.78, 121.21, 124.42, 124.47, 124.74, 125.16, 125.49, 125.83, 126.08, 126.17, 126.73, 127.05, 131.58, 151.81, 168.94 .

5.2 Synthesis of 2-(pyren-1-yloxy) acetic acid 3

The reaction of alkaline hydrolysis of the ester **2** (1 g, 3.0 mmol) was performed by refluxing in ethanol during an hour. The amount of potassium hydroxide added to reaction has consisted to 1.68 g or 30.0 mmol. After the filtration the solution was evaporated to dryness. The water had added to residue and the product was precipitated by hydrochloric acid and filtrated. The yield was 67 %.

^{1}H NMR (400 MHz, DMSO-d_6) δ ppm 5.08 (s, 2 H) 7.65 (d, *J*=8.53 Hz, 1 H) 7.95 - 8.08 (m, 3 H) 8.11 -8.26 (m, 4 H) 8.45 (d, *J*=9.29 Hz, 1 H); ^{13}C NMR (101 MHz, DMSO-*d*6) δ ppm 65.53, 107.85, 109.80, 119.45,120.82, 123.97, 124.14, 124.35, 124.85, 124.87, 124.91, 125.60,126.30, 127.06, 130.94, 131.07, 151.68, 169.97.

5.3 Synthesis of ethyl 5-(pyren-1-yloxy)pentanoate 4

Dry ethyl 5-bromovalerate (1.17 g, 5.6 mmol) and potassium carbonate (10 g, 72.36 mmol) were added to a solution of **1** (1 g, 4.5 mmol) in dry acetonitrile. The reaction mixture was stirred at 60 ° C for 48 hours under argon. The resulting product extracted by methylene. The solution was evaporated under reduced pressure, the residue re-crystallized from ethanol. The yield was 95 %.

^{1}H NMR (400 MHz, CHLOROFORM-*d*) δ ppm 1.23 - 1.29 (m, 3 H) 1.97 - 2.09 (m, 4 H) 2.44 - 2.52 (m, 2H) 4.09 - 4.22 (m, 2 H) 4.31 - 4.37 (m, 2 H) 7.52 (d, *J*=8.53 Hz, 1 H) 7.85 - 7.90 (m, 1 H) 7.92 - 7.98 (m, 2H) 8.03 (d, *J*=9.03 Hz, 1 H) 8.06 - 8.13 (m, 3 H) 8.46 (d, *J*=9.29 Hz, 1 H); ^{13}C NMR (101 MHz, CHLOROFORM-*d*) δ ppm 14.23, 21.86, 28.92, 34.01, 60.32, 68.32, 108.99, 120.37, 121.21, 124.09, 124.18,124.92, 125.19, 125.42 , 125.81, 126.03, 126.30,127.20, 131.67, 131.71, 152.97, 173.43 .

5.4 Synthesis of 5-(pyren-1-yloxy)pentanoic acid 5

The reaction of alkaline hydrolysis of the ester **2** (0.7 g, 2.0 mmol) was performed by refluxing in ethanol during an hour. The amount of potassium hydroxide added to reaction has consisted to 1.12 g or 20.0 mmol. The resulting reaction mixture was evaporated *in vacuo*. The water had added to residue and the product was precipitated by hydrochloric acid and filtrated. The yield was 85 %.

^{1}H NMR (400 MHz, CHLOROFORM-*d*) δ ppm 2.09 (br. s., 5 H) 2.52 - 2.60 (m, 2 H) 4.33 - 4.40 (m, 2 H) 7.51 - 7.56 (m, 1 H) 7.86 - 7.90 (m, 1 H) 7.93 - 7.98 (m, 2 H) 8.04 (d, *J*=9.29 Hz, 1 H) 8.06 - 8.13 (m, 3 H) 8.46 (d, *J*=9.03 Hz, 1 H); ^{13}C NMR (101 MHz, DMSO-*d*6) δ ppm 21.41, 28.34 , 33.37, 68.17, 71.68, 73.72, 109.75, 119.34, 120.79, 124.09, 124.15, 124.30, 124.48, 124.63, 124.94, 125.97, 126.25, 126.36, 127.27, 131.08, 131.23, 152.62, 174.38.

6. Photophysical properties offluorophores

6.1 Summary of photophysical data of chemosensors 1-5

Table S2 Data of absorption and emission of **1-5** sensors

Sensor	Absorption (nm)	Emission (nm)	Stokes shift (nm)
1	241,266,277,345, 363,383	385,406	40
2	256,266,277,333 345,361,381	381,402	33
3	241,266,277,345 362,382	383, 403	37
4	256,266,277,333 345,361,381	383, 403	33
5	241,266,277,345 362,382	384, 405	39

Table S3 Data of absolute quantum yields and lifetime of **1-5** sensors

Sensor	Φ_f	τ, ns
1	98,04	15,59
2	15,51	14,22
3	92,77	18,31
4	22,77	12,86
5	93,24	15,59

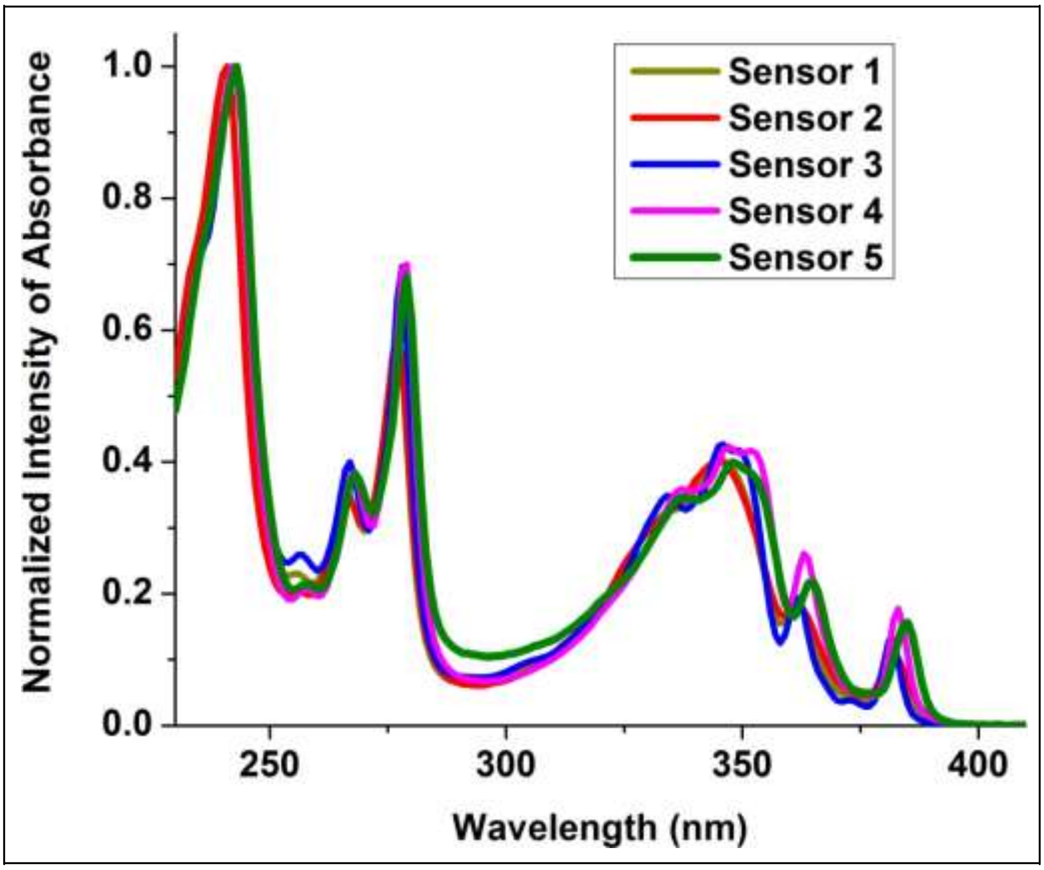

Fig.S3 Absorbance spectra of sensors **1-5**

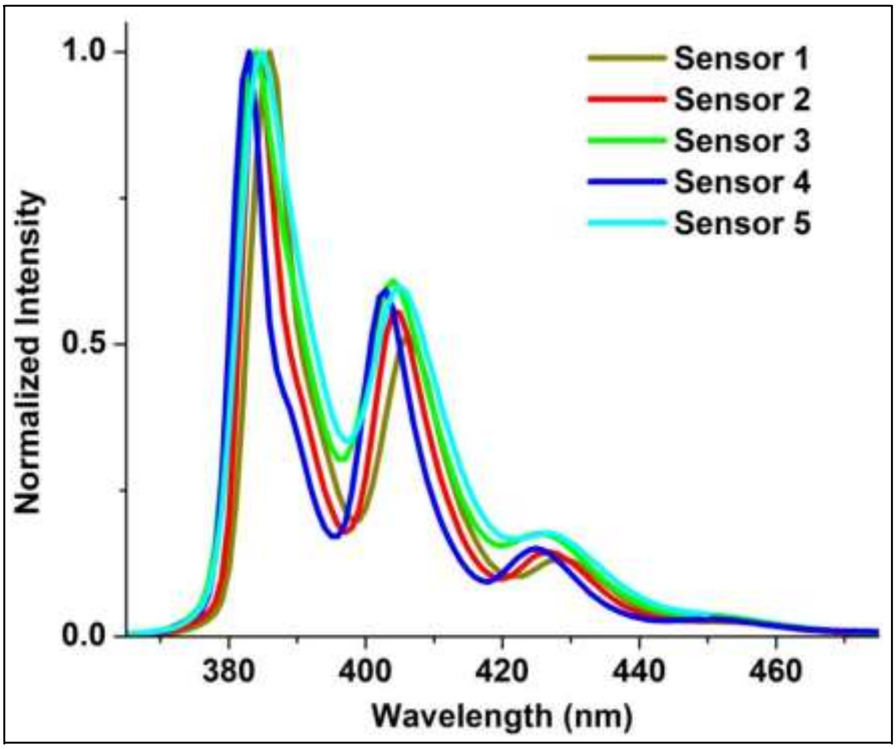

Fig.S4 Emission spectra of sensors **1-5**

6.2 1-Pyrenol (sensor 1)

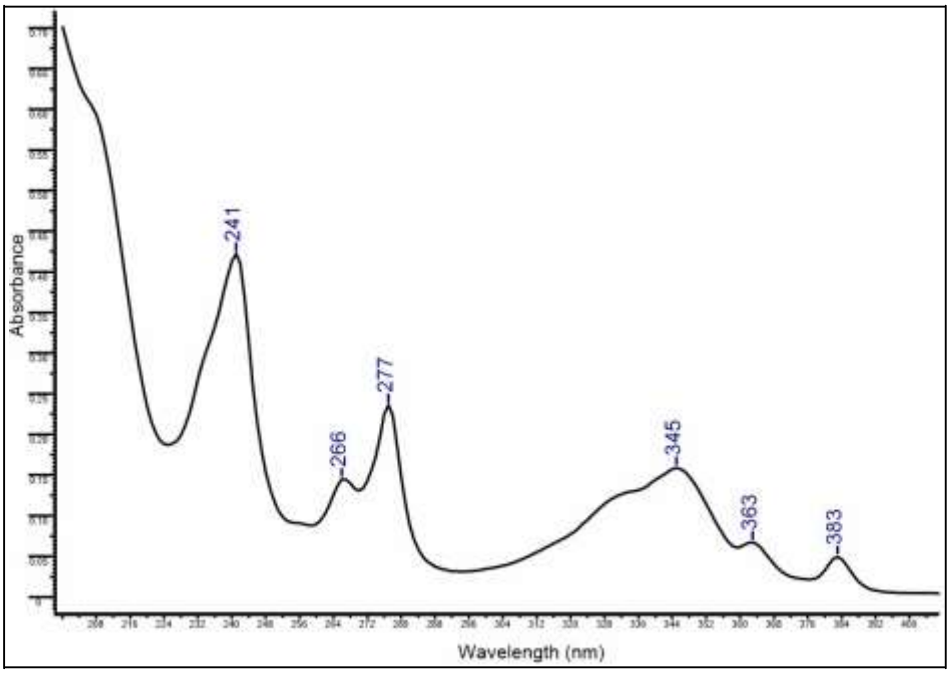

Fig.S5 UV-Vis spectrum of sensor **1**

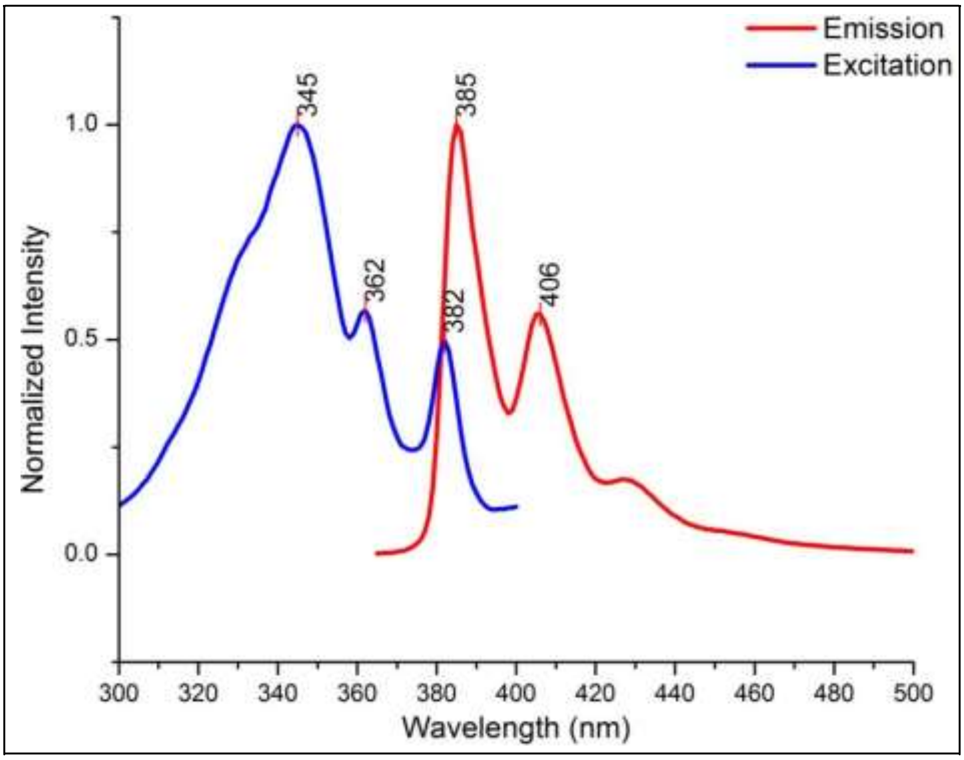

Fig.S6 Fluorescence excitation and emission spectra of sensor **1**

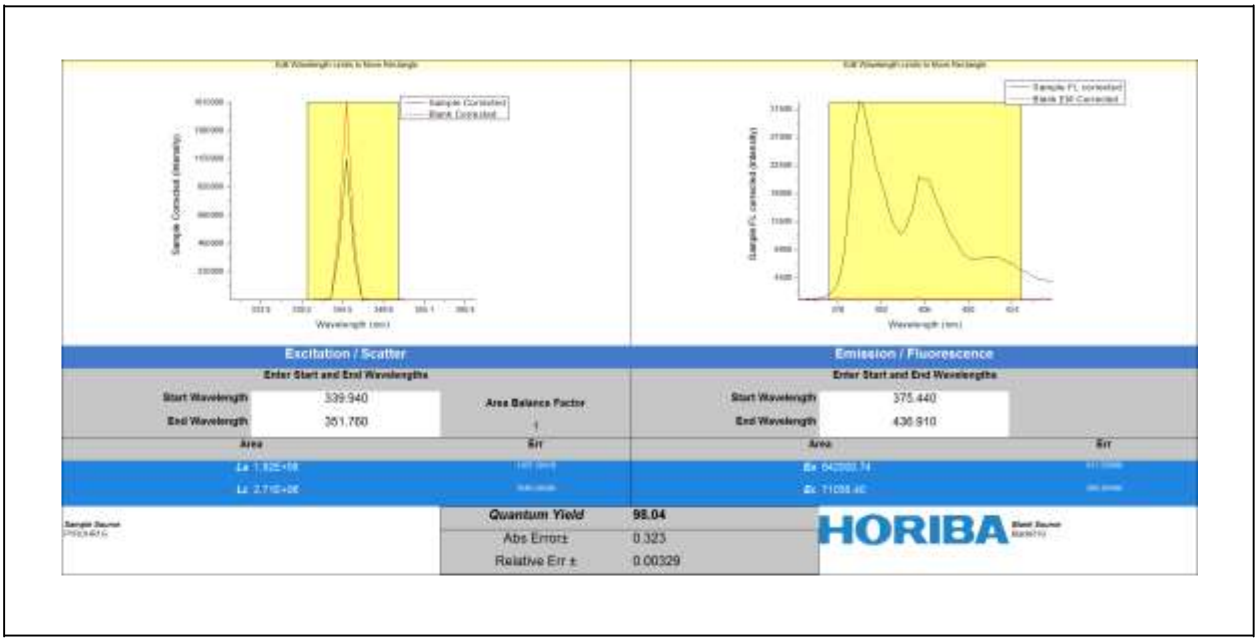

Fig.S7 PLQY of sensor **1**

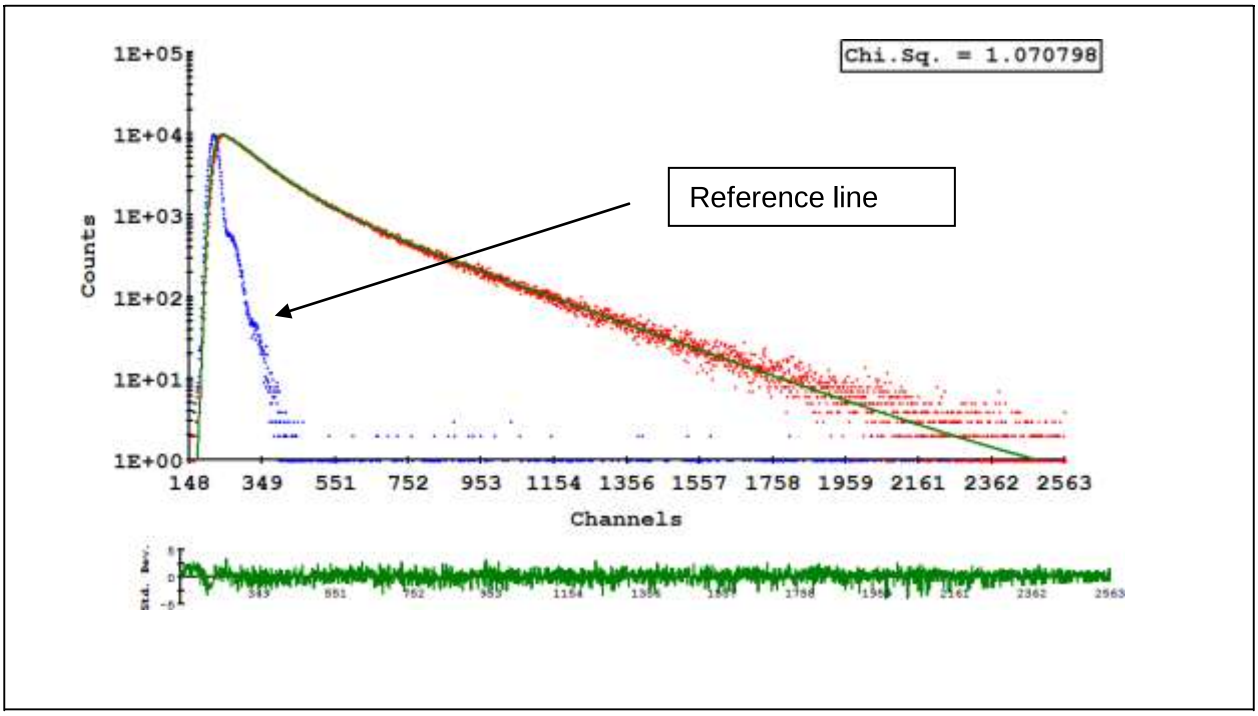

Fig.S8 TCSPC measurement of sensor **1**

6.3 Ethyl 2-(pyren-1-yloxy) acetate (sensor 2)

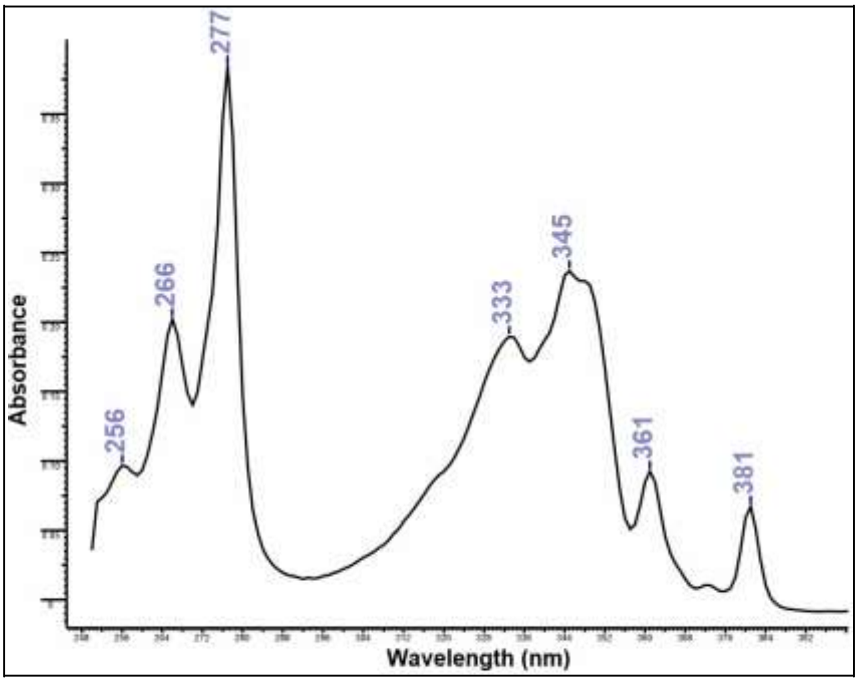

Fig.S9 UV-Vis spectrum of sensor **2**

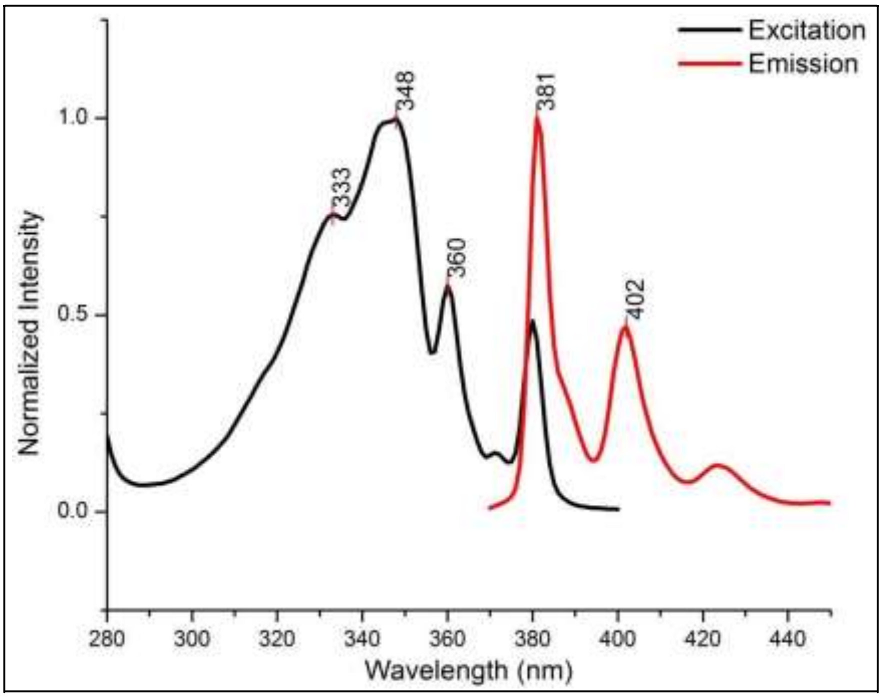

Fig.S10 Fluorescence excitation and emission spectra of sensor **2**

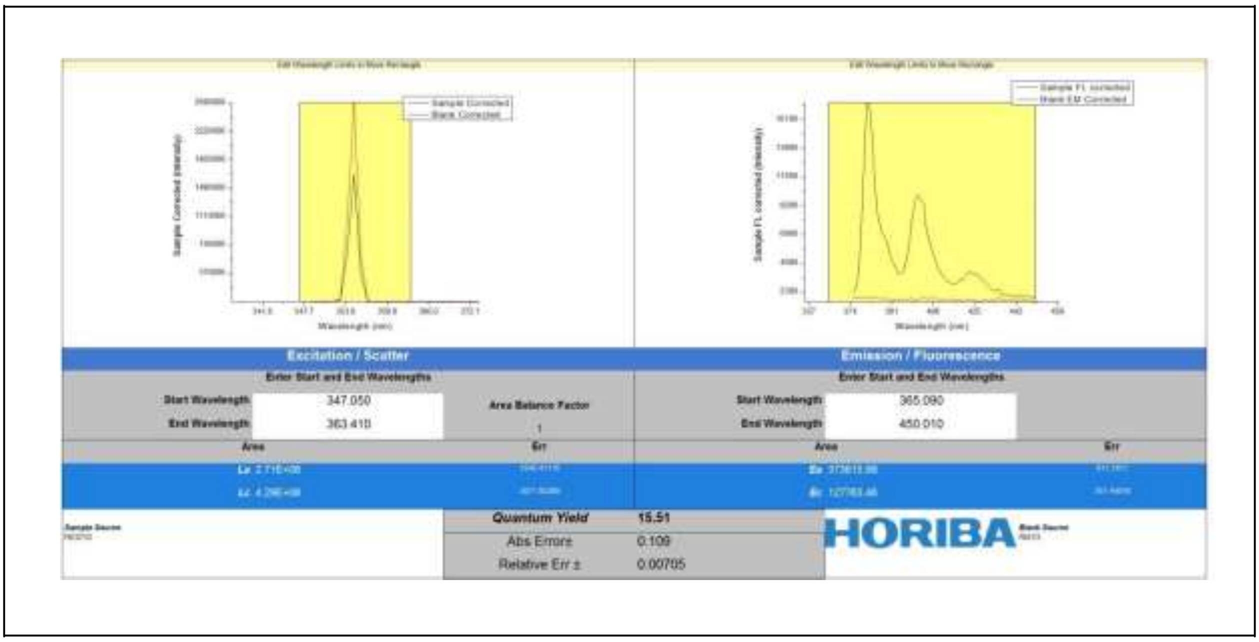

Fig.S11 PLQY of sensor **2**

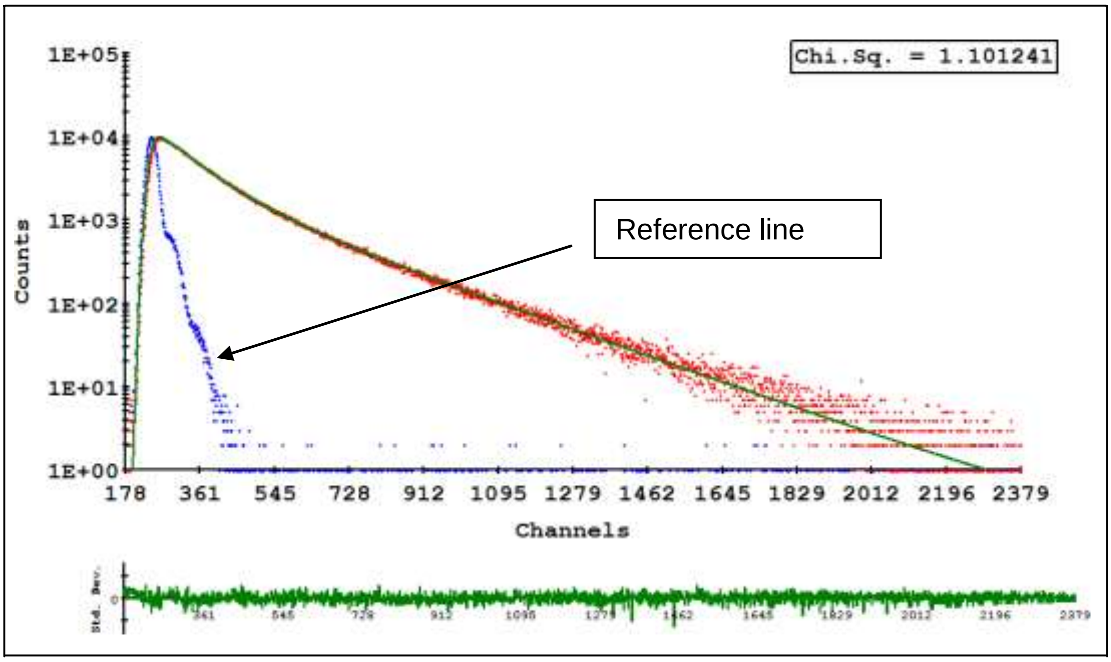

Fig.S12 TCSPC measurement of sensor **2**

6.4 2-(Pyren-1-yloxy) acetic acid (sensor 3)

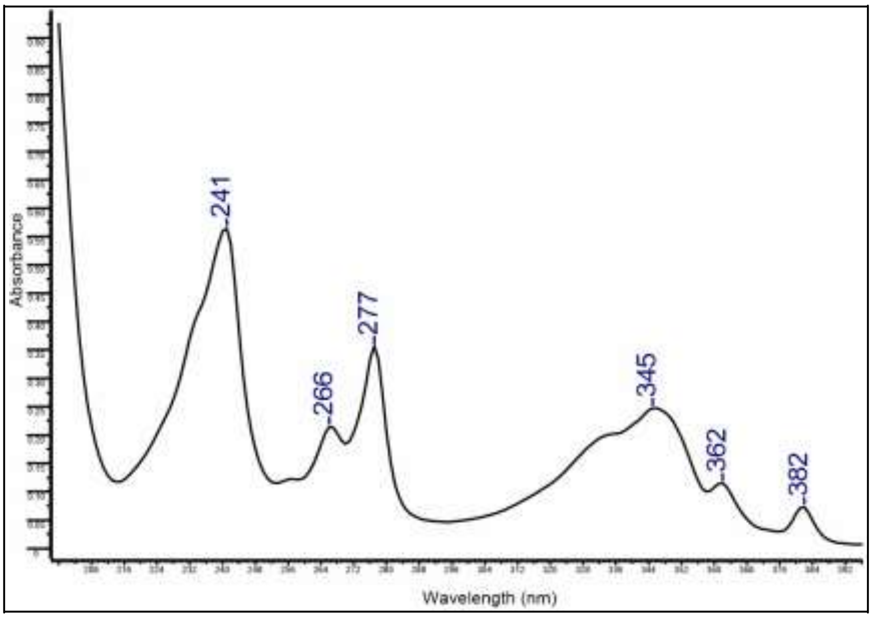

Fig.S13 UV-Vis spectrum of sensor **3**

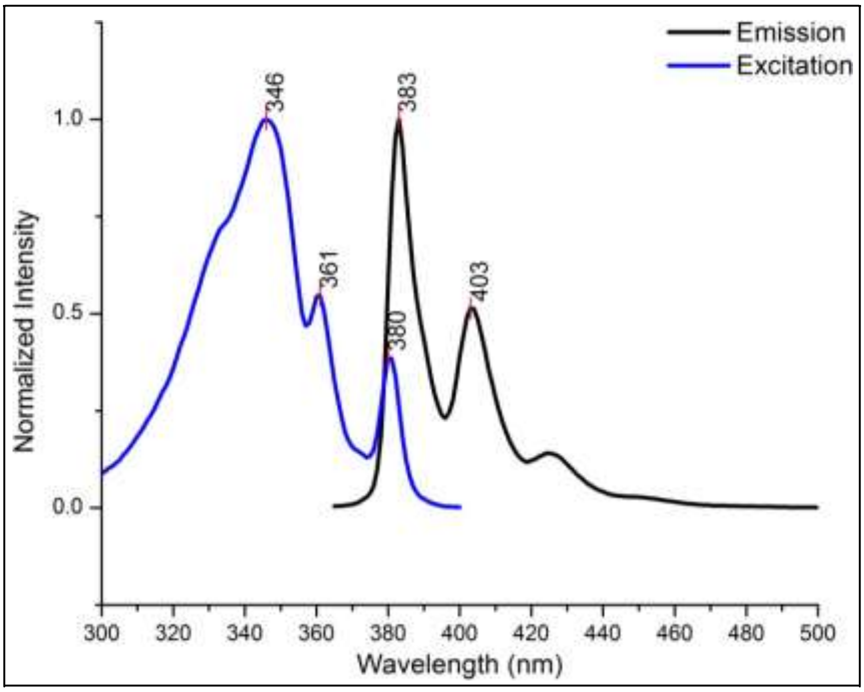

Fig.S14 Fluorescence excitation and emission spectra of sensor **3**

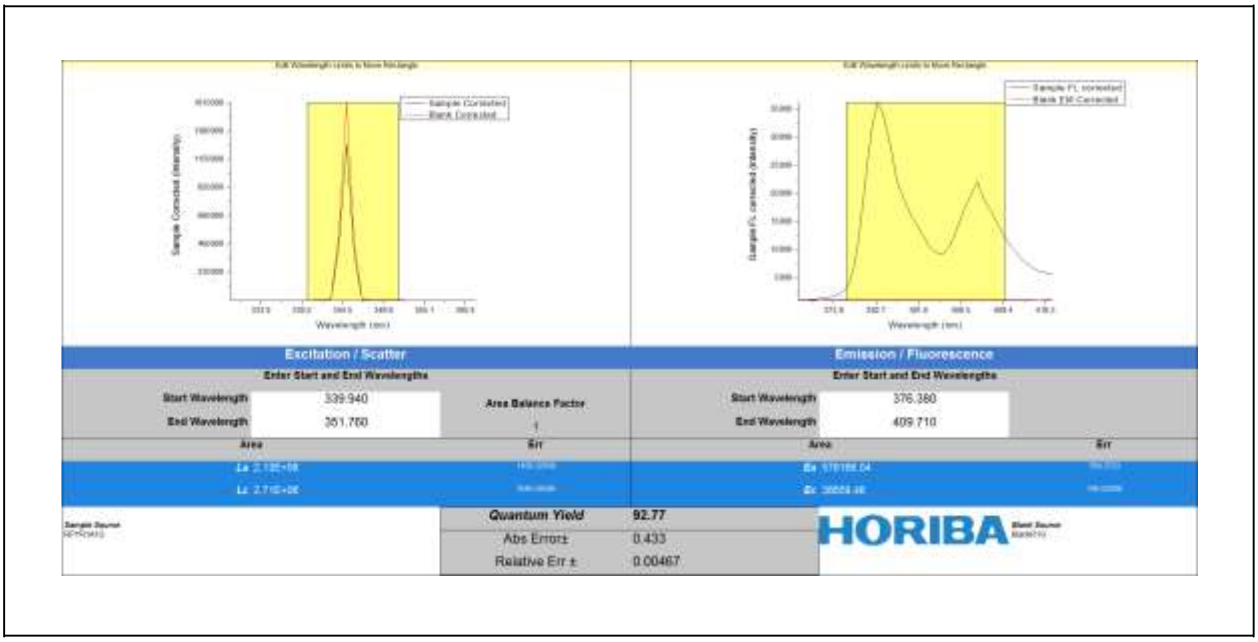

Fig.S15 PLQY of sensor **3**

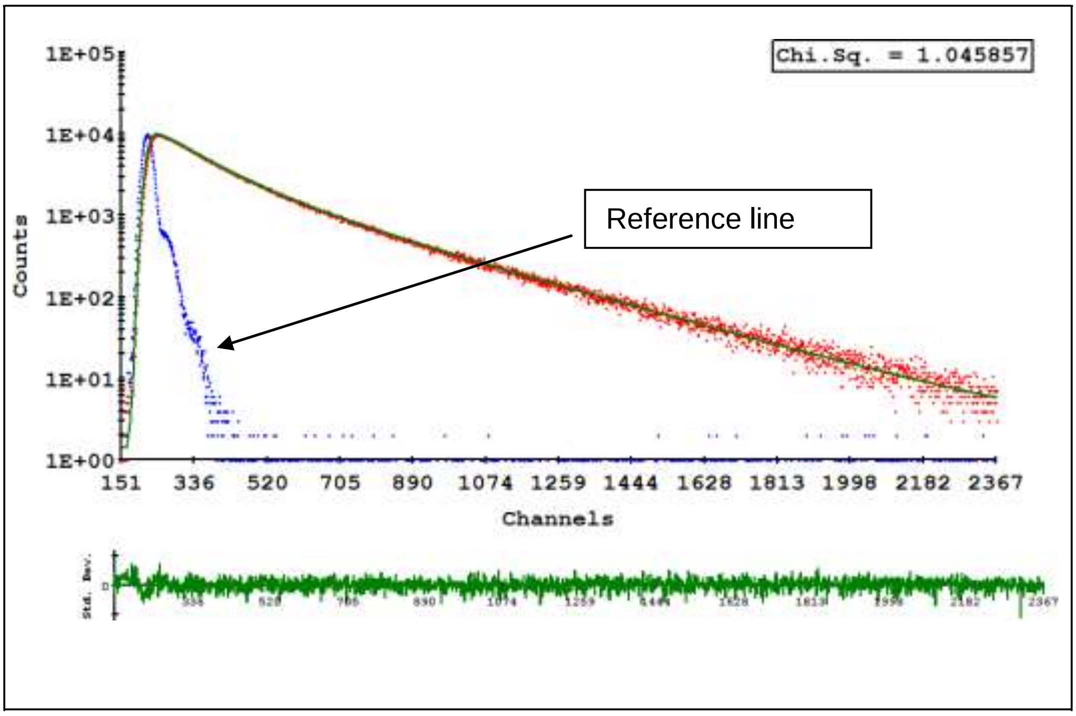

Fig.S16 TCSPC measurement of sensor **3**

6.5 Ethyl 5-(pyren-1-yloxy)pentanoate (sensor 4)

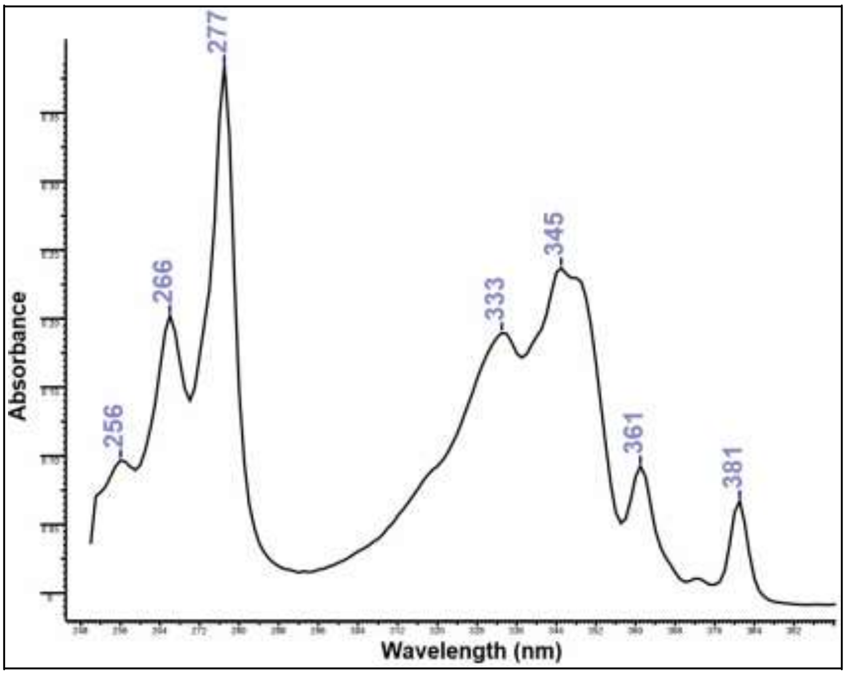

Fig.S17 UV-Vis spectrum of sensor **4**

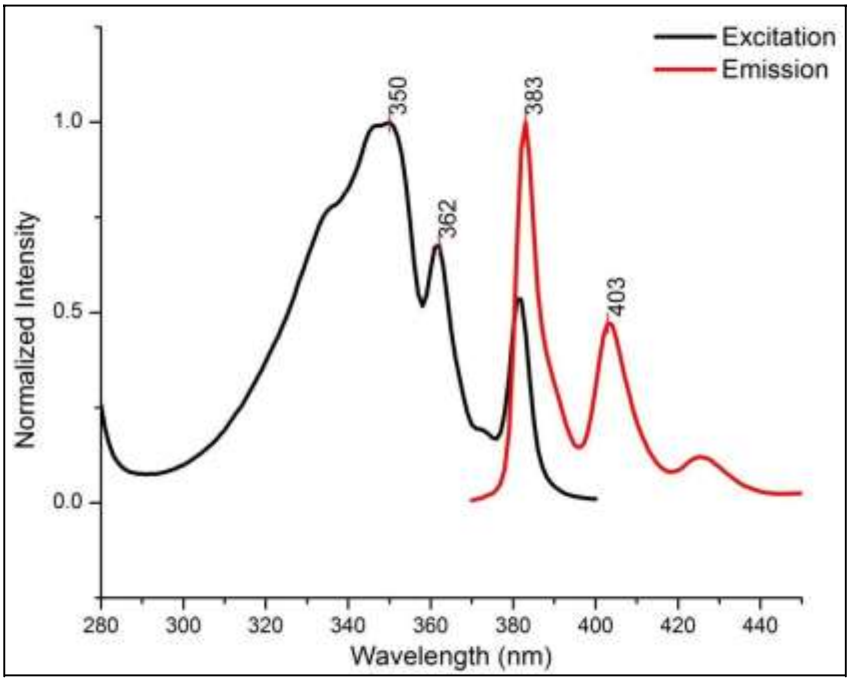

Fig.S18 Fluorescence excitation and emission spectra of sensor **4**

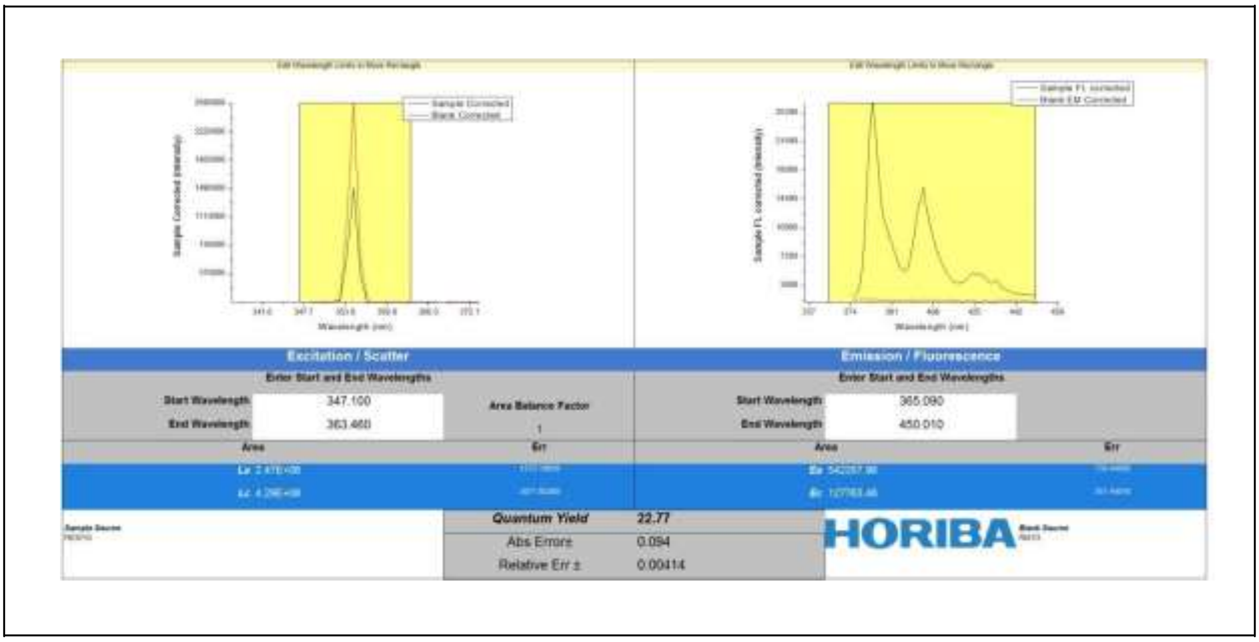

Fig.S19 PLQY of sensor **4**

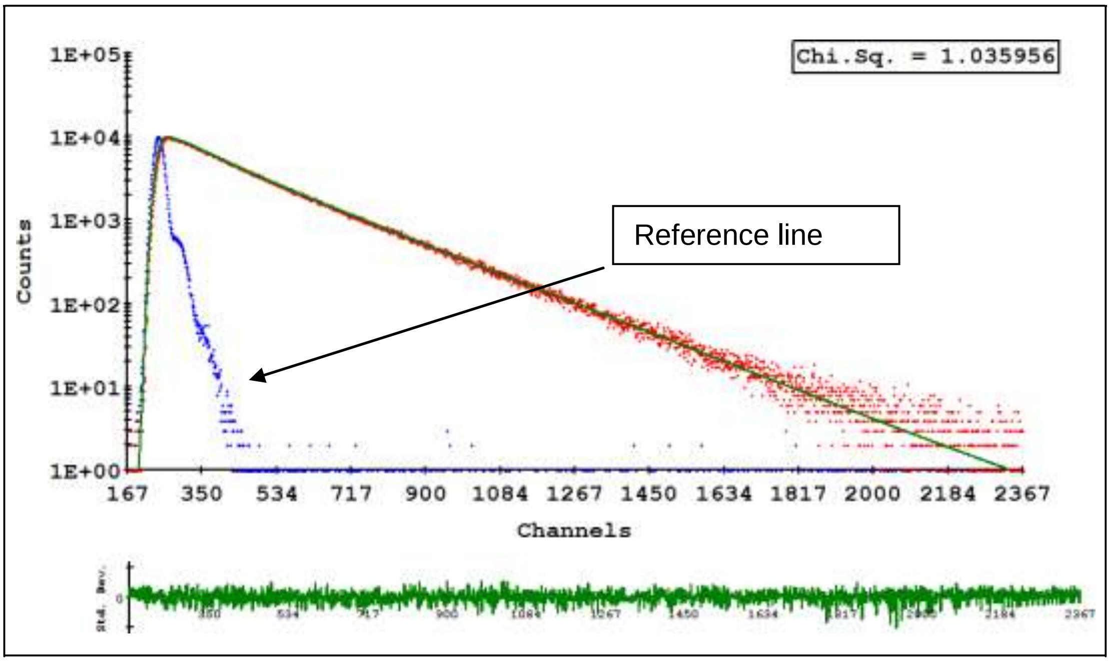

Fig.S20 TCSPC measurement of sensor **4**

6.6 5-(Pyren-1-yloxy)pentanoic acid (sensor 5)

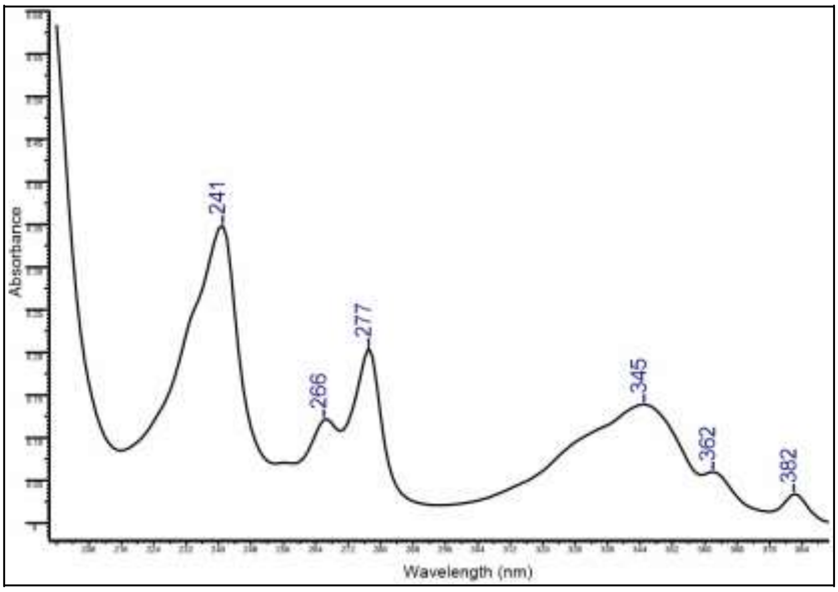

Fig.S21 UV-Vis spectrum of sensor **5**

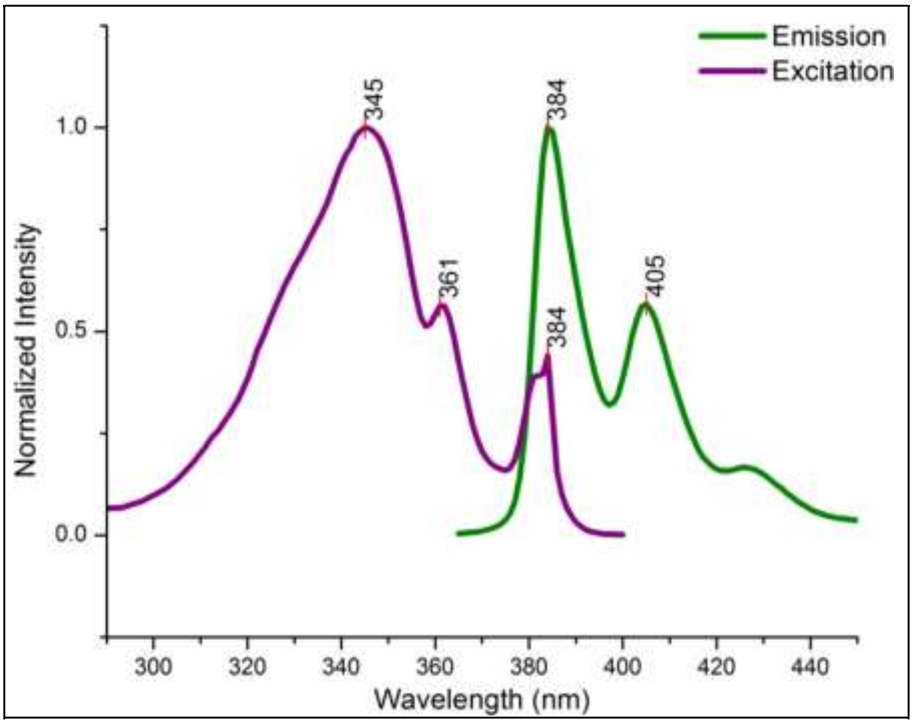

Fig.S22 Fluorescence excitation and emission spectra of sensor **5**

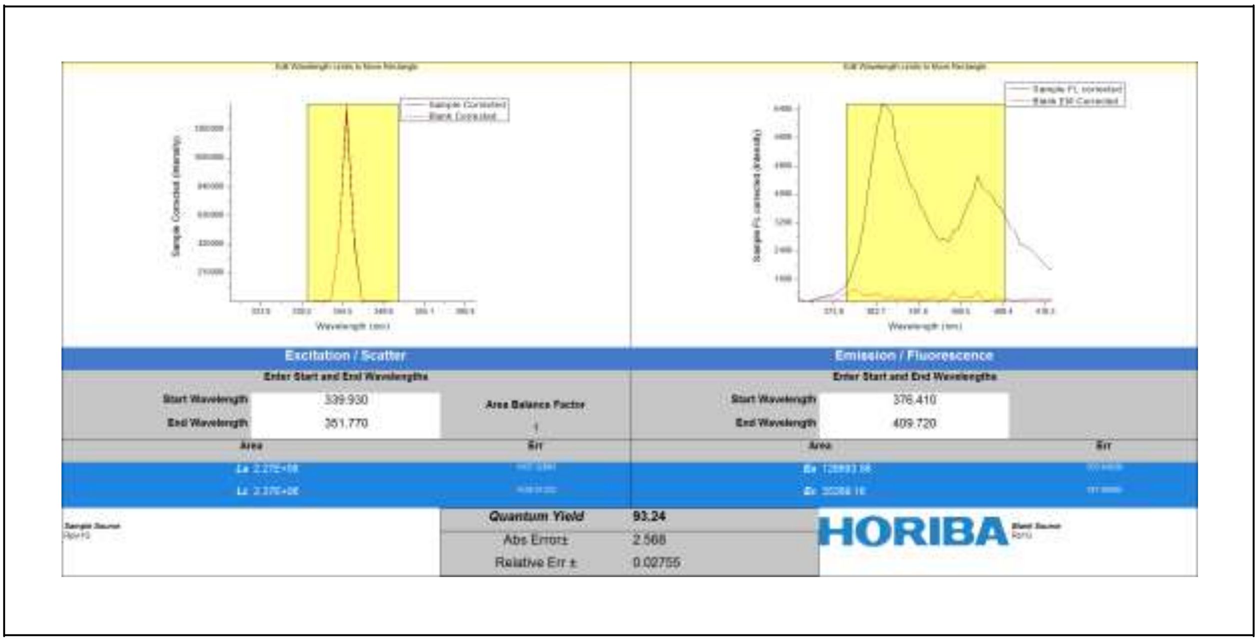

Fig.S23 PLQY of sensor **5**

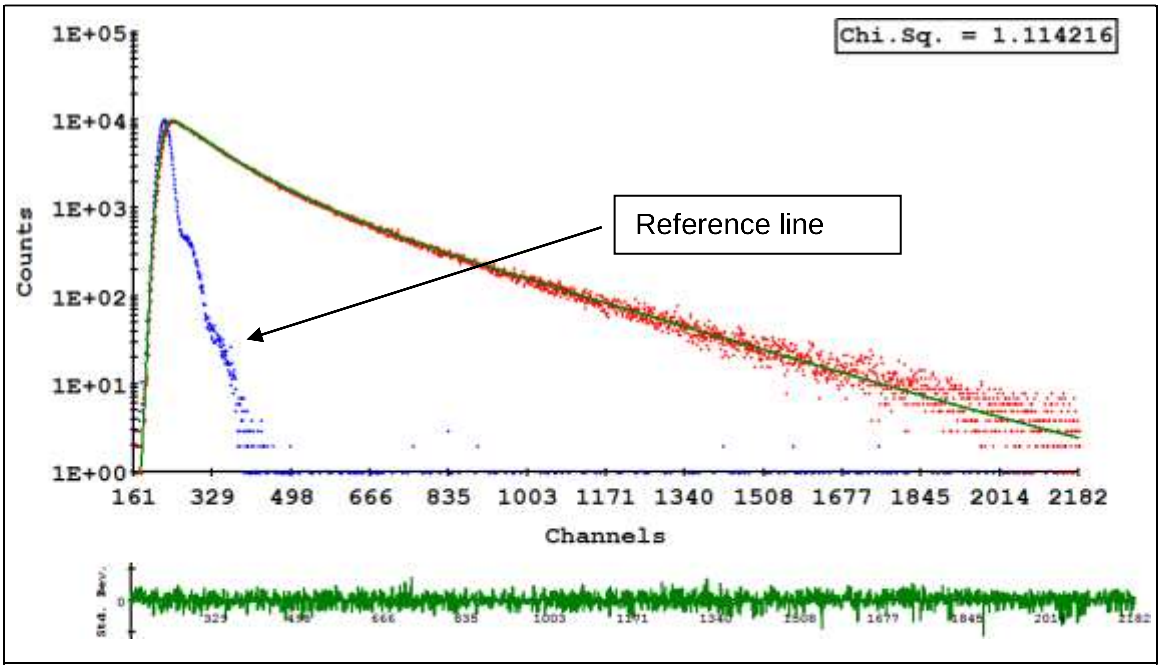

Fig.S24 TCSPC measurement of sensor **5**

7 Studies of sensor's fluorescence quenching responce

7.1 Stern-Volmer quenching constants for the sensors 1-5

Table S4 Summary of Stern-Volmer rate constants of sensors **1-5**

#	K_{SV}^{DMNB} (1x10^5),M^-1	K_{SV}^{PETN} (1x10^5),M^-1	K_{SV}^{TNG} (1x10^5),M^-1	K_{SV}^{RDX} (1x10^5),M^-1
1	**0,001(7)**	0,000(7)	**0,001(9)**	**-**
2	**1,264(1)**	0,623(9)	**0,951(5)**	**0,687(9)**
3	**0,451(8)**	0,322(2)	**0,629(1)**	**0,692(1)**
4	**1,292(1)**	1,010(5)	**1,264(9)**	**0,569(8)**
5	**6,421(7)**	1,217(4)	**3,453(3)**	**1,533(5)**

Table S5 Limit of detection (LOD)

#	ppb(DMNB)	ppb(PETN)	ppb(TNG)	ppb(RDX)
5	~12	~21	~15	~15

Table S6 Quenching efficiency

#	Q.Ef (DMNB),%	Q.Ef(PETN),%	Q.Ef(TNG),%	Q.Ef(RDX),%
2	11	5	8	5
3	3	2	4	4
4	11	5	8	5
5	39	15	21	12

Table S7 Quenching sphere radii, based on Perrin's model

#	r_s^{DMNB} ,nm	r_s^{PETN} , nm	r_s^{TNG} ,nm	r_s^{RDX} , nm
1	4	3	4	-
2	36	29	33	30
3	26	23	29	30
4	37	34	36	28
5	59	36	50	38

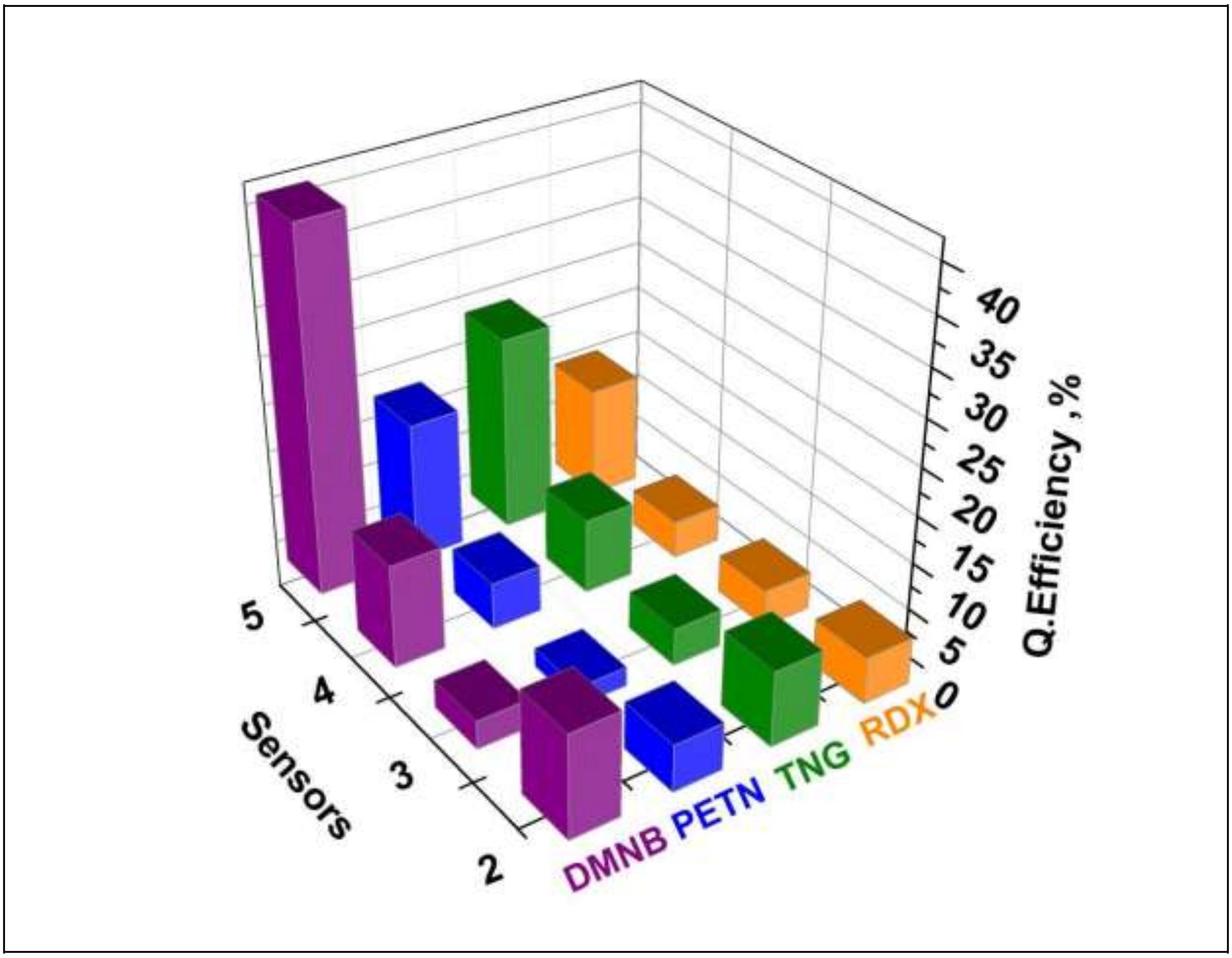

Fig.S25 Quenching efficiency of sensors **2-5** at different concentrations of nitro explosives

7.2 Sensor 1

Table S8 Fluorescence quenching experiment of **1** upon addition DMNB

Solution of sensor 1	Concentrate of sensor 1, M	Solution of quencher	Concentrate of quencher, M
25% water solution of THF	1.0×10^{-5} M	CH_3CN	2.0×10^{-2} M

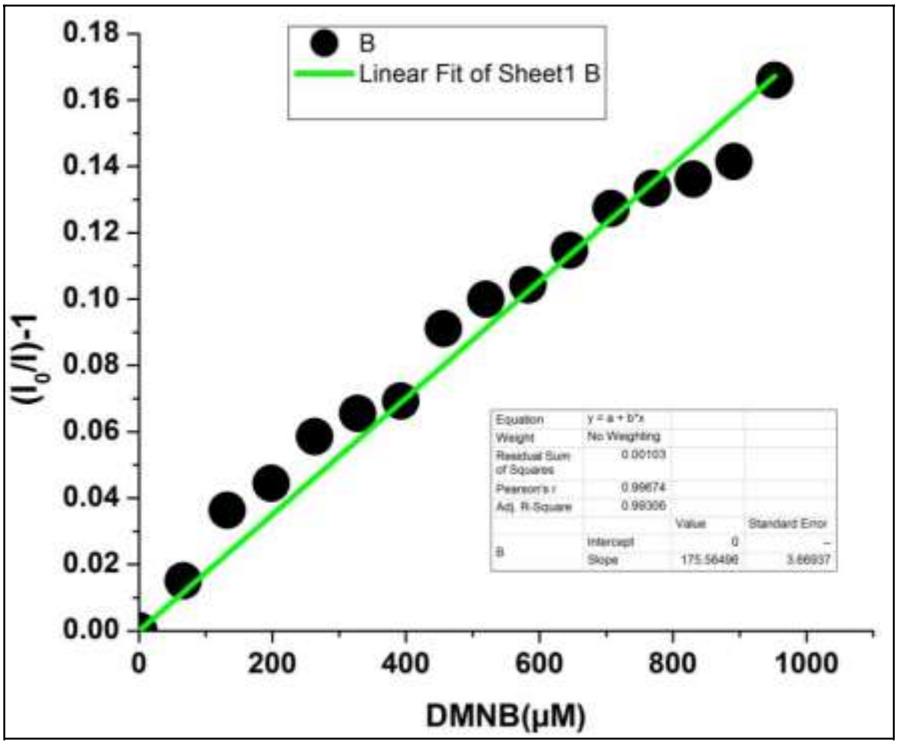

Fig.S26 Stern-Volmer plot

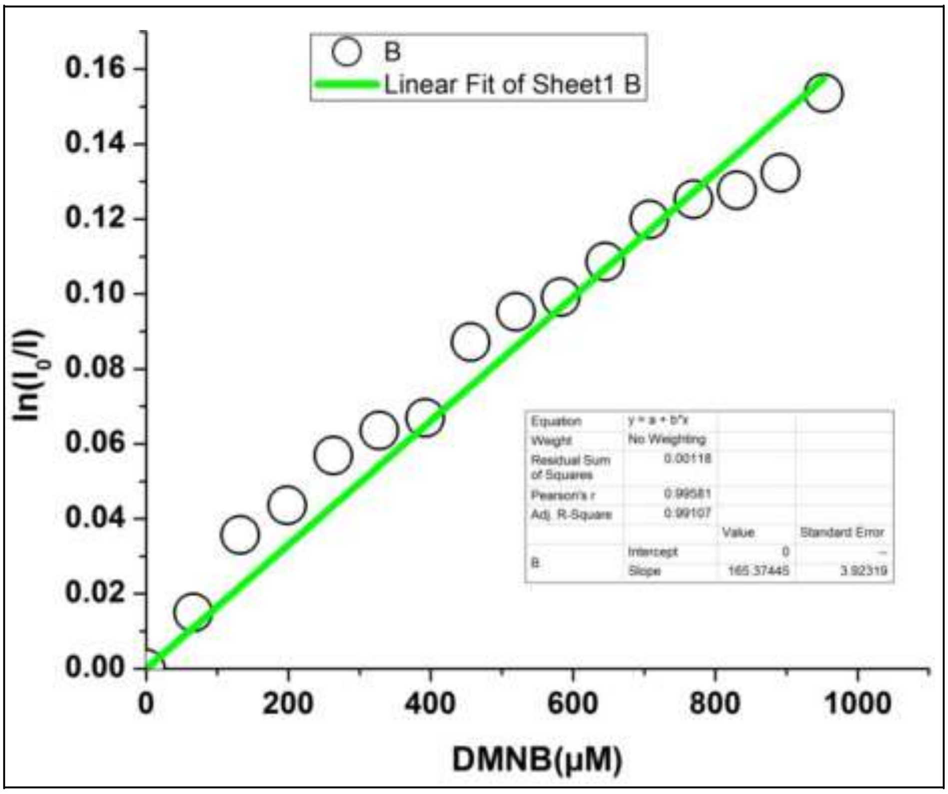

Fig.S27 Perrin plot

Table S9 Fluorescence quenching experiment of **1** upon addition PETN

Solution of sensor 1	Concentrate of sensor 1, M	Solution of quencher	Concentrate of quencher, M
25% water solution of THF	1.0×10^{-5} M	CH_3CN	2.0×10^{-2} M

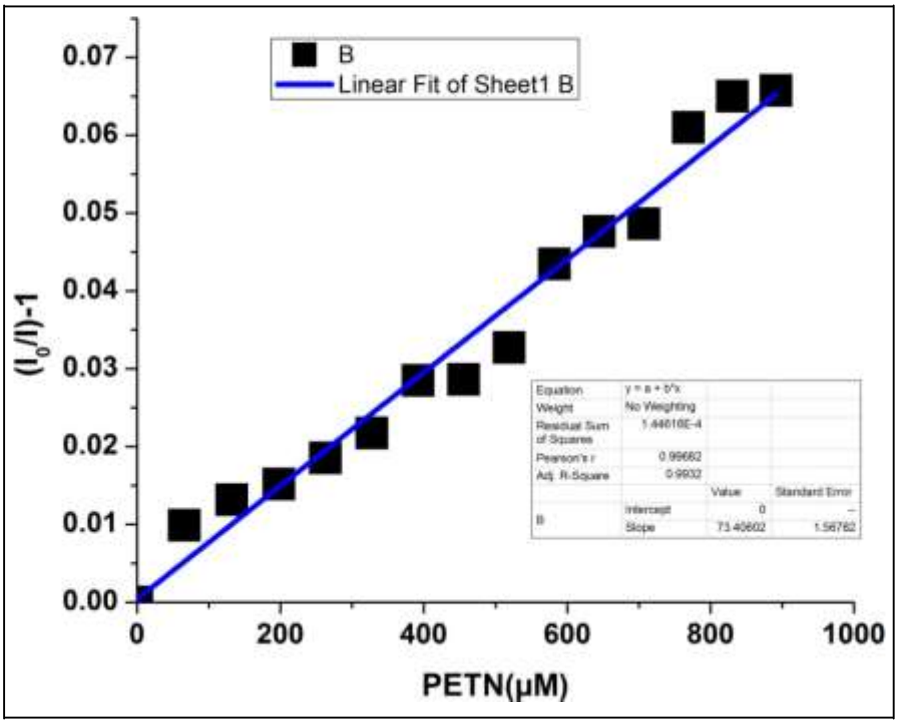

Fig.S28 Stern-Volmer plot

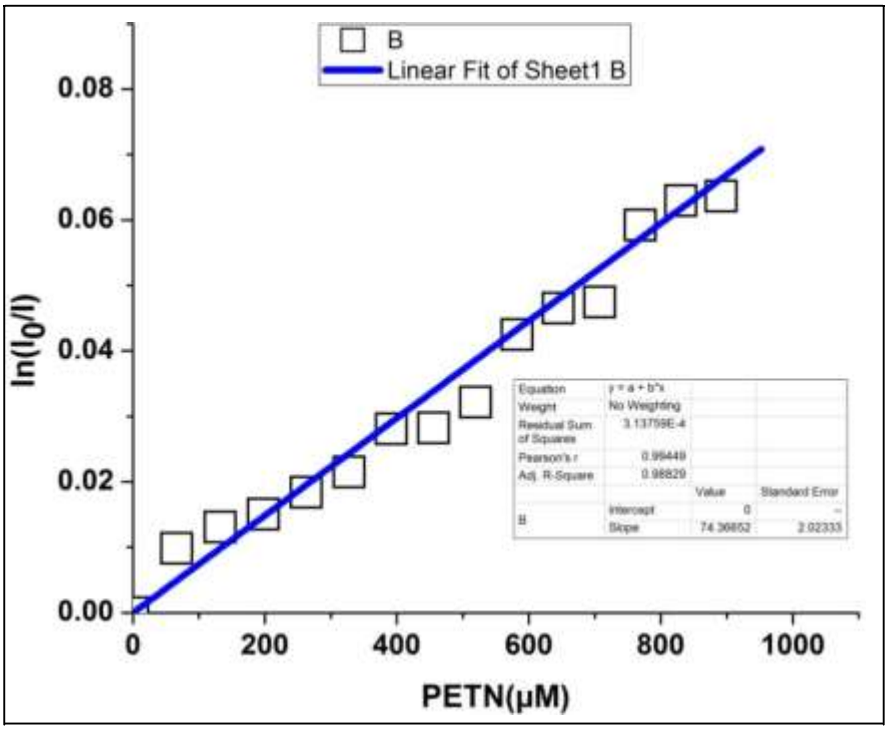

Fig.S29 Perrin plot

Table S10. Fluorescence quenching experiment of **1** upon addition TNG

Solution of sensor 1	Concentrate of sensor 1, M	Solution of quencher	Concentrate of quencher, M
25% water solution of THF	1.0×10^{-5} M	CH_3CN	2.0×10^{-2} M

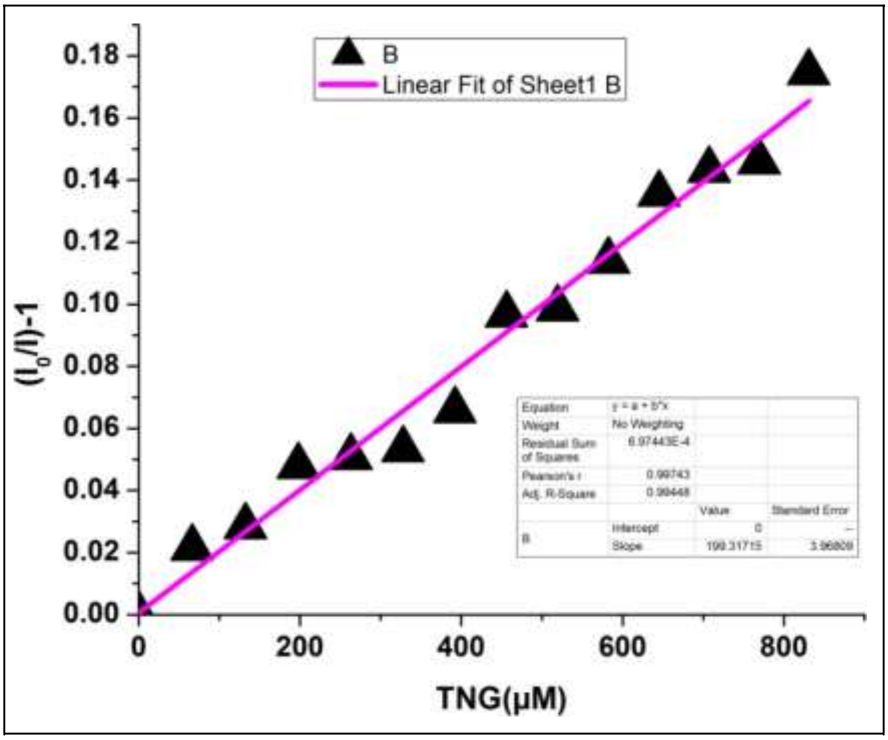

Fig.S30 Stern-Volmer plot

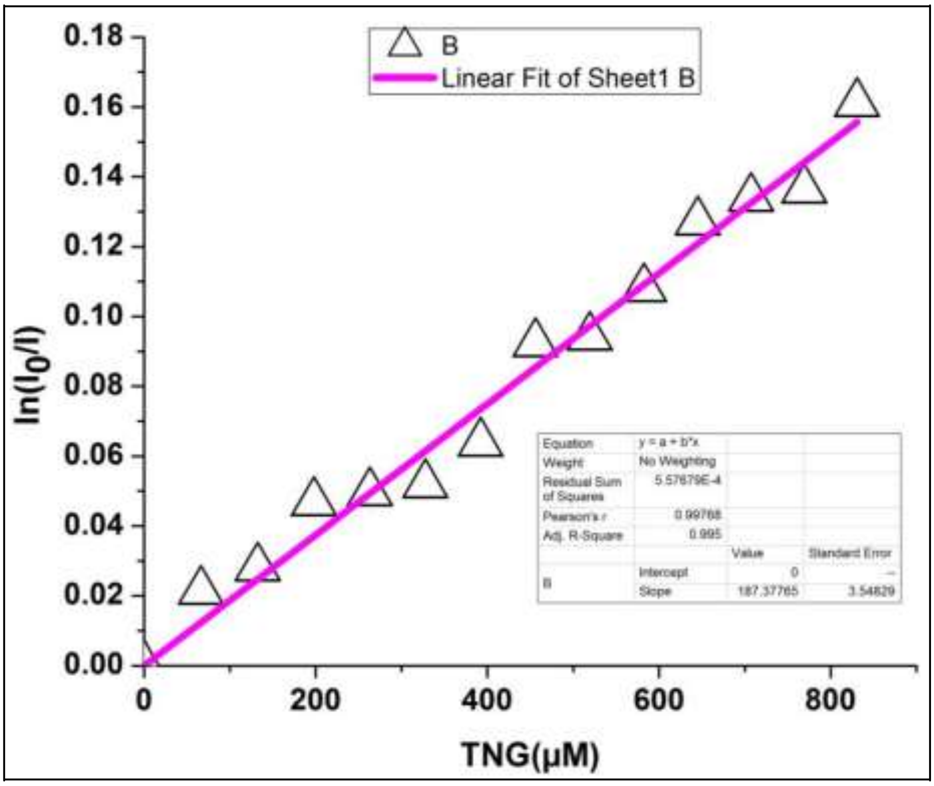

Fig.S31 Perrin plot

Table S11. Summary of the data of the fluorescence quenching experiments for the sensor **1** by using Single Point method

μM	DMNB (I_0/I)-1	PETN (I_0/I)-1	TNG (I_0/I)-1
0.00	0.00	0.00	0.00
66.45	0.02	0.01	0.02
132.45	0.04	0.01	0.03
198.02	0.04	0.02	0.05
263.16	0.06	0.02	0.05
327.87	0.07	0.02	0.05
392.16	0.07	0.03	0.07
456.03	0.09	0.03	0.10
519.48	0.10	0.03	0.10
582.52	0.10	0.04	0.11
645.16	0.11	0.05	0.14
707.40	0.13	0.05	0.14
769.23	0.13	0.06	0.15
830.67	0.14	0.06	0.17
891.72	0.14	0.07	0.17
952.38	0.17	0.09	0.18

DMNB		PETN		TNG	
Q.Ef,%	ppm	Q.Ef,%	ppm	Q.Ef,%	ppm
0.0	0.0	0.0	0.0	0.00	0.0
1.5	11.7	1.0	21.0	2.11	15.1
3.5	23.3	1.3	41.9	2.76	30.1
4.3	34.9	1.5	62.6	4.56	45.0
5.5	46.3	1.8	83.2	4.83	59.7
6.2	57.7	2.1	103.6	5.05	74.4
6.5	69.0	2.8	123.9	6.17	89.0
8.3	80.3	2.8	144.1	8.81	103.5
9.1	91.4	3.2	164.2	8.98	117.9
9.4	102.5	4.2	184.1	10.23	132.2
10.3	113.5	4.5	203.9	11.94	146.5
11.3	124.5	4.6	223.5	12.53	160.6
11.8	135.4	5.7	243.1	12.74	174.6
12.0	146.2	6.1	262.5	14.87	188.6
12.4	156.9	6.2	281.8	15.90	202.4
14.2	167.6	8.0	301.0	16.87	216.2

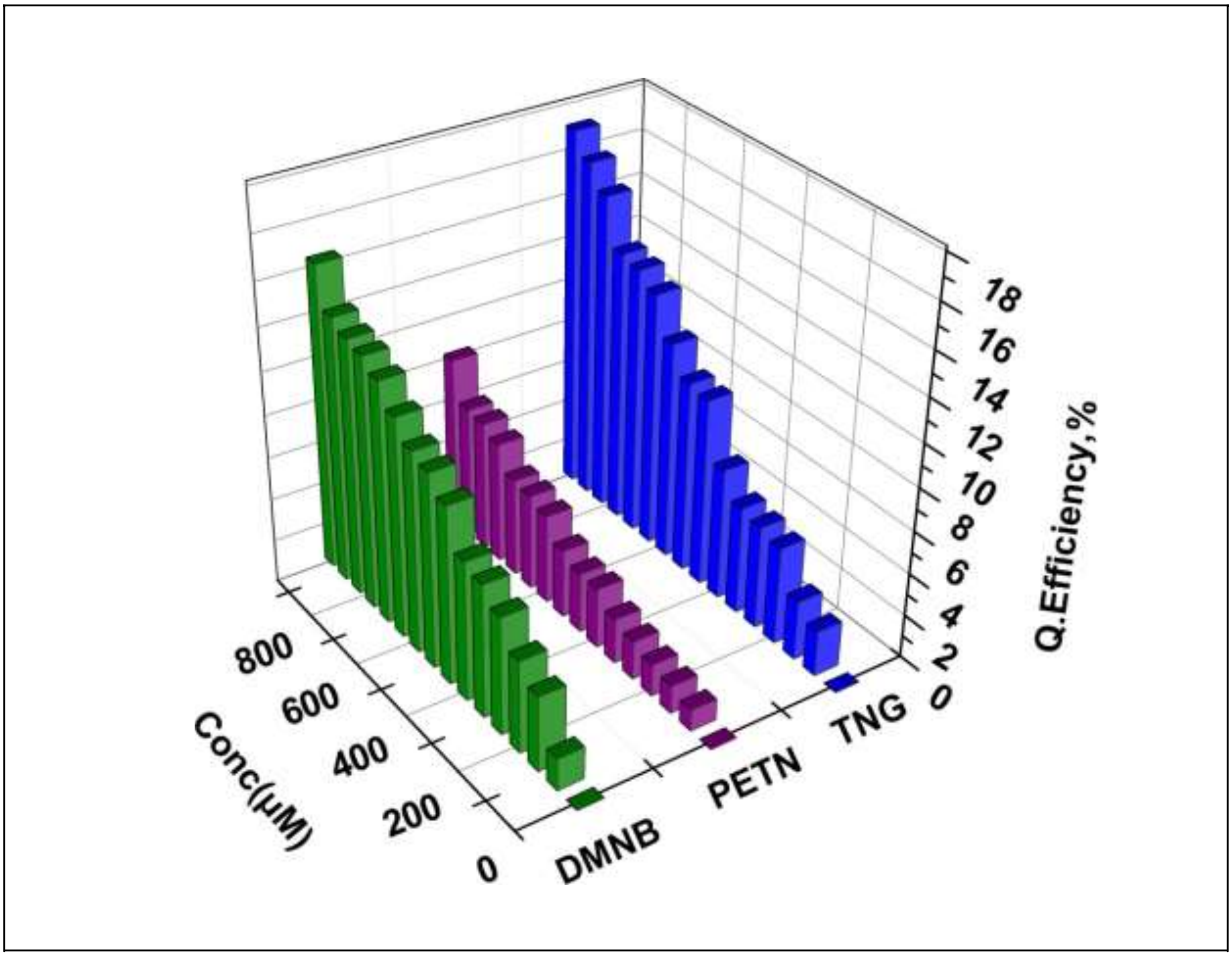

Fig.S32. Quenching efficiency of sensor **1** at different concentrations of nitro explosives

7.3 Sensor 2

Table S12. Fluorescence quenching experiment of **2** upon addition DMNB

Solution of sensor 2	Concentrate of sensor 2, M	Solution of quencher	Concentrate of quencher, M
25% water solution of THF	1.0×10^{-6} M	CH_3CN	2.0×10^{-5} M

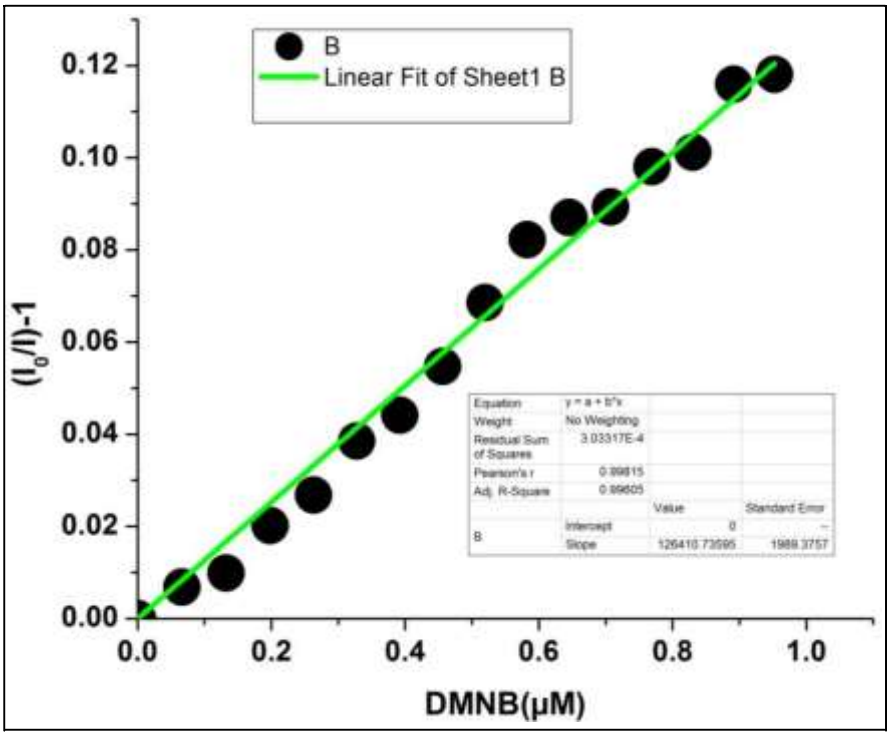

Fig.S33 Stern-Volmer plot

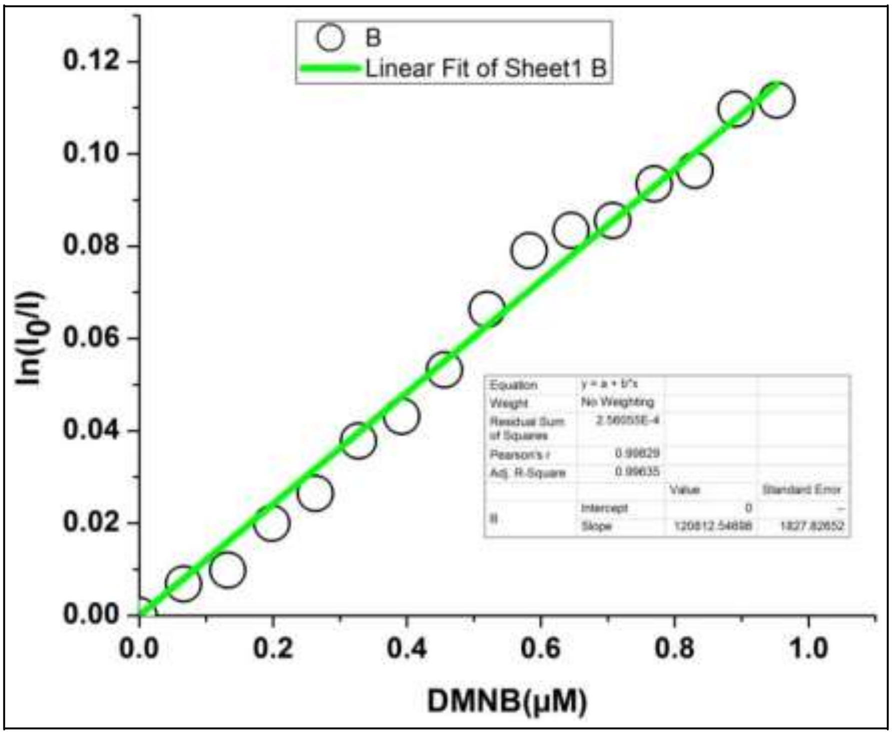

Fig.S34 Perrin plot

Table S13 Fluorescence quenching experiment of **2** upon addition PETN

Solution of sensor 2	Concentrate of sensor 2, M	Solution of quencher	Concentrate of quencher, M
25% water solution of THF	1.0×10^{-6} M	CH_3CN	2.0×10^{-5} M

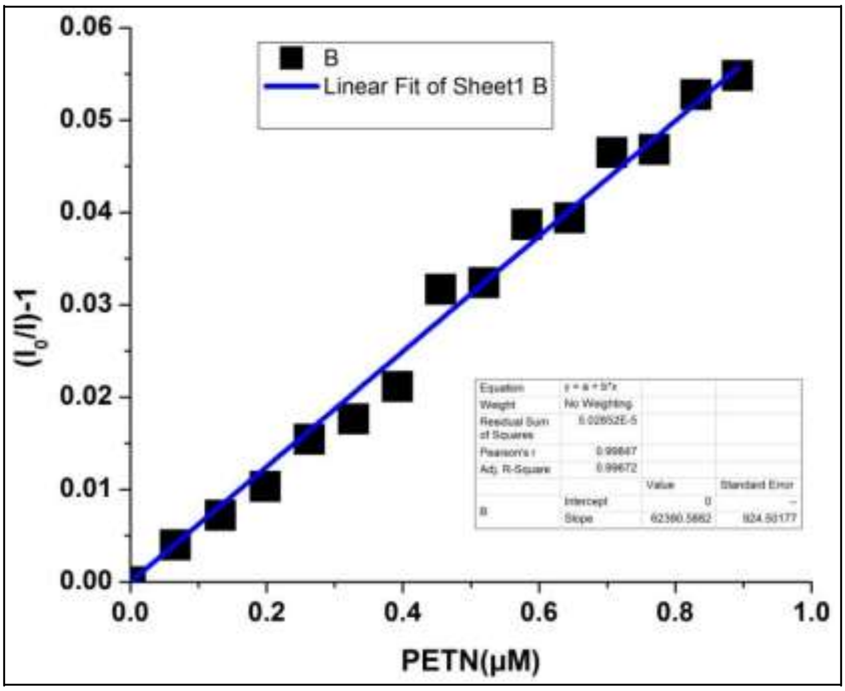

Fig.S35 Stern-Volmer plot

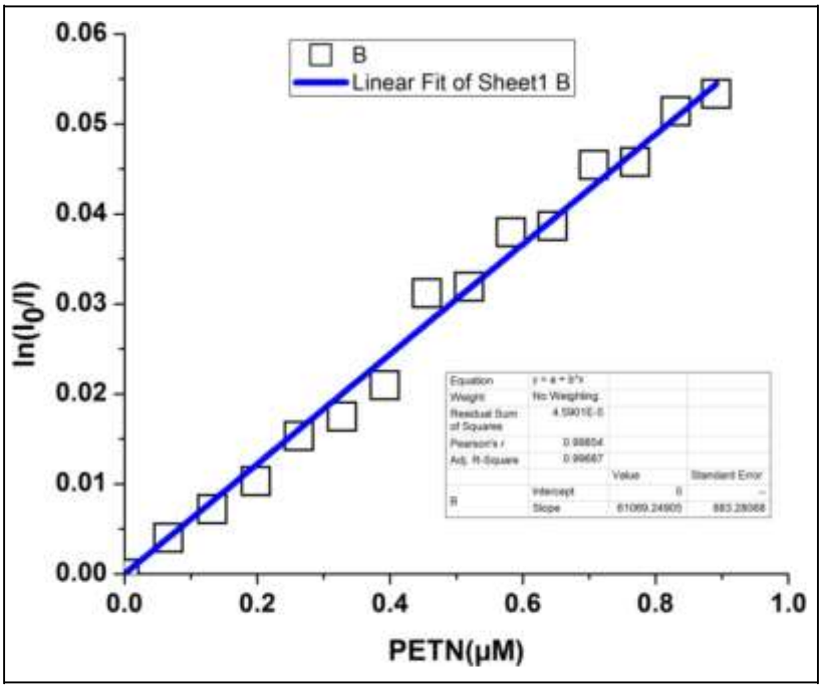

Fig.S36 Perrin plot

Table S14. Fluorescence quenching experiment of **2** upon addition TNG

Solution of sensor 2	Concentrate of sensor 2, M	Solution of quencher	Concentrate of quencher, M
25% water solution of THF	1.0×10^{-6} M	CH_3CN	2.0×10^{-5} M

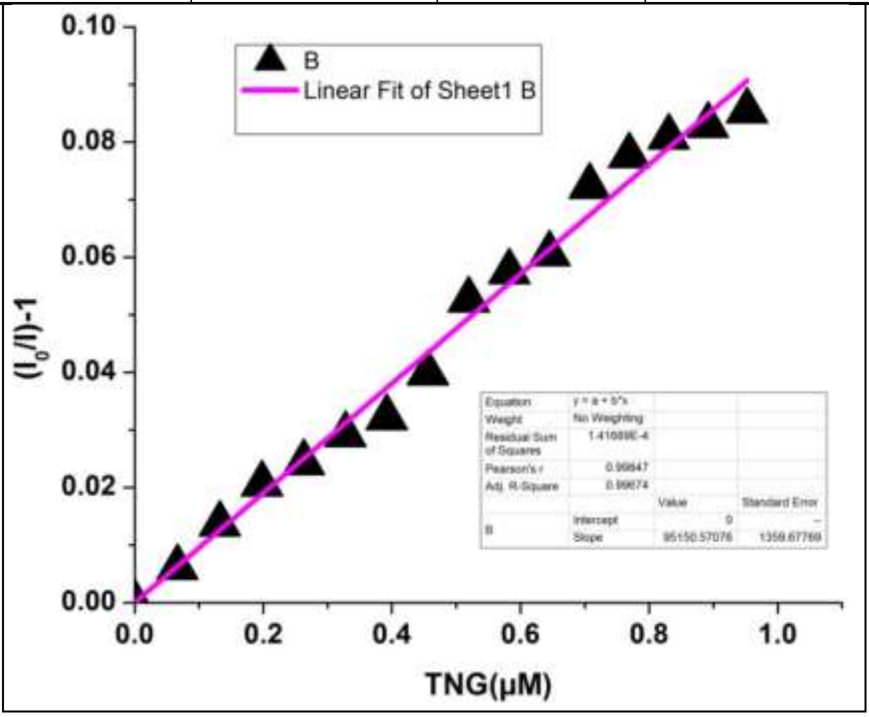

Fig.S37 Stern-Volmer plot

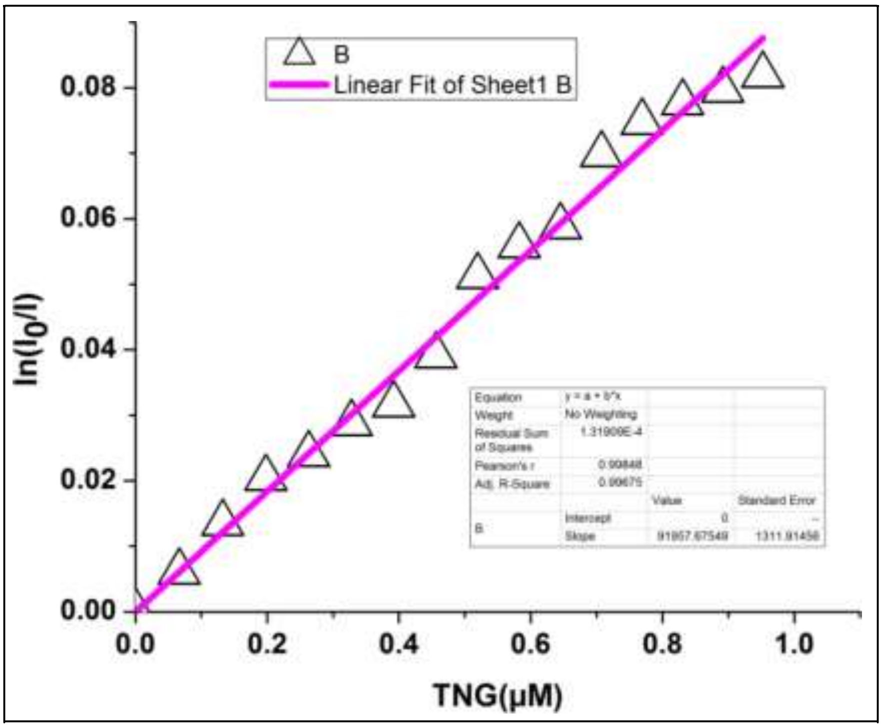

Fig.S38 Perrin plot

Table S15. Fluorescence quenching experiment of **2** upon addition RDX

Solution of sensor 2	Concentrate of sensor 2, M	Solution of quencher	Concentrate of quencher, M
25% water solution of THF	1.0×10^{-6} M	CH_3CN	2.0×10^{-5} M

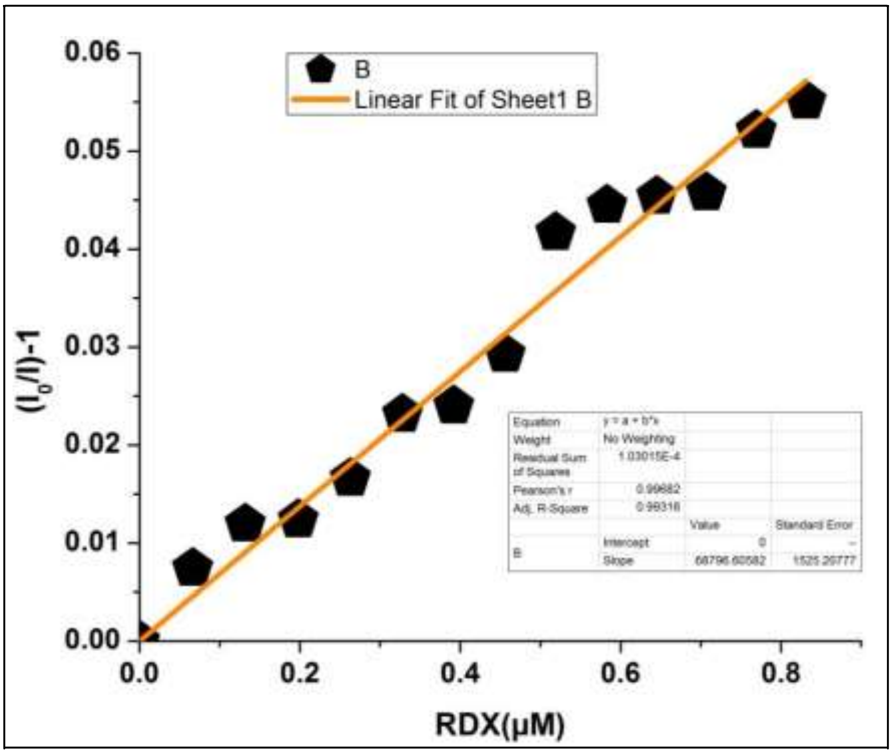

Fig.S39 Stern-Volmer plot

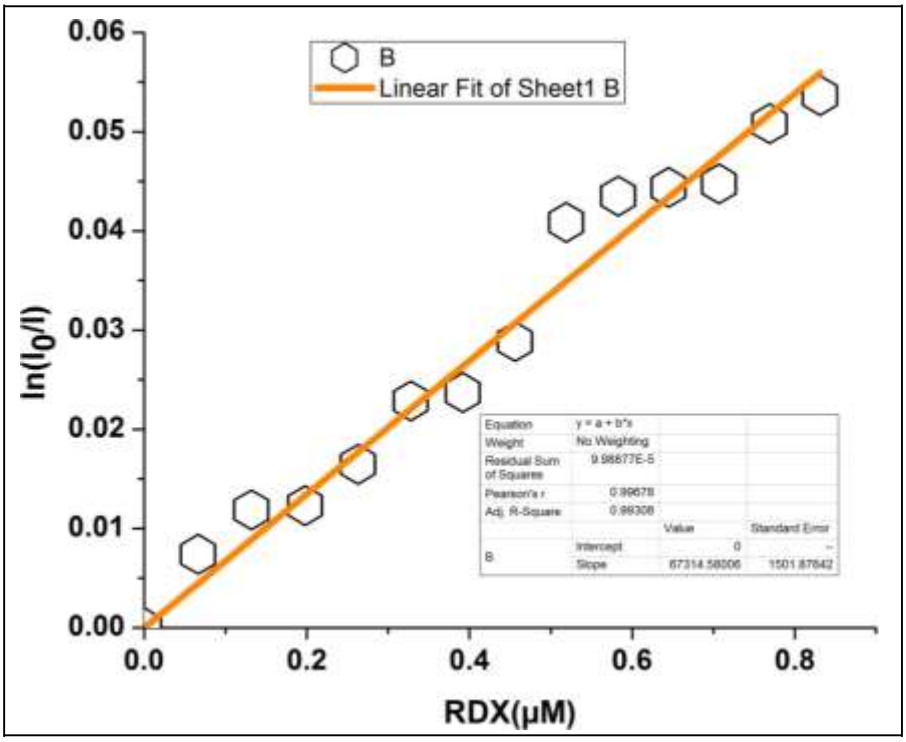

Fig.S40 Perrin plot

Table S16. Summary data of experiments fluorescence quenching of sensor **2** by using Single Point method

μM	**DMNB (I_0/I)-1**	**PETN (I_0/I)-1**	**TNG (I_0/I)-1**	**RDX (I_0/I)-1**
0.000	0.000	0.000	0.000	0,0000
0.066	0.007	0.004	0.006	0,0074
0.132	0.010	0.007	0.014	0,0119
0.198	0.020	0.010	0.021	0,0124
0.263	0.027	0.015	0.024	0,0166
0.328	0.039	0.018	0.029	0,0231
0.392	0.044	0.021	0.032	0,0240
0.456	0.055	0.032	0.040	0,0293
0.519	0.069	0.032	0.053	0,0417
0.583	0.082	0.039	0.057	0,0445
0.645	0.087	0.039	0.061	0,0454
0.707	0.089	0.046	0.072	0,0458
0.769	0.098	0.047	0.078	0,0521
0.831	0.101	0.053	0.081	0,0551
0.892	0.116	0.055	0.083	0,0000
0.952	0.118	0.000	0.085	0,0000

DMNB		**PETN**		**TNG**		**RDX**	
Q.Ef,%	**ppb**	**Q.Ef,%**	**ppb**	**Q.Ef,%**	**ppb**	**Q.Ef,%**	**ppb**
0.00	0.00	0.00	0.00	0.00	0.00	0.00	0.00
0.68	11.69	0.40	21.00	0.61	15.08	0,74	14,75
0.98	23.31	0.71	41.85	1.34	30.07	1,18	29,40
1.98	34.85	1.02	62.57	2.02	44.95	1,22	43,96
2.61	46.32	1.52	83.16	2.37	59.74	1,63	58,42
3.71	57.70	1.73	103.61	2.84	74.43	2,26	72,79
4.23	69.02	2.07	123.92	3.11	89.02	2,34	87,06
5.19	80.26	3.07	144.10	3.83	103.52	2,84	101,24
6.42	91.43	3.14	164.16	4.99	117.92	4,00	115,32
7.59	102.52	3.73	184.08	5.43	132.23	4,26	129,32
8.01	113.55	3.79	203.87	5.71	146.45	4,34	143,23
8.20	124.50	4.44	223.54	6.74	160.58	4,38	157,04
8.93	135.38	4.47	243.08	7.20	174.62	4,95	170,77
9.19	146.20	5.01	262.49	7.48	188.56	5,22	184,41
10.39	156.94	5.20	281.78	7.66	202.42	0.00	0.00
10.56	167.62	0.00	0.00	7.87	216.19	0.00	0.00

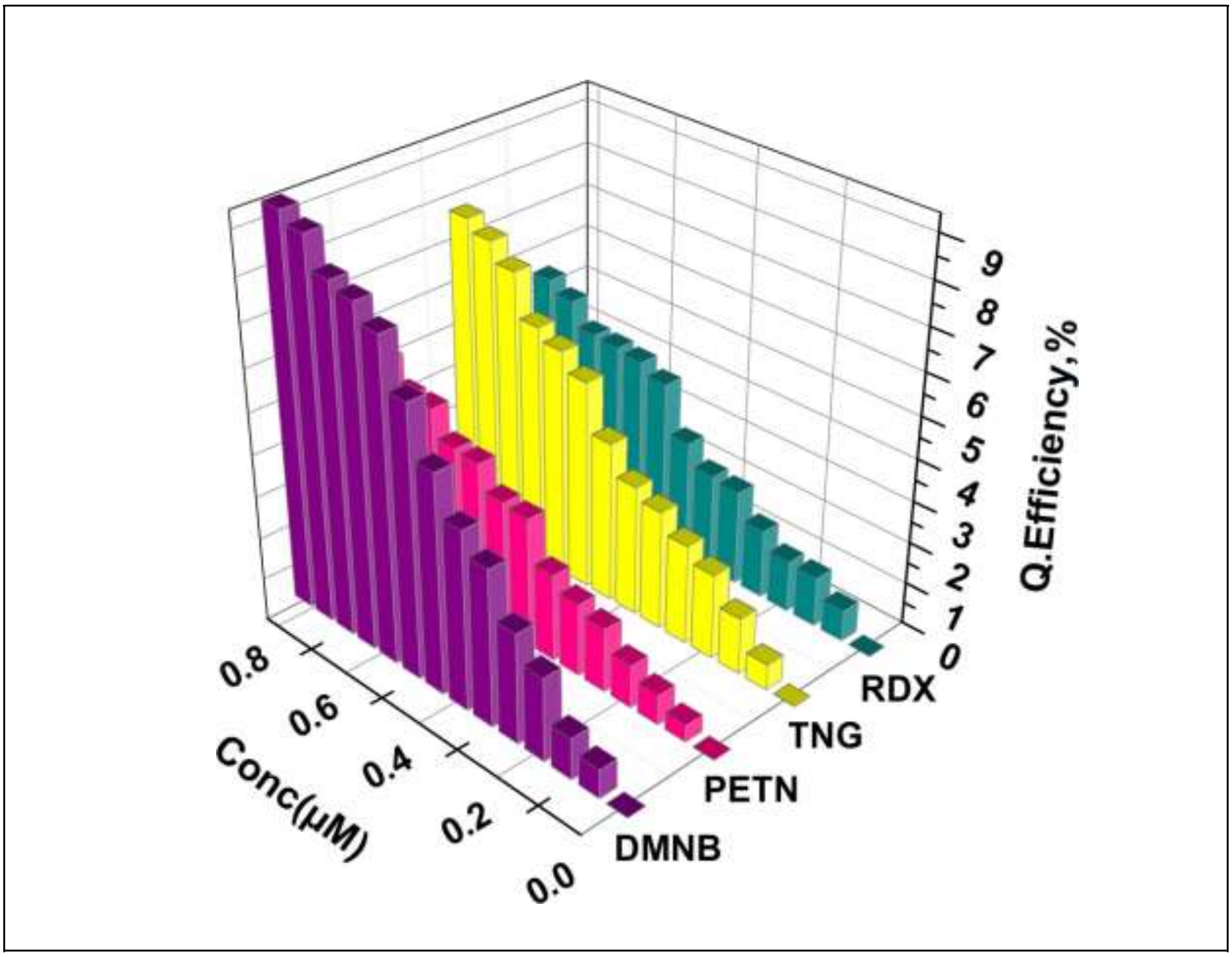

Fig.S41 Quenching efficiency of sensor **2** at different concentrations of nitro explosives

7.4 Sensor 3

Table S17 Fluorescence quenching experiment of **3** upon addition DMNB

Solution of sensor 3	Concentrate of sensor 3, M	Solution of quencher	Concentrate of quencher, M
Potassium salt in water	1.0×10^{-6} M	CH_3CN	2.0×10^{-5} M

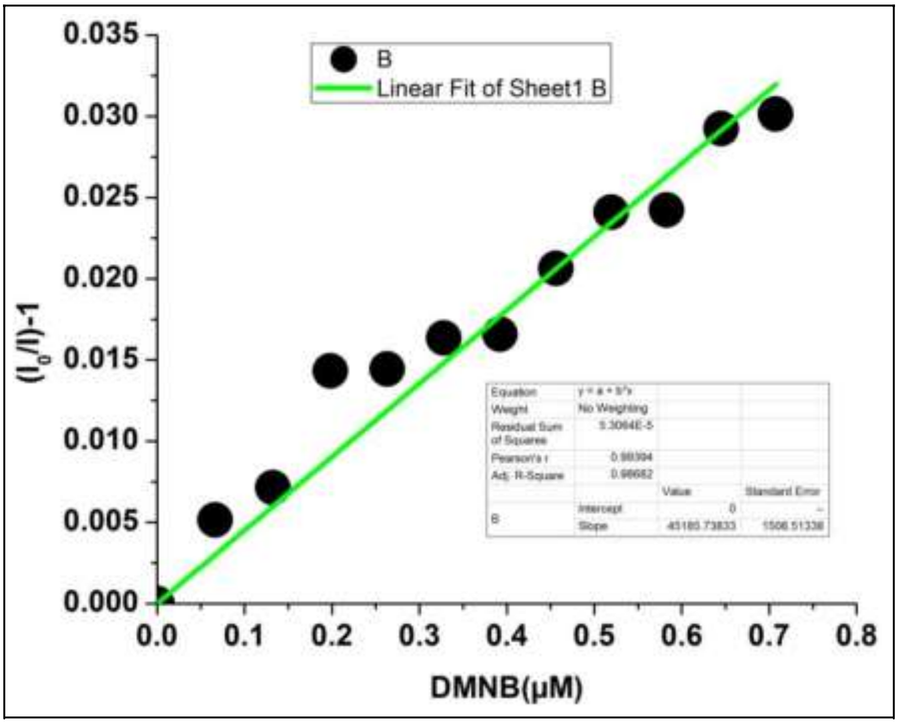

Fig.S42 Stern-Volmer plot

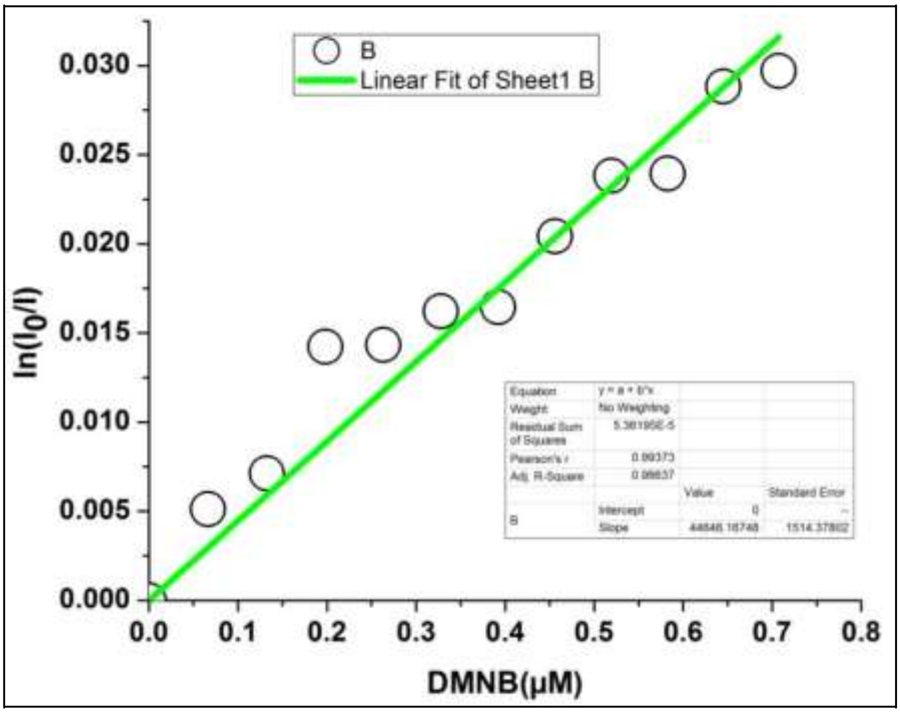

Fig.S43 Perrin plot

Table S18 Fluorescence quenching experiment of **3** upon addition PETN

Solution of	Concentrate of	Solution of	Concentrate of

sensor 3	sensor 3, M	quencher	quencher, M
Potassium salt in water	1.0×10^{-6} M	CH_3CN	2.0×10^{-5} M

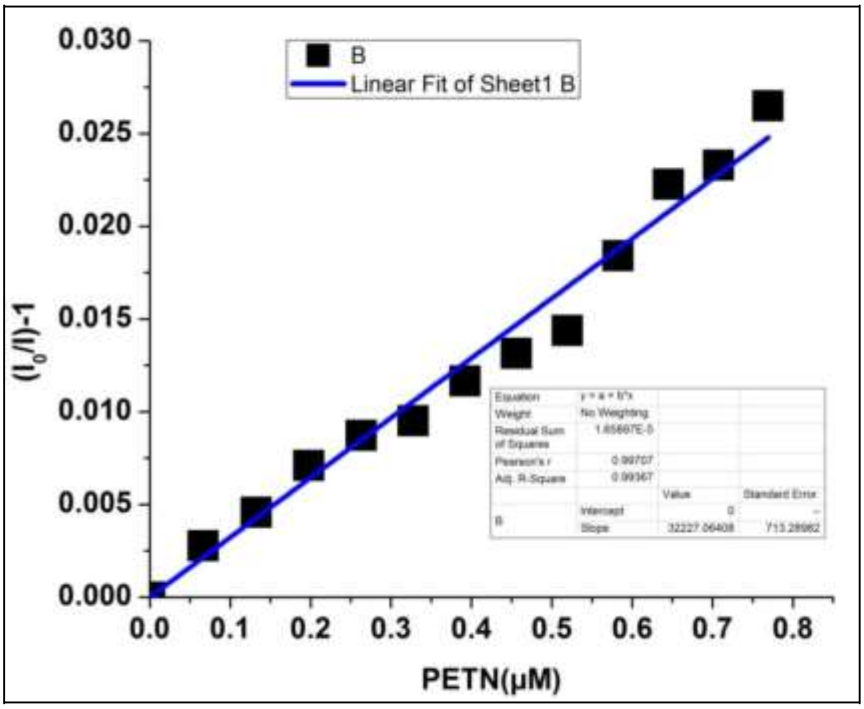

Fig.S44 Stern-Volmer plot

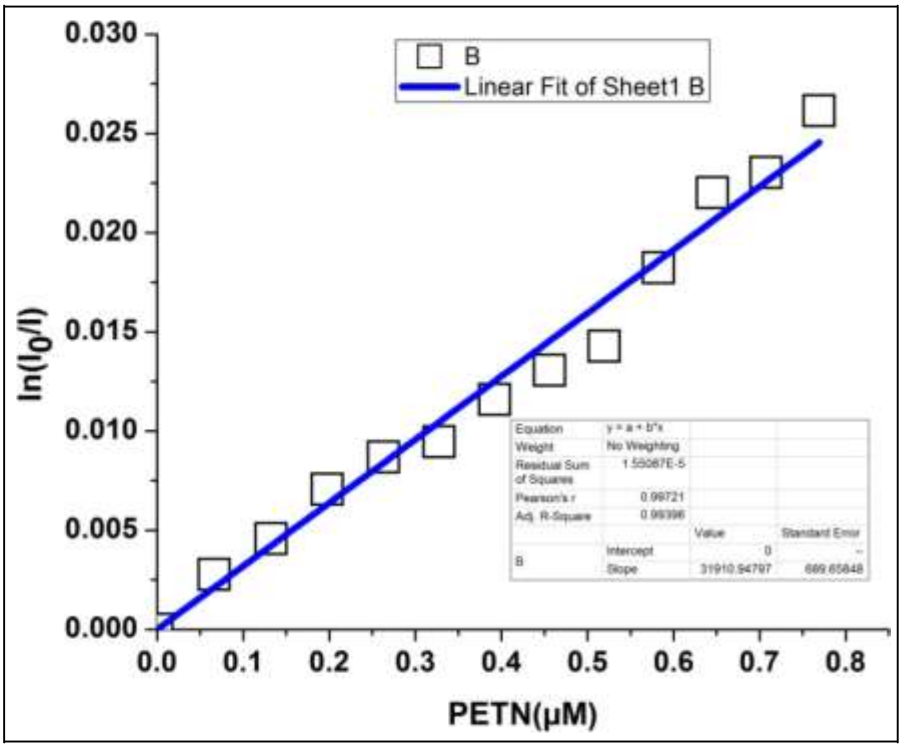

Fig.S45 Perrin plot

Table S19 Fluorescence quenching experiment of **3** upon addition TNG

Solution of sensor 3	Concentrate of sensor 3, M	Solution of quencher	Concentrate of quencher, M
Potassium salt in water	1.0×10^{-6} M	CH_3CN	2.0×10^{-5} M

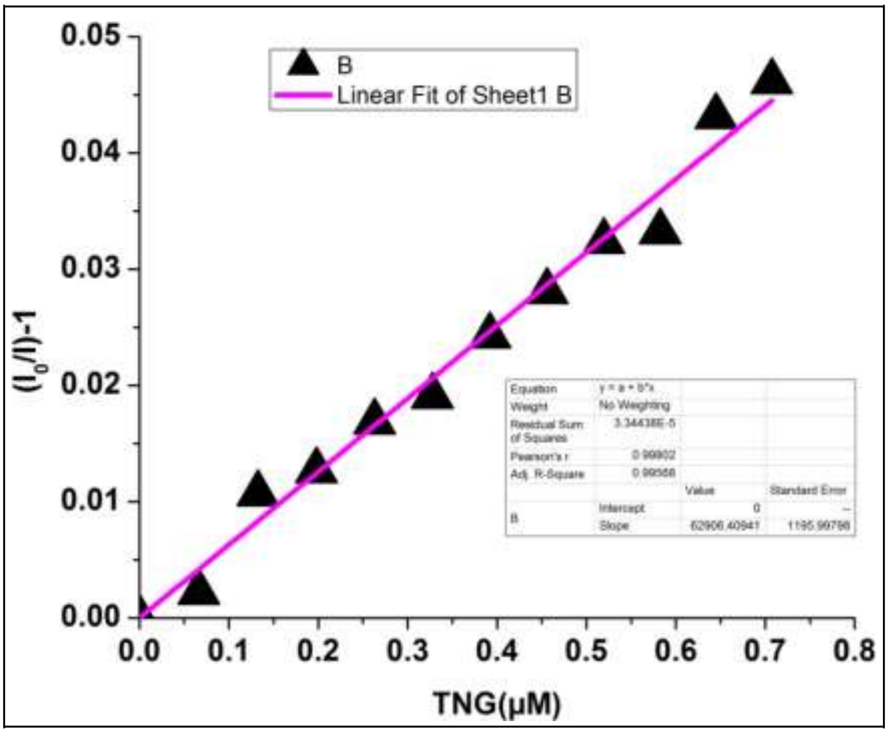

Fig.S46 Stern-Volmer plot

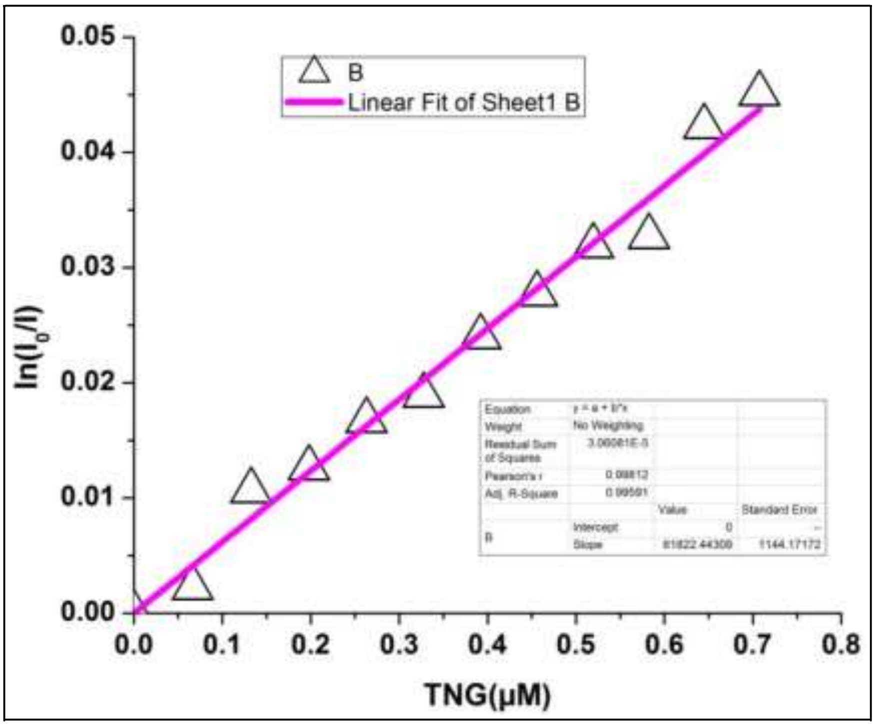

Fig.S47 Perrin plot

Table S20 Fluorescence quenching experiment of **3** upon addition RDX

Solution of sensor 3	Concentrate of sensor 3, M	Solution of quencher	Concentrate of quencher, M
Potassium salt in water	1.0×10^{-6} M	CH_3CN	2.0×10^{-5} M

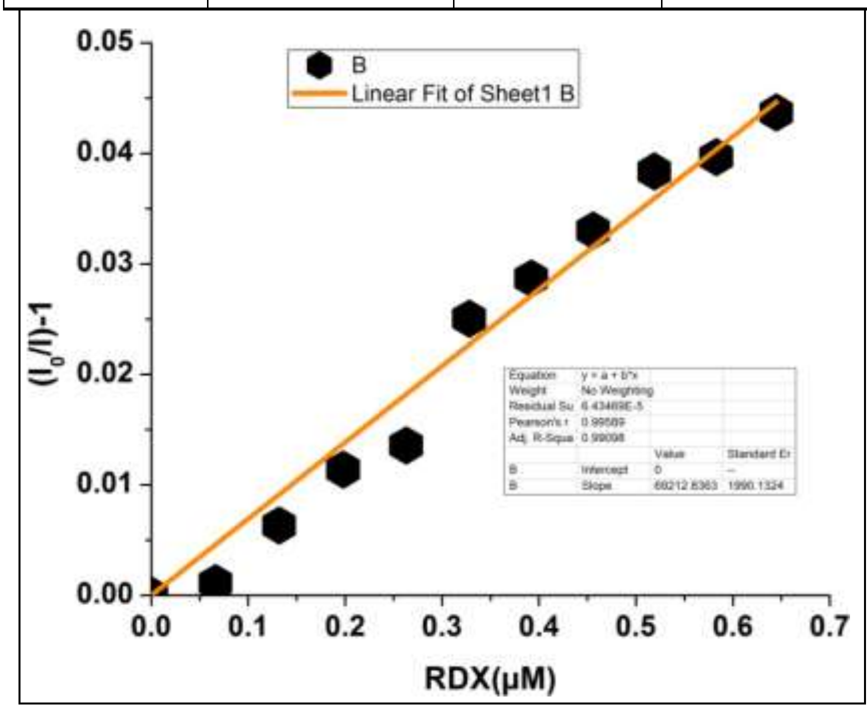

Fig.S48 Stern-Volmer plot

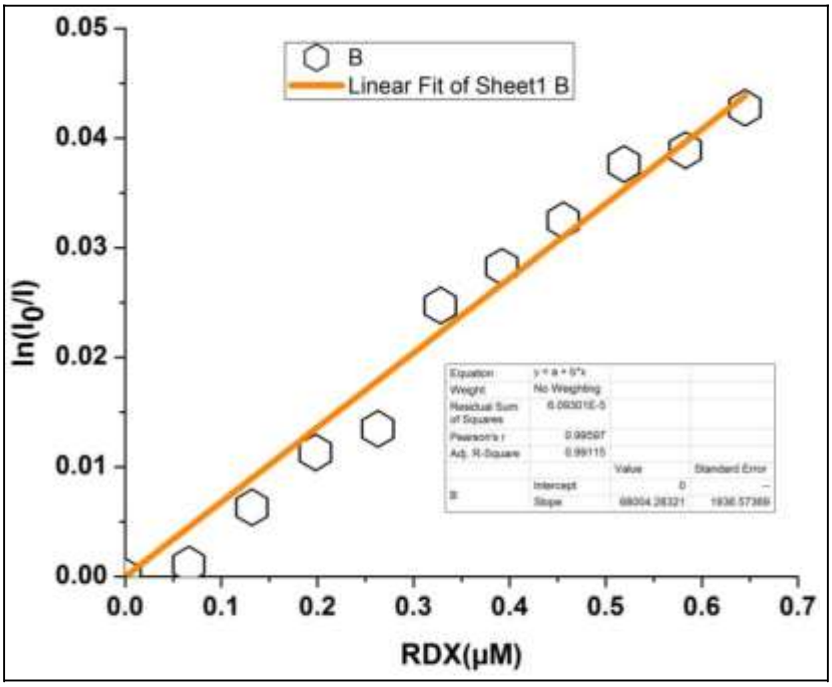

Fig.S49 Perrin plot

Table S21 Summary data of experiments fluorescence quenching of sensor **3** by using Single Point method

μM	**DMNB (I_0/I)-1**	**PETN (I_0/I)-1**	**TNG (I_0/I)-1**	**RDX (I_0/I)-1**
0.000	0.000	0.000	0.000	0,0000
0.066	0.005	0.003	0.002	0,0011
0.132	0.007	0.005	0.011	0,0063
0.198	0.014	0.007	0.013	0,0114
0.263	0.014	0.009	0.017	0,0136
0.328	0.016	0.009	0.019	0,0250
0.392	0.017	0.012	0.024	0,0287
0.456	0.021	0.013	0.028	0,0330
0.519	0.024	0.014	0.032	0,0384
0.583	0.024	0.018	0.033	0,0397
0.645	0.029	0.022	0.043	0,0437
0.707	0.030	0.023	0.046	0,0000

DMNB		**PETN**		**TNG**		**RDX**	
Q.Ef,%	**ppb**	**Q.Ef,%**	**ppb**	**Q.Ef,%**	**ppb**	**Q.Ef,%**	**ppb**
0.00	0.00	0.00	0.00	0.00	0.00	0,00	0,00
0.51	11.69	0.28	21.00	0.22	15.08	0,11	14,75
0.71	23.31	0.46	41.85	1.06	30.07	0,63	29,40

1.41	34.85	0.70	62.57	1.25	44.95	1,13	43,96
1.42	46.32	0.86	83.16	1.66	59.74	1,34	58,42
1.61	57.70	0.94	103.61	1.87	74.43	2,44	72,79
1.63	69.02	1.15	123.92	2.37	89.02	2,79	87,06
2.02	80.26	1.30	144.10	2.73	103.52	3,20	101,24
2.35	91.43	1.42	164.16	3.14	117.92	3,69	115,32
2.37	102.52	1.81	184.08	3.21	132.23	3,81	129,32
2.84	113.55	2.18	203.87	4.13	146.45	4,19	143,23
2.93	124.50	2.28	223.54	4.41	160.58	0,00	0,00

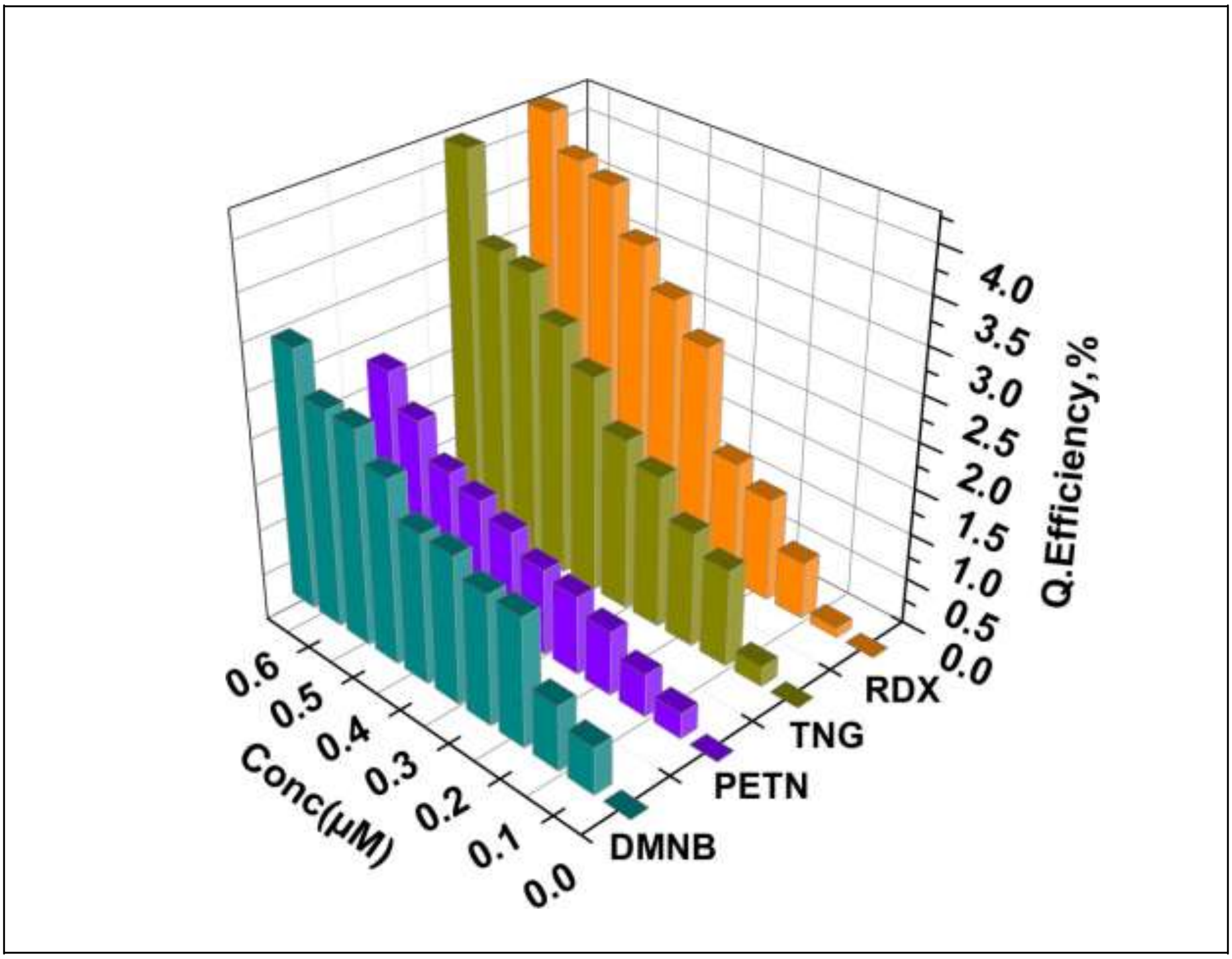

Fig.S50 Quenching efficiency of sensor **3** at different concentrations of nitro explosives

7.5 Sensor 4

Table S22 Fluorescence quenching experiment of **4** upon addition DMNB

Solution of sensor 4	Concentrate of sensor 4, M	Solution of quencher	Concentrate of quencher, M
25% water solution of THF	1.0×10^{-6} M	CH_3CN	2.0×10^{-5} M

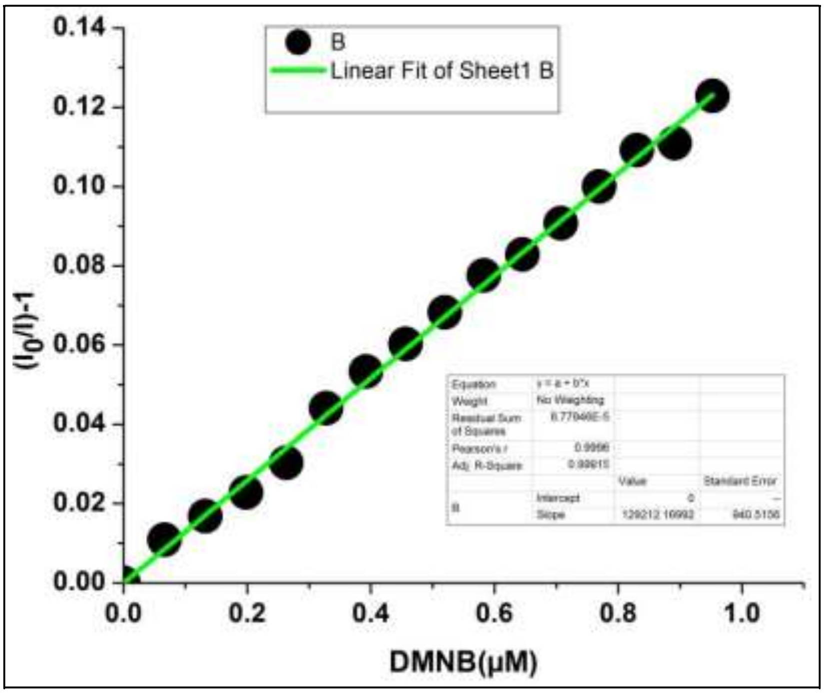

Fig.S51 Stern-Volmer plot

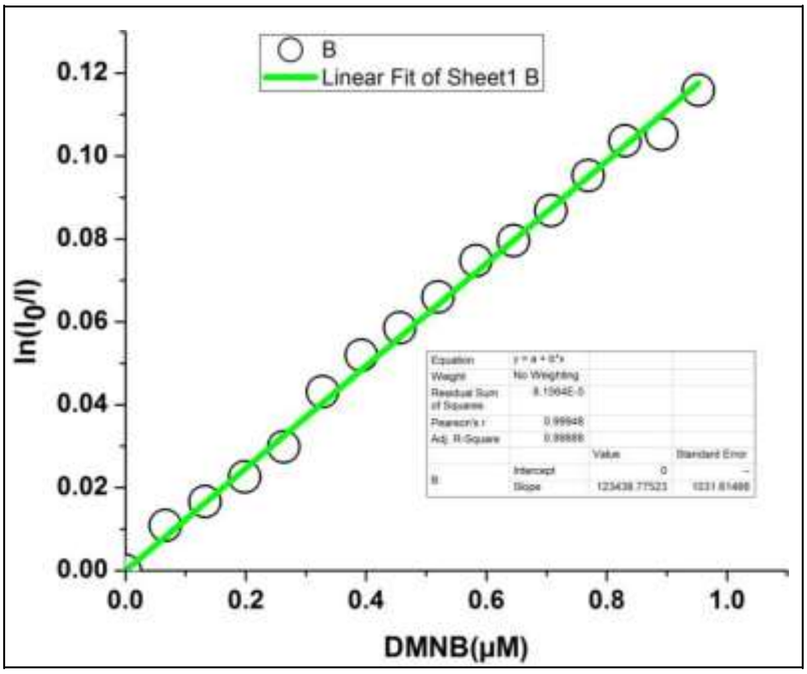

Fig.S52 Perrin plot

Table S23 Fluorescence quenching experiment of **4** upon addition PETN

Solution of sensor 4	Concentrate of sensor 4, M	Solution of quencher	Concentrate of quencher, M
25% water	1.0×10^{-6} M	CH_3CN	2.0×10^{-5} M

solution of THF			

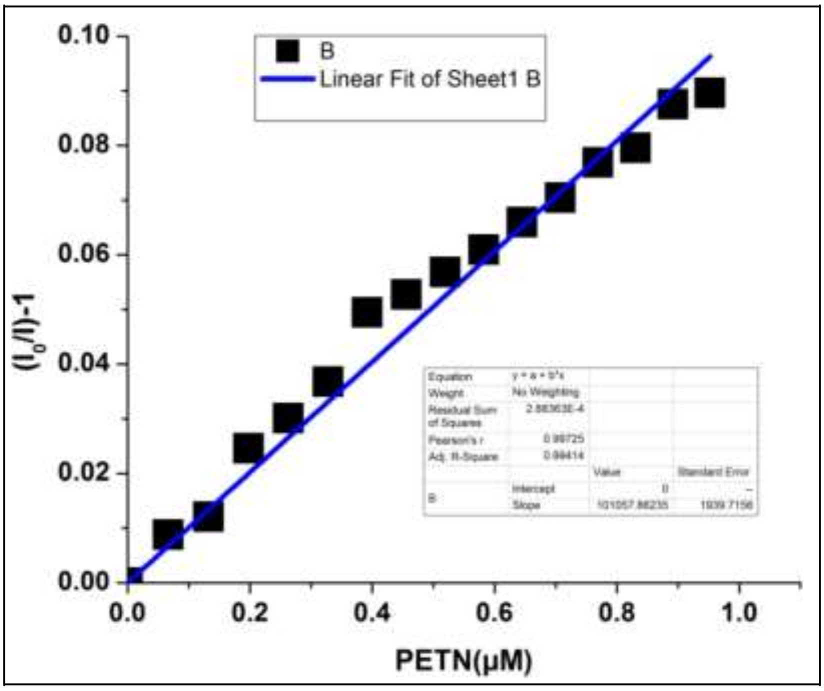

Fig.S53 Stern-Volmer plot

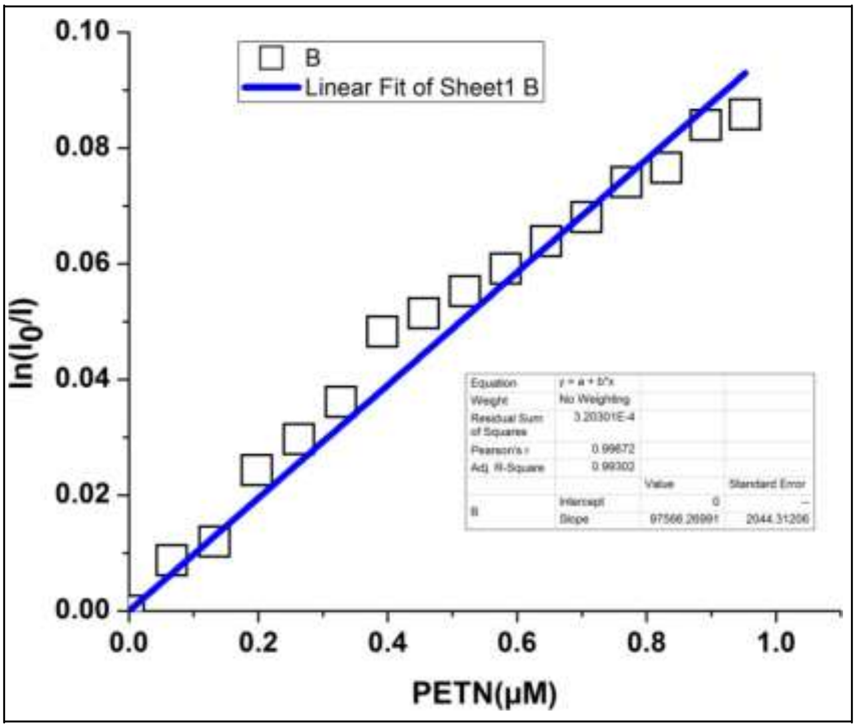

Fig.S54 Perrin plot

Table S24 Fluorescence quenching experiment of **4** upon addition TNG

Solution of sensor 4	Concentrate of sensor 4, M	Solution of quencher	Concentrate of quencher, M
25% water solution of THF	1.0 ×10^{-6} M	CH_3CN	2.0 × 10^{-5} M

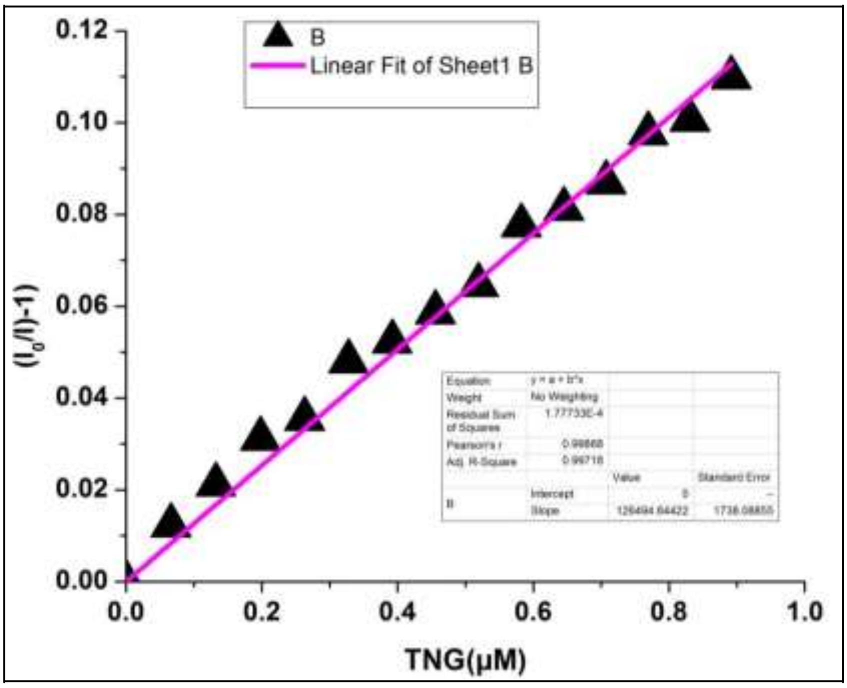

Fig.S55 Stern-Volmer plot

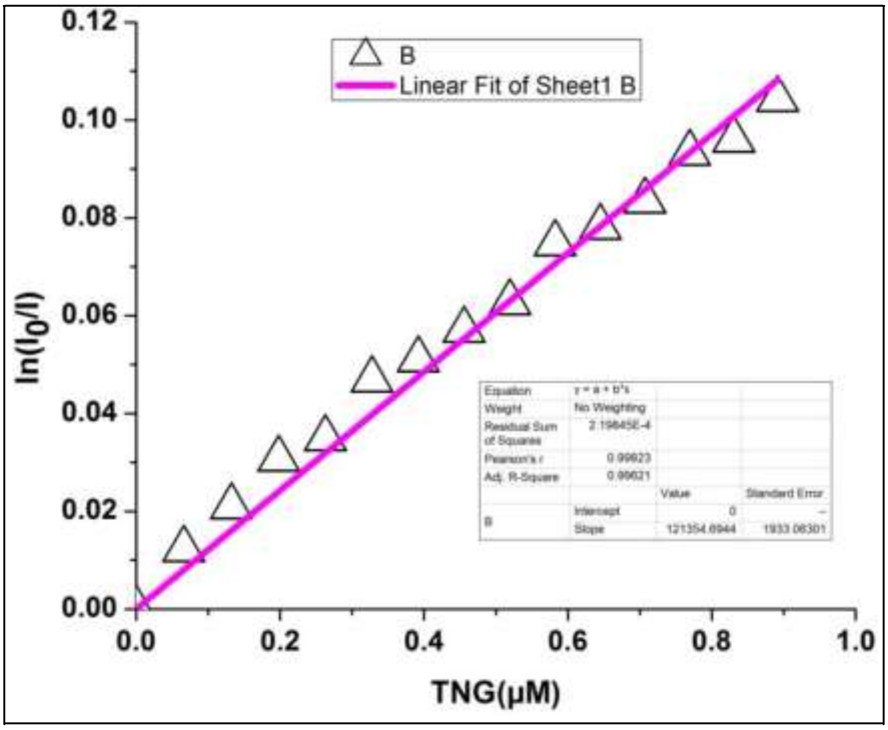

Fig.S56 Perrin plot

Table S25 Fluorescence quenching experiment of **4** upon addition RDX

Solution of sensor 4	Concentrate of sensor 4, M	Solution of quencher	Concentrate of quencher, M
25% water solution of THF	1.0×10^{-6} M	CH_3CN	2.0×10^{-5} M

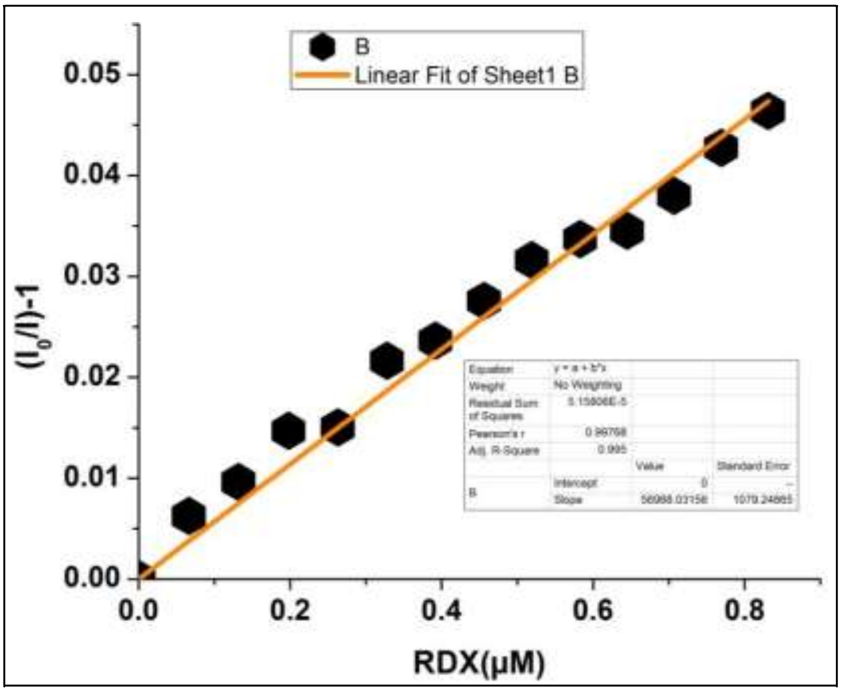

Fig.S57 Stern-Volmer plot

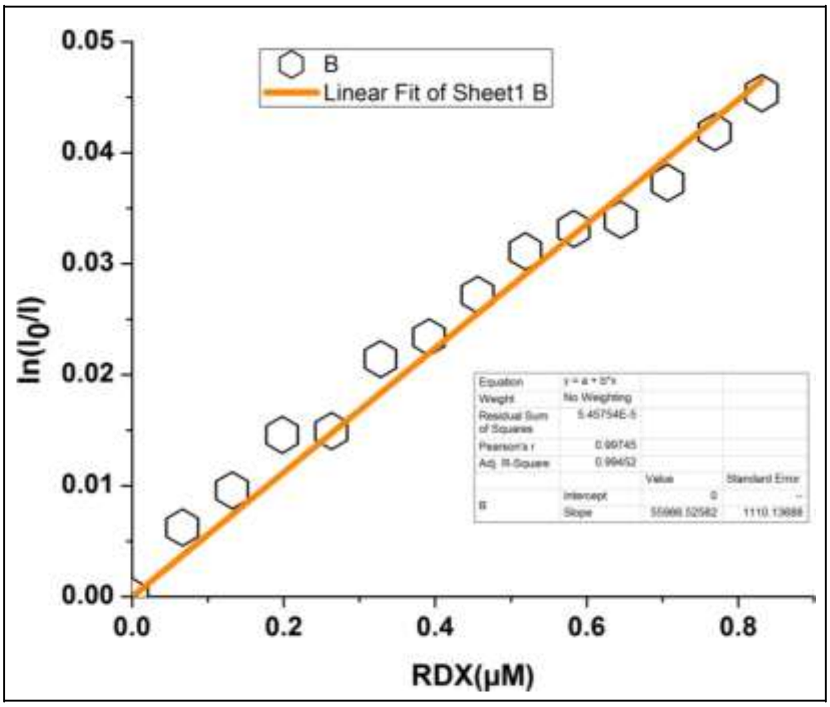

Fig.S58 Perrin plot

Table S26. Summary data of fluorescence quenching experiments for the sensor **4** by using Single Point method

µM	DMNB (I_0/I)-1	PETN (I_0/I)-1	TNG (I_0/I)-1	RDX (I_0/I)-1
0.000	0.000	0.000	0.000	0,000
0.066	0.007	0.004	0.006	0,006
0.132	0.010	0.007	0.014	0,010
0.198	0.020	0.010	0.021	0,014
0.263	0.027	0.015	0.024	0,015
0.328	0.039	0.018	0.029	0,022
0.392	0.044	0.021	0.032	0,024
0.456	0.055	0.032	0.040	0,028
0.519	0.069	0.032	0.053	0,032
0.583	0.082	0.039	0.057	0,034
0.645	0.087	0.039	0.061	0,035
0.707	0.089	0.046	0.072	0,038
0.769	0.098	0.047	0.078	0,043
0.831	0.101	0.053	0.081	0.000
0.892	0.116	0.055	0.083	0.000
0.952	0.118	0.000	0.085	0.000

DMNB		PETN		TNG		RDX	
Q.Ef,%	ppb	Q.Ef,%	ppb	Q.Ef,%	ppb	Q.Ef,%	ppb
0.00	0.00	0.00	0.00	0.00	0.00	0,00	0,00
0.68	11.69	0.40	21.00	0.61	15.08	0,62	14,75
0.98	23.31	0.71	41.85	1.34	30.07	0,95	29,40
1.98	34.85	1.02	62.57	2.02	44.95	1,45	43,96
2.61	46.32	1.52	83.16	2.37	59.74	1,48	58,42
3.71	57.70	1.73	103.61	2.84	74.43	2,12	72,79
4.23	69.02	2.07	123.92	3.11	89.02	2,31	87,06
5.19	80.26	3.07	144.10	3.83	103.52	2,68	101,24
6.42	91.43	3.14	164.16	4.99	117.92	3,06	115,32
7.59	102.52	3.73	184.08	5.43	132.23	3,26	129,32
8.01	113.55	3.79	203.87	5.71	146.45	3,34	143,23
8.20	124.50	4.44	223.54	6.74	160.58	3,66	157,04
8.93	135.38	4.47	243.08	7.20	174.62	4,10	170,77
9.19	146.20	5.01	262.49	7.48	188.56	4,30	0,00
10.39	156.94	5.20	281.78	7.66	202.42	4,60	0,00
10.56	167.62	0.00	0.00	7.87	216.19	0,00	0,00

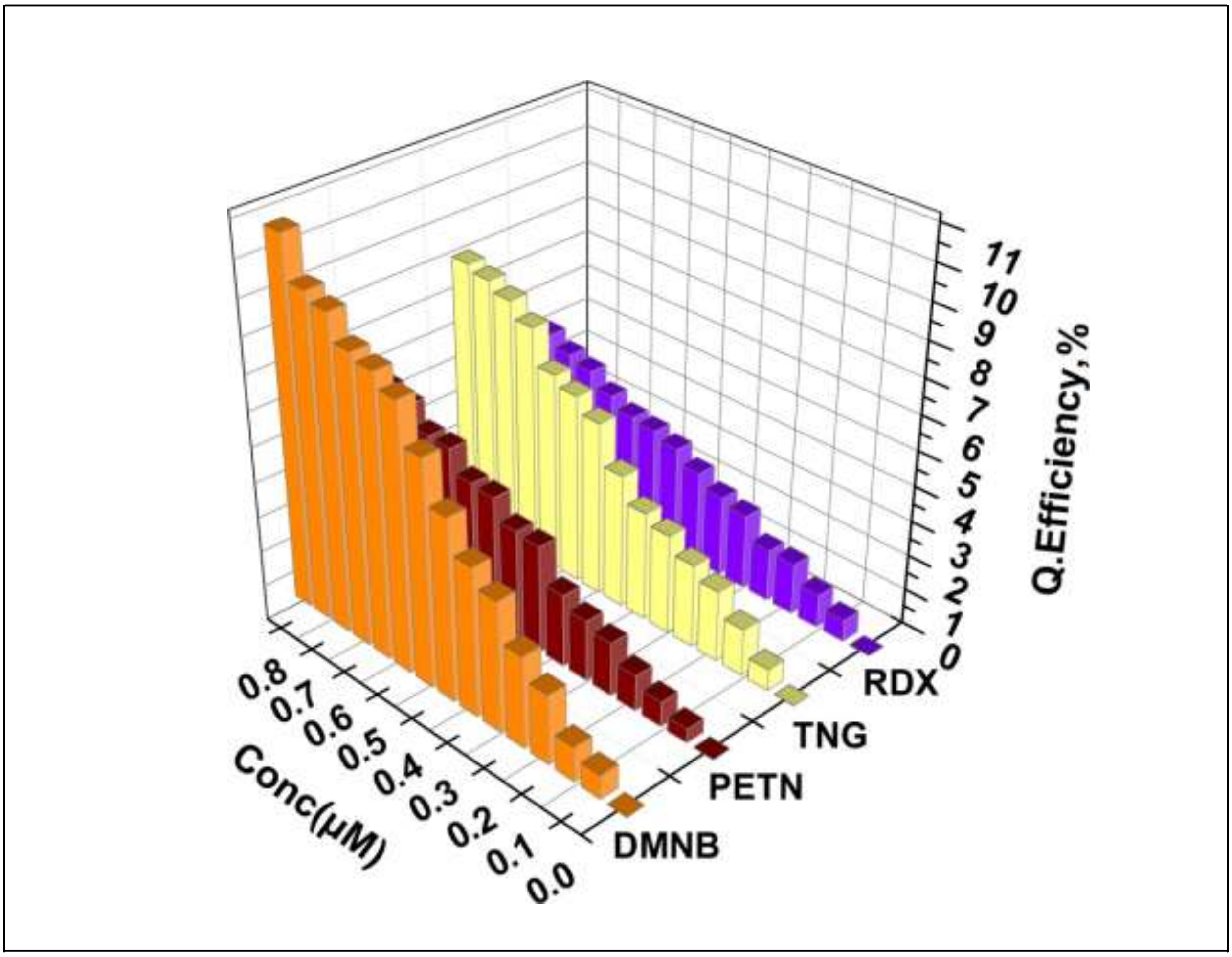

Fig.S59 Quenching efficiency of sensor **4** at different concentrations of nitro explosives

7.6 Sensor 5

Table S27 Fluorescence quenching experiment of **5** upon addition DMNB

Solution of sensor 5	Concentrate of sensor 5, M	Solution of quencher	Concentrate of quencher, M
Potassium salt in water	1.0×10^{-6} M	CH_3CN	2.0×10^{-5} M

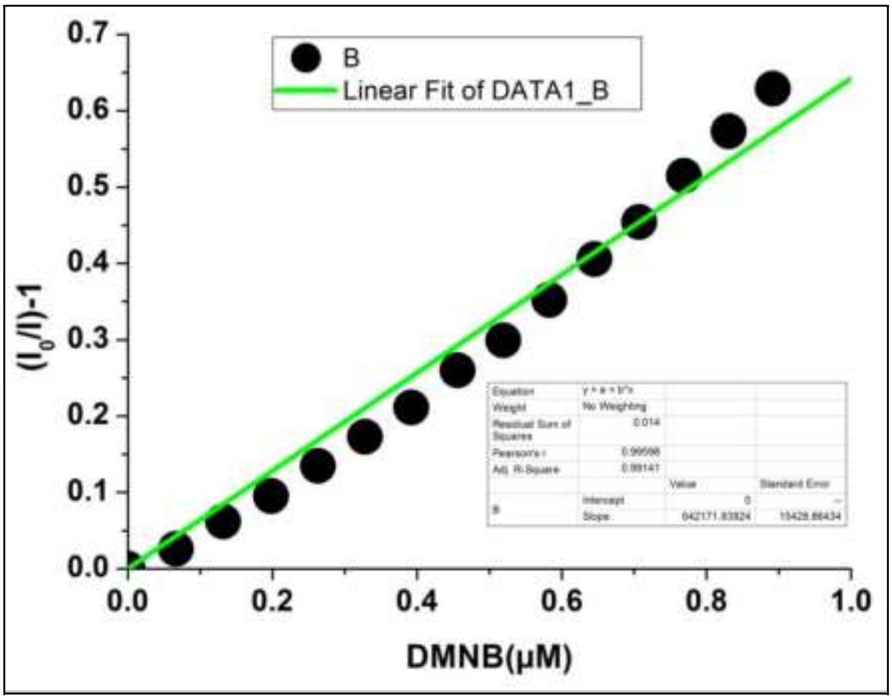

Fig.S60 Stern-Volmer plot

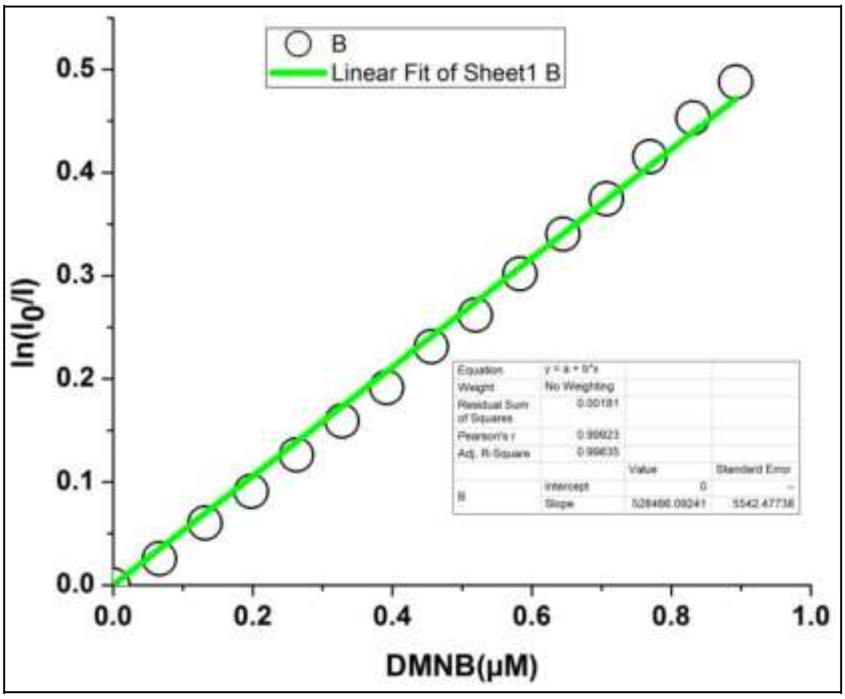

Fig.S61 Perrin plot

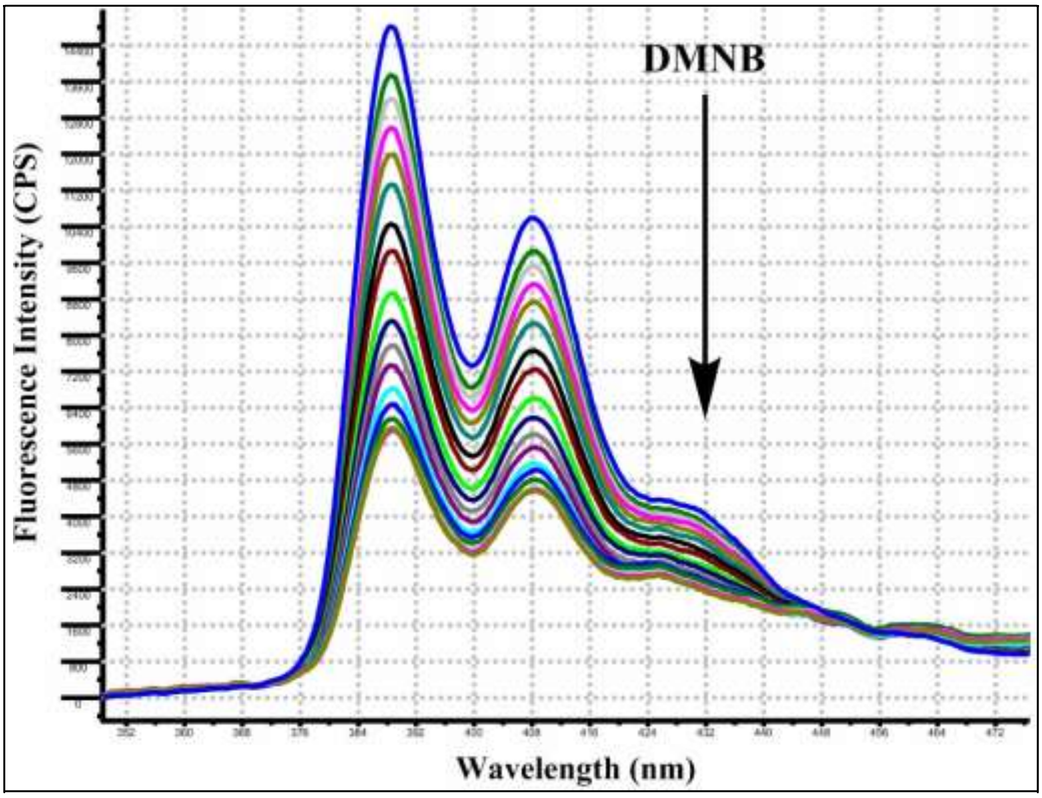

Fig.S62 Fluorescence quenching of the sensor **5** with DMNB in water

Table S28. Fluorescence quenching experiment of **5** upon addition PETN

Solution of sensor 5	Concentrate of sensor 5, M	Solution of quencher	Concentrate of quencher, M
Potassium salt in water	1.0×10^{-6} M	CH_3CN	2.0×10^{-5} M

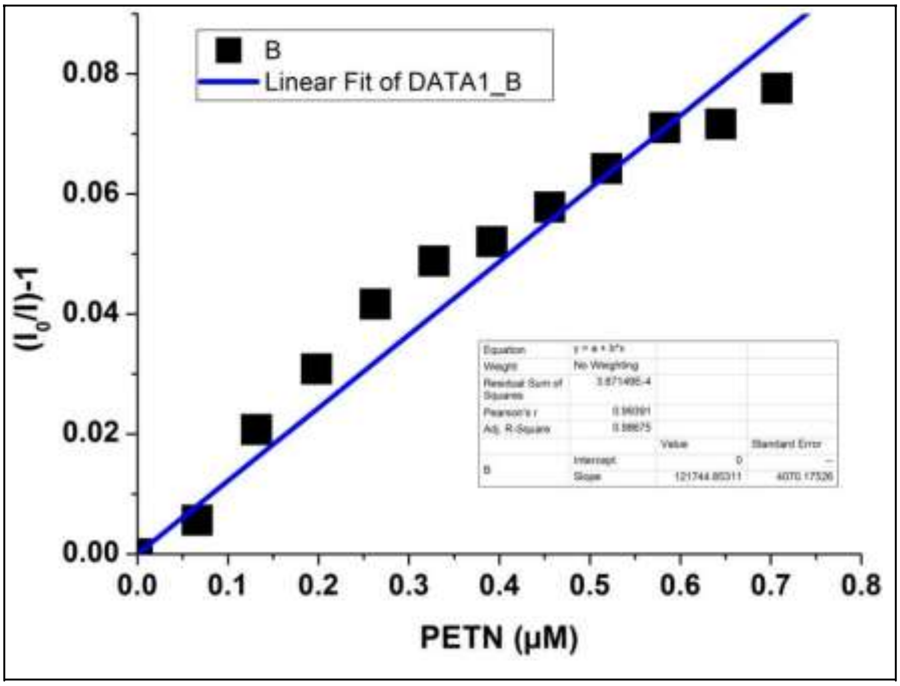

Fig.S63 Stern-Volmer plot

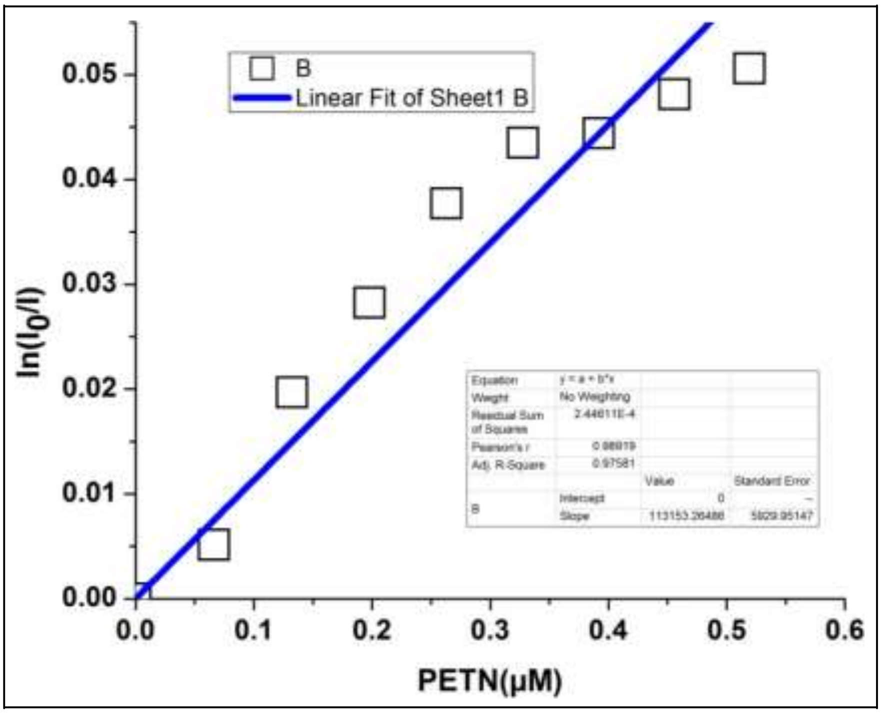

Fig.S64 Perrin plot

Fig.S46 Fluorescence quenching of the sensor **5** with DMNB in water

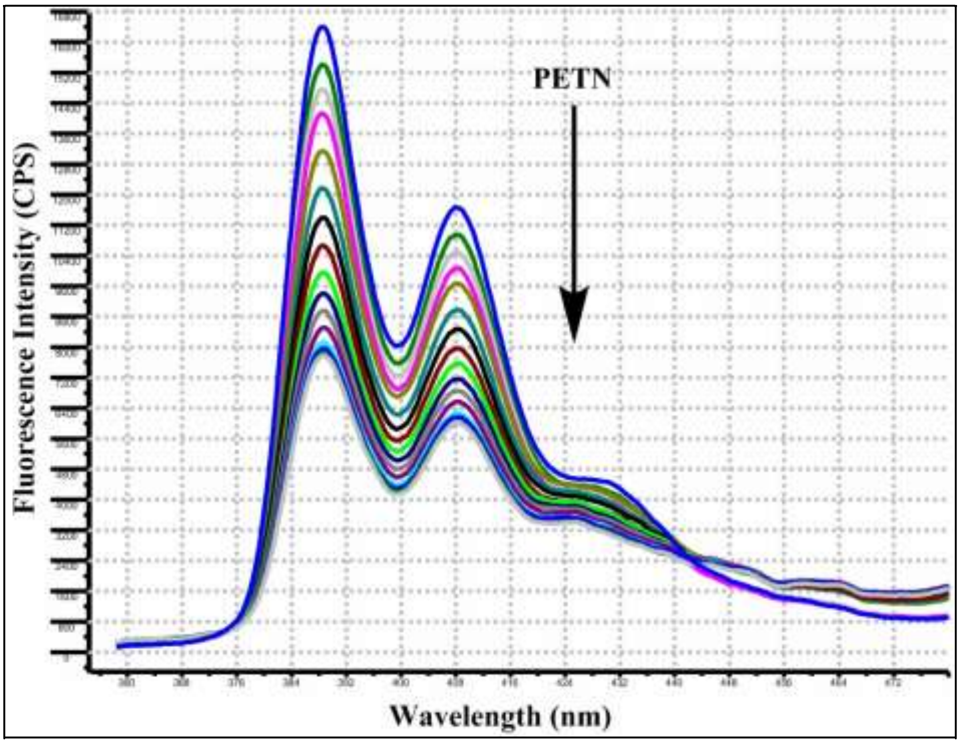

Fig.S65 Fluorescence quenching of the sensor **5** with PETN in water

Table S29. Fluorescence quenching experiment of **5** upon addition TNG

Solution of sensor 5	Concentrate of sensor 5, M	Solution of quencher	Concentrate of quencher, M
Potassium salt in water	1.0×10^{-6} M	CH_3CN	2.0×10^{-5} M

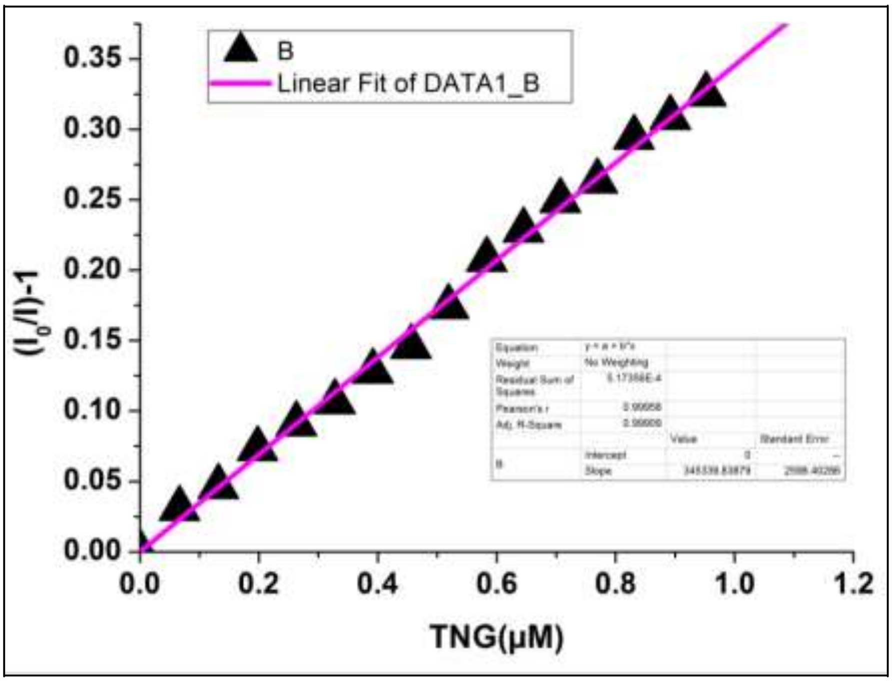

Fig.S66 Stern-Volmer plot

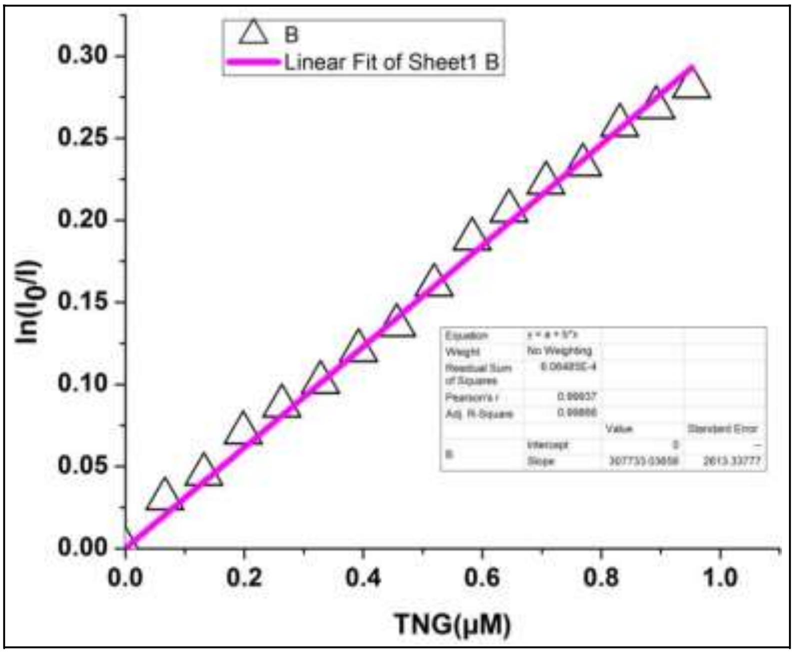

Fig.S67 Perrin plot

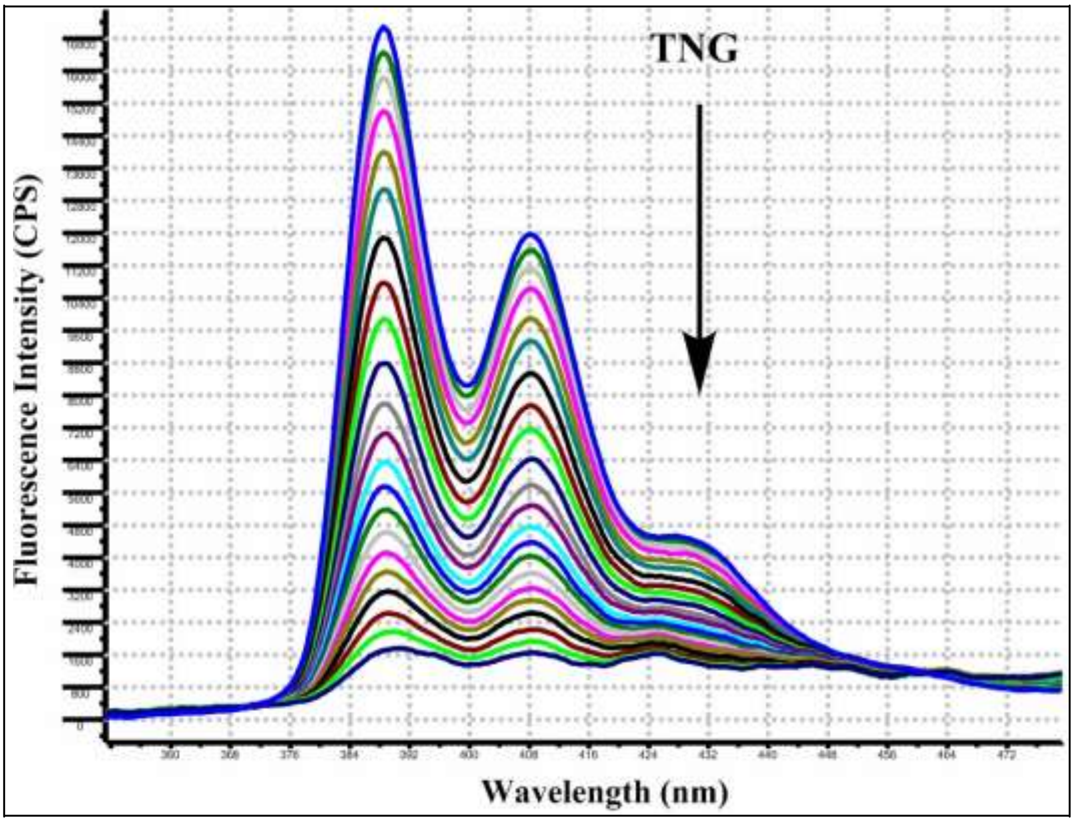

Fig.S68 Fluorescence quenching of the sensor **5** with TNG in water

Table S30. Fluorescence quenching experiment of **5** upon addition RDX

Solution of sensor 5	Concentrate of sensor 5, M	Solution of quencher	Concentrate of quencher, M
Potassium salt in water	1.0×10^{-6} M	CH_3CN	2.0×10^{-5} M

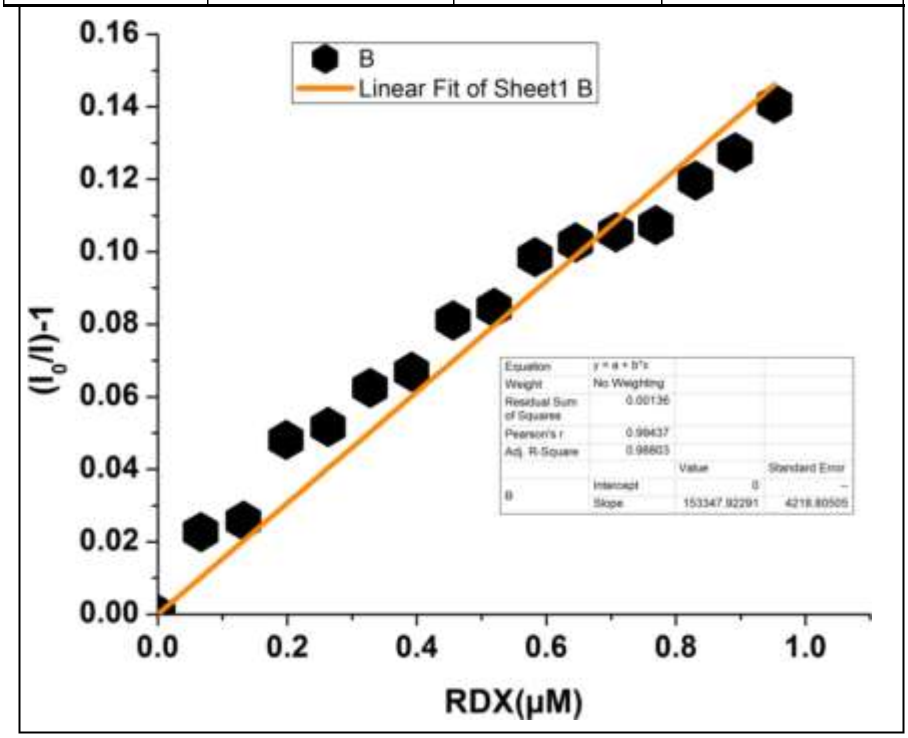

Fig.S69 Stern-Volmer plot

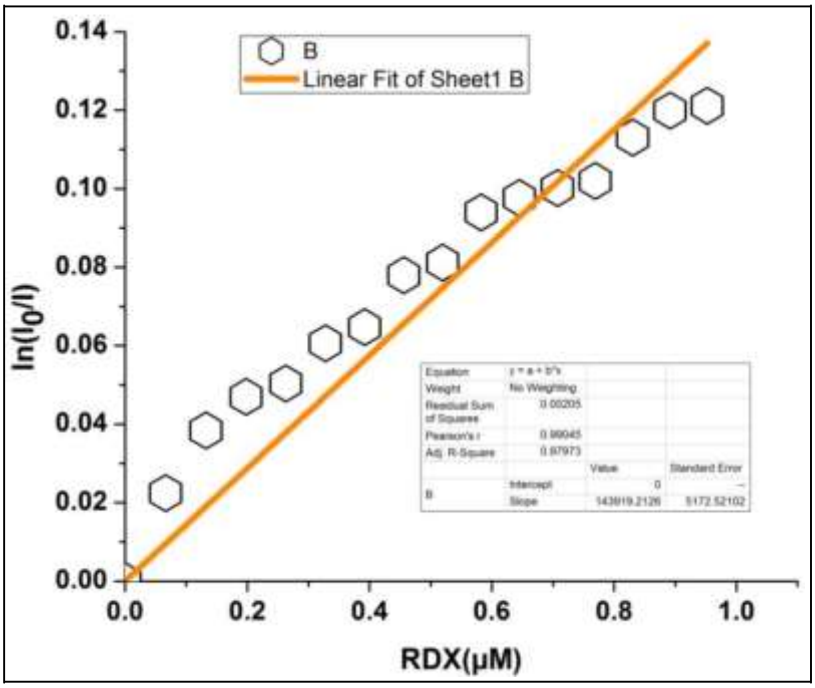

Fig.S70 Perrin plot

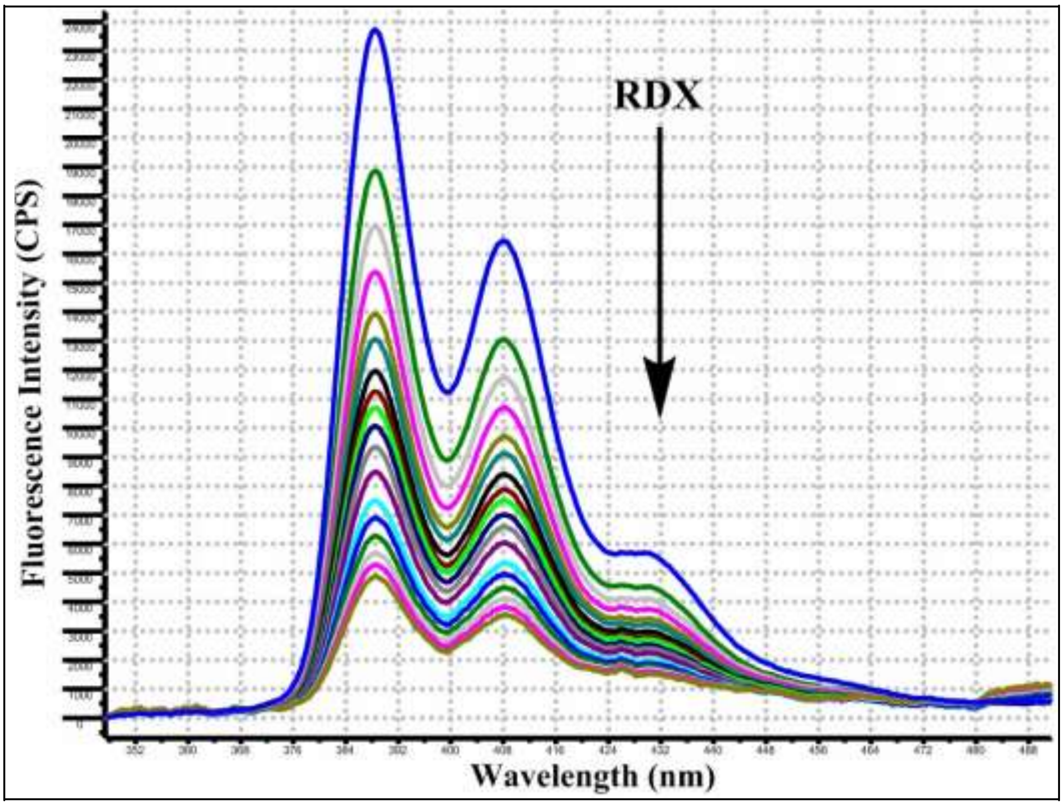

Fig.S71 Fluorescence quenching of the sensor **5** with RDX in water

Table S31. Summary data of fluorescence quenching experiments for the sensor **5** by using Single Point method

μM	DMNB (I_0/I)-1	PETN (I_0/I)-1	TNG (I_0/I)-1	RDX (I_0/I)-1
0.000	0.000	0.000	0.000	0.000
0.066	0.026	0.006	0.031	0.066
0.132	0.062	0.021	0.046	0.132
0.198	0.095	0.031	0.073	0.198
0.263	0.135	0.042	0.091	0.263
0.328	0.173	0.049	0.106	0.328
0.392	0.211	0.052	0.128	0.392
0.456	0.260	0.058	0.146	0.456
0.519	0.299	0.064	0.174	0.519
0.583	0.352	0.071	0.207	0.583
0.645	0.405	0.072	0.228	0.645
0.707	0.454	0.078	0.249	0.707
0.769	0.515	0.182	0.263	0.769
0.831	0.573	0.000	0.294	0.831
0.892	0.629	0.000	0.308	0.892
0.952	0.000	0.000	0.325	0.952

DMNB		PETN		TNG		RDX	
Q.Ef,%	**ppb**	**Q.Ef,%**	**ppb**	**Q.Ef,%**	**ppb**	**Q.Ef,%**	**ppb**
0.00	0.00	0.00	0.00	0.00	0.00	0.00	0.00
2.52	11.69	3.24	21.00	2.98	15.08	2.22	14.75
5.83	23.31	6.10	41.85	4.42	30.07	2.51	29.40
8.70	34.85	8.62	62.57	6.80	44.95	4.59	43.96
11.87	46.32	9.41	83.16	8.32	59.74	4.91	58.42
14.72	57.70	10.80	103.61	9.62	74.43	5.88	72.79
17.44	69.02	11.66	123.92	11.36	89.02	6.27	87.06
20.64	80.26	12.93	144.10	12.71	103.52	7.50	101.24
23.04	91.43	14.34	164.16	14.82	117.92	7.79	115.32
26.04	102.52	14.55	184.08	17.18	132.23	8.97	129.32
28.85	113.55	14.63	203.87	18.59	146.45	9.30	143.23
31.24	124.50	15.24	223.54	19.96	160.58	9.53	157.04
33.98	135.38	15.39	243.08	20.84	174.62	9.70	170.77
36.43	146.20	0.00	0.00	22.73	188.56	10.69	184.41
38.60	0.00	0.00	0.00	23.56	202.42	11.30	197.96
0.00	0.00	0.00	0.00	24.52	216.19	12.35	211.43

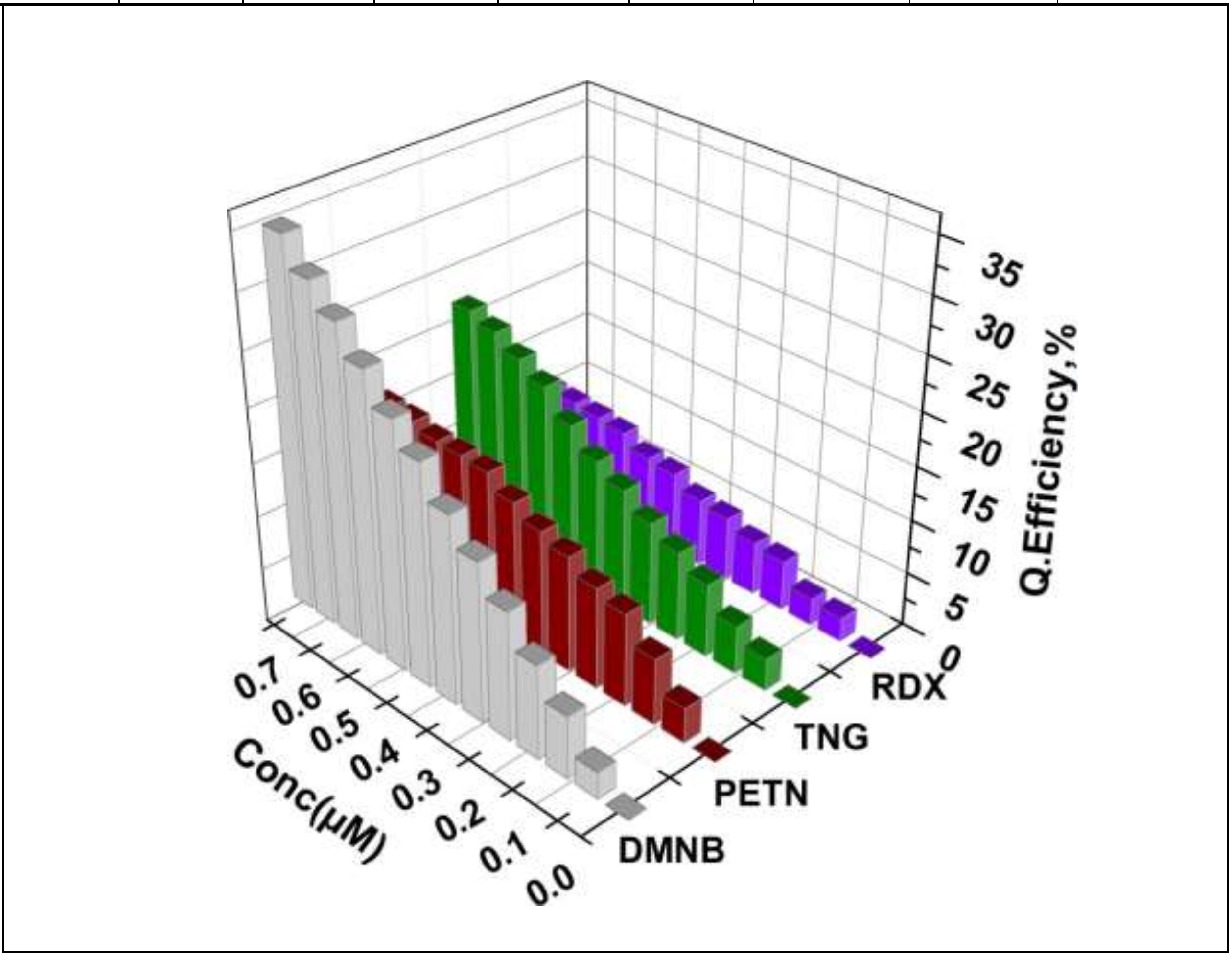

Fig.S72 Quenching efficiency of sensor **5** at different concentrations of nitro explosives

8 UV-visible titration study of sensor 5

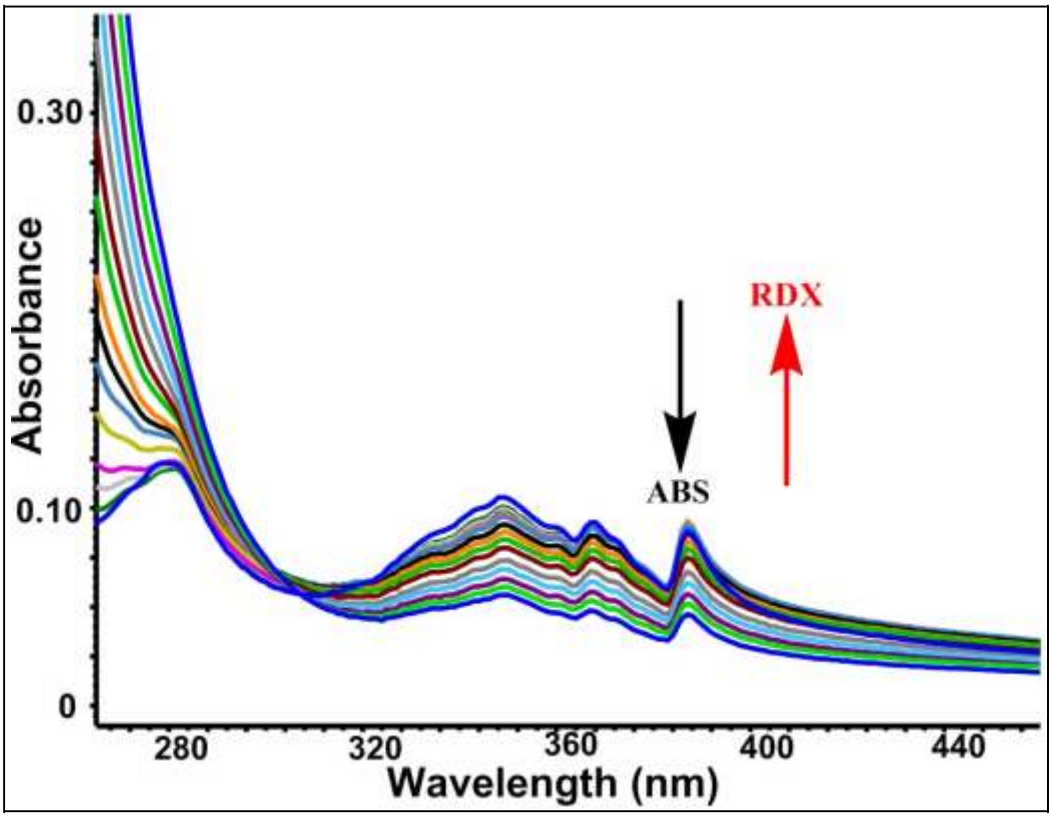

Fig.S73 UV titration of sensor **5** by RDX

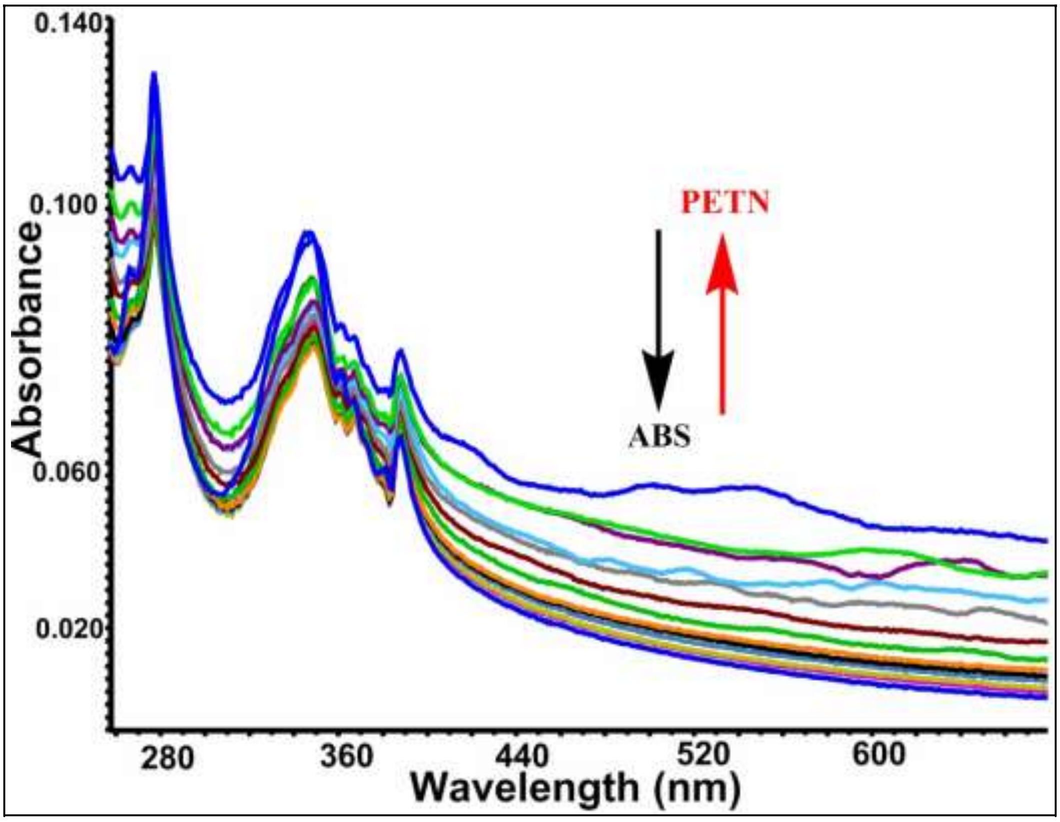

Fig.S74 UV titration of sensor **5** by PETN

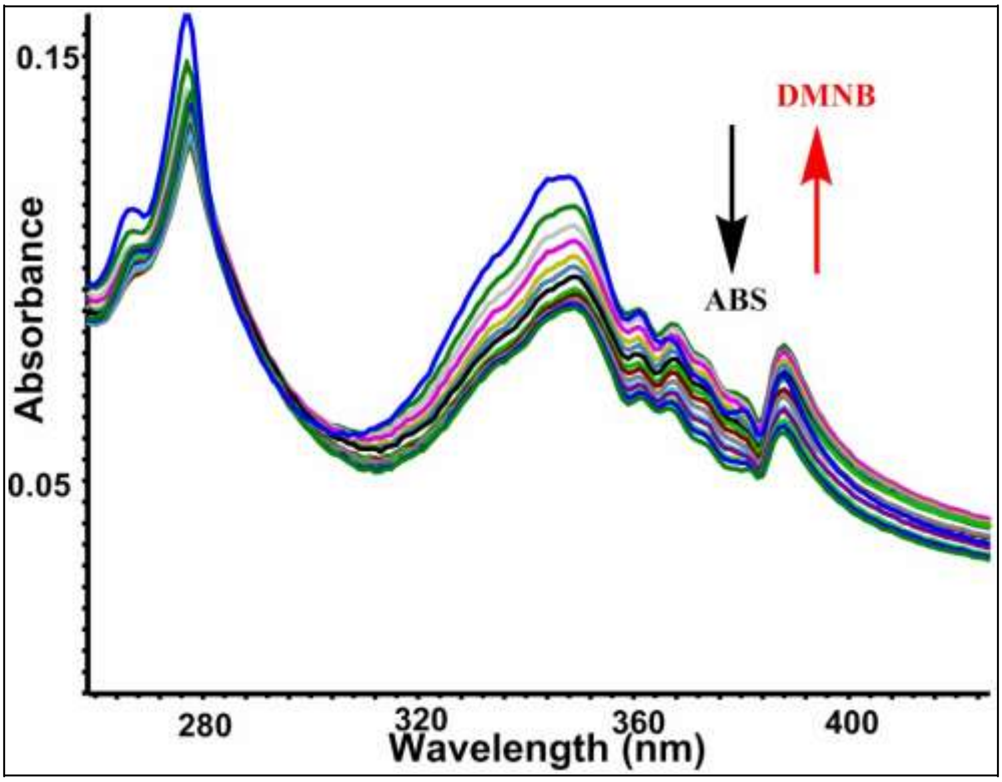

Fig.S75 UV titration of sensor **5** by DMNB

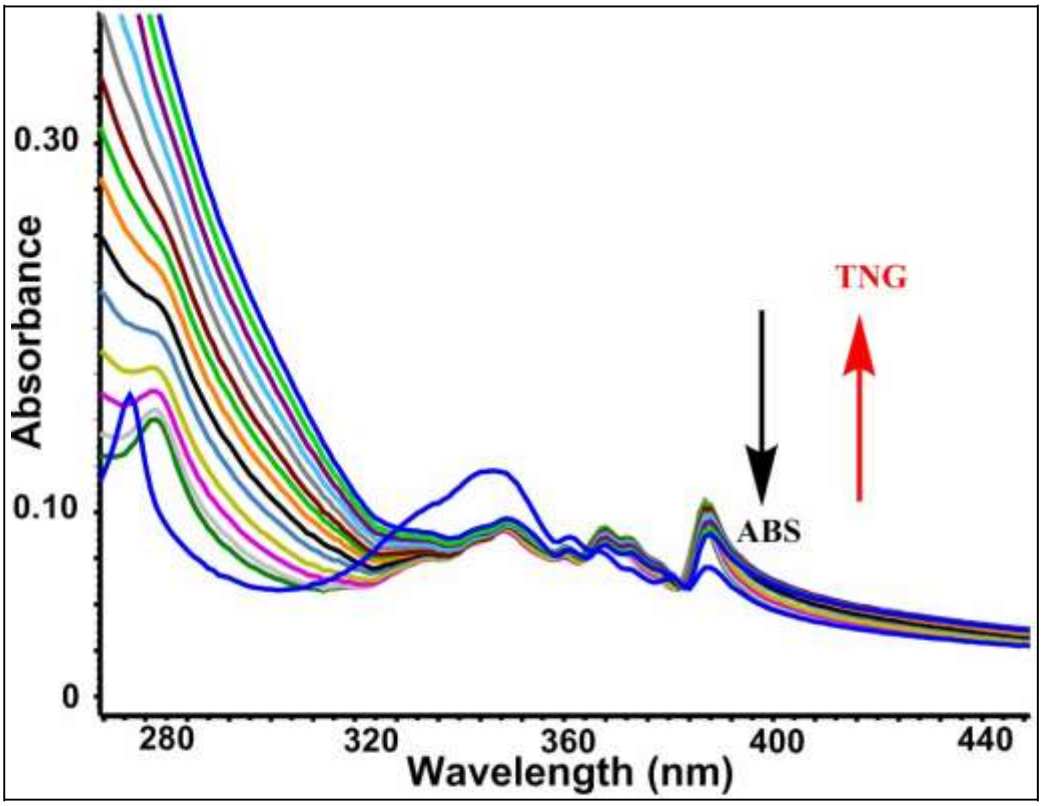

Fig.S76 UV titration of sensor **5** by TNG

9 Time-resolved fluorescence emission (TCSPC)

Table S32 Lifetime data of **5** at different mole ratios of PETN

Mole ratio sensor 5 opp. PETN	Lifetime τ (ns)
0,00	16,07
1:0,2	16,16
1:0,4	16,11
1:0,6	16,07
1:0,8	16,23
1:1	16,15

1:1,2	16,24
1:1,4	16,08
1:1,6	16,19
1:1,8	16,11
1:2	16,23
1:3	16,20

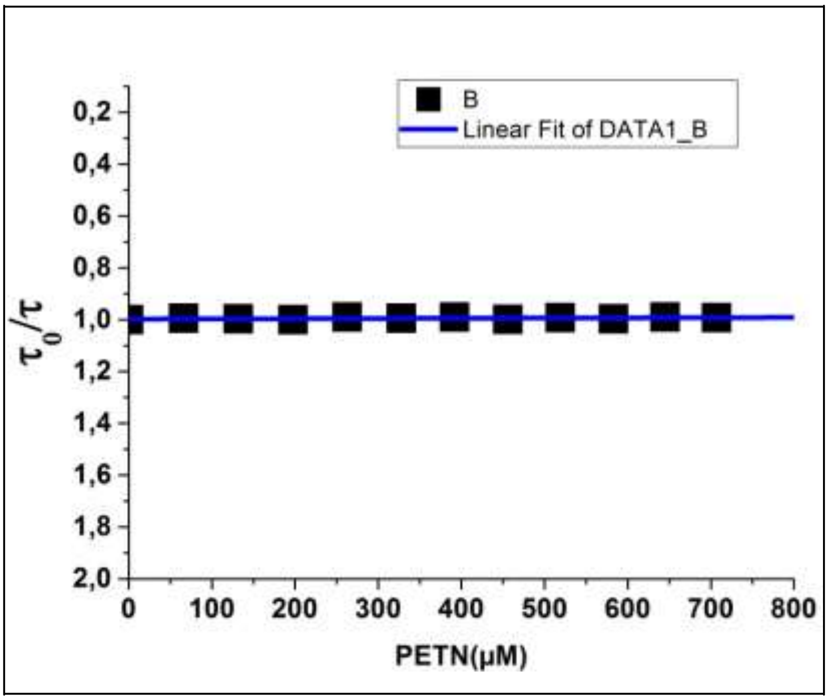

Fig.S77 The graphical result of Time-resolved fluorescence titration of **5** by PETN (no change in LT)

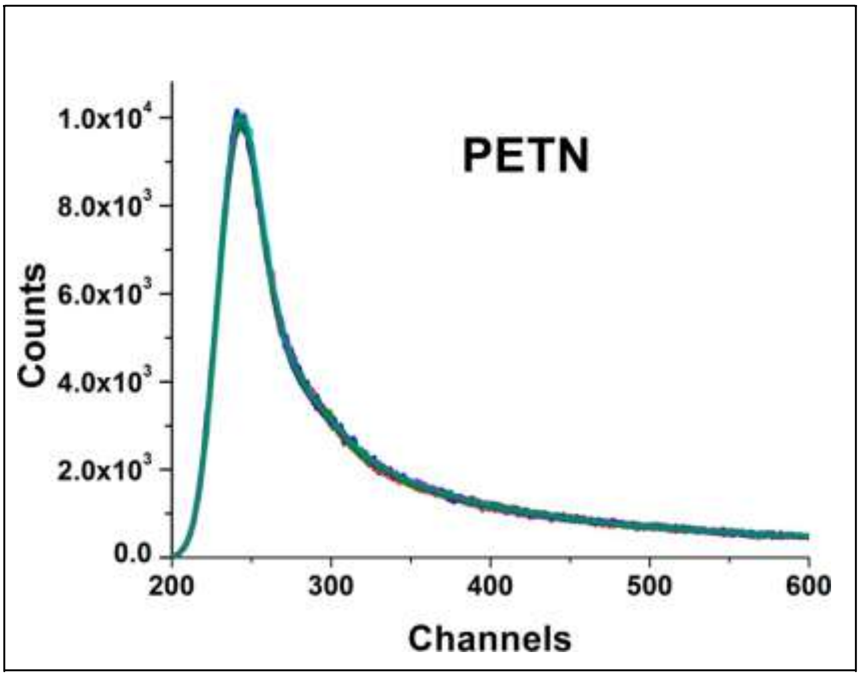

Fig.S78 2D fluorescence decay profiles for sensor **5** shows no change upon addition of PETN

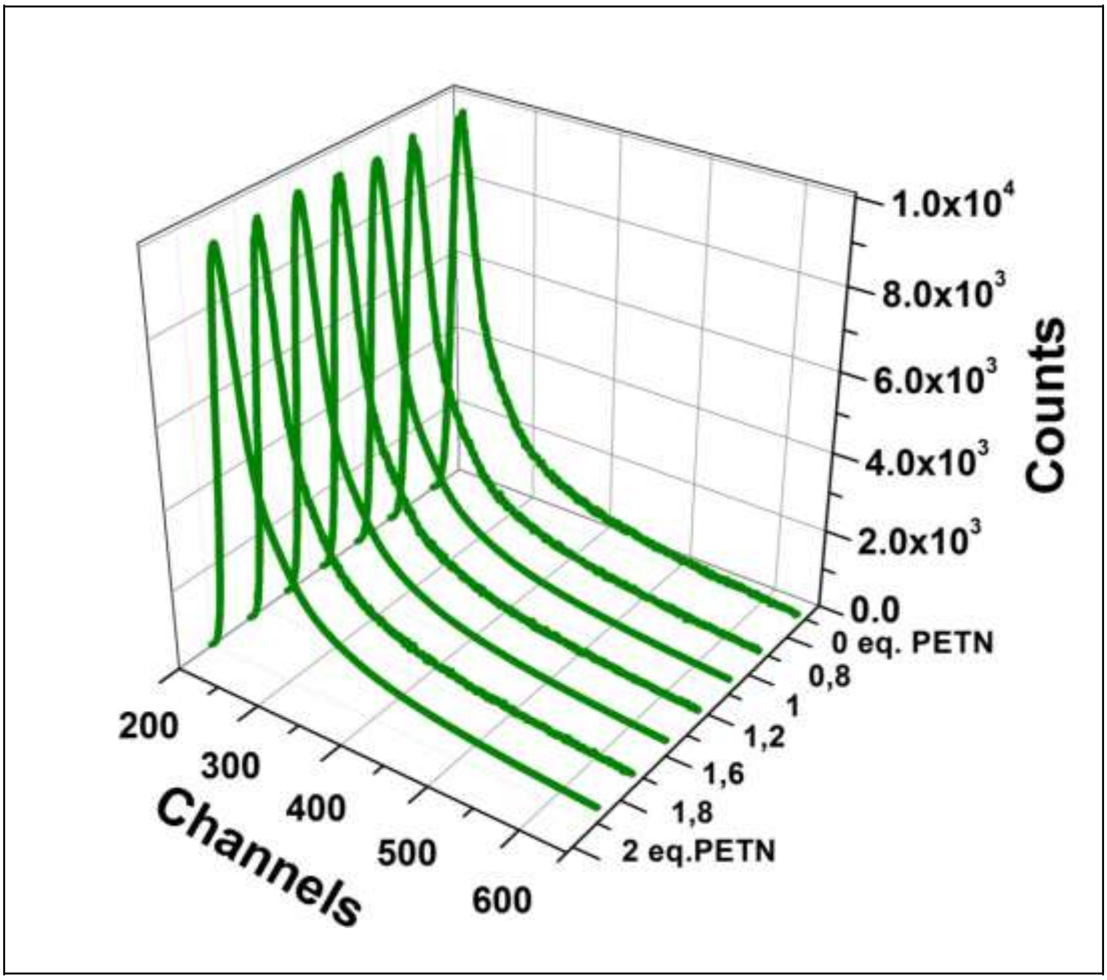

Fig.S79 3D fluorescence decay profiles for sensor **5** shows no change upon addition of PETN

10 Quenching efficiency of 2-5 sensors

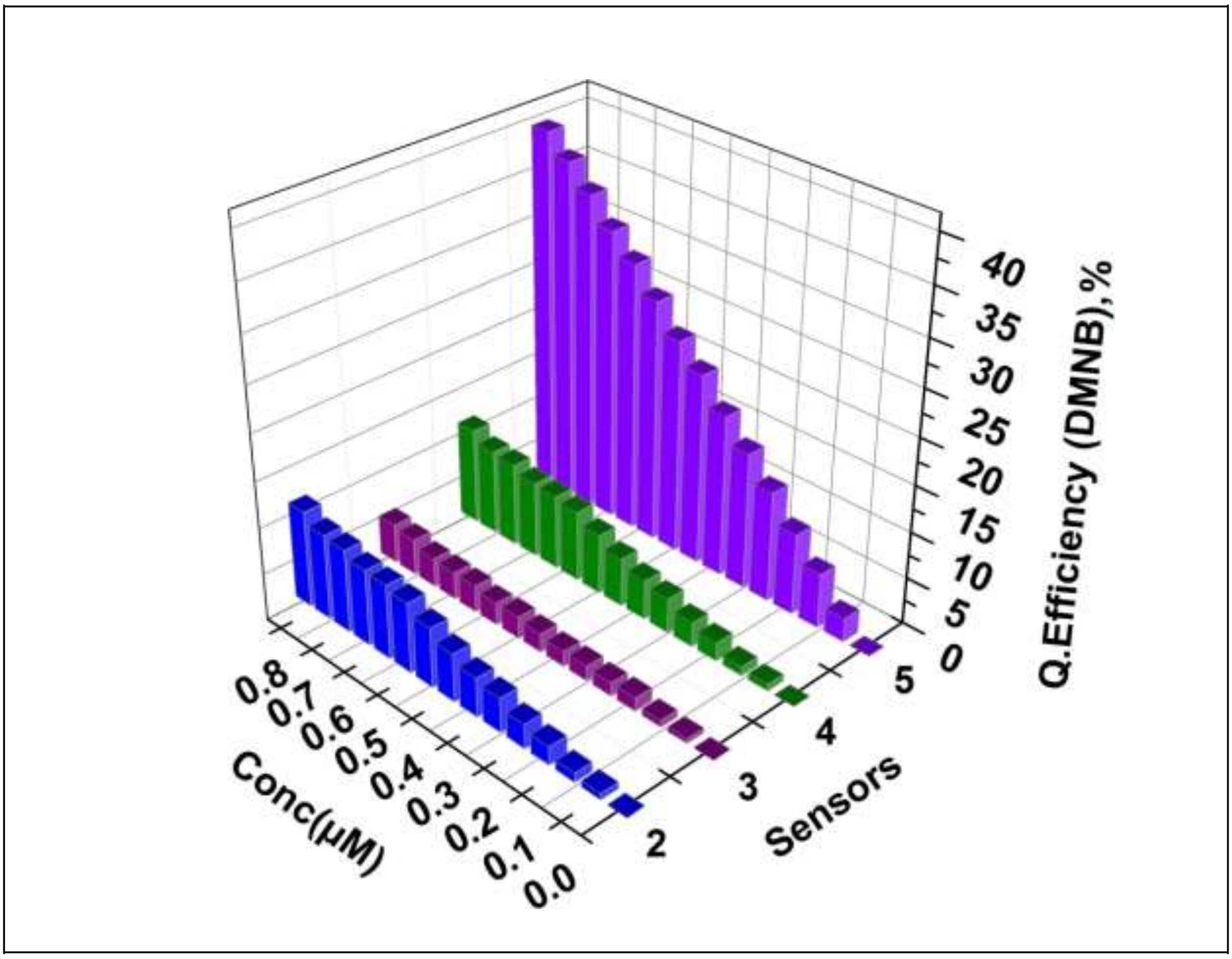

Fig.S80 Quenching efficiency of **2-5** sensors at different concentrations of DMNB

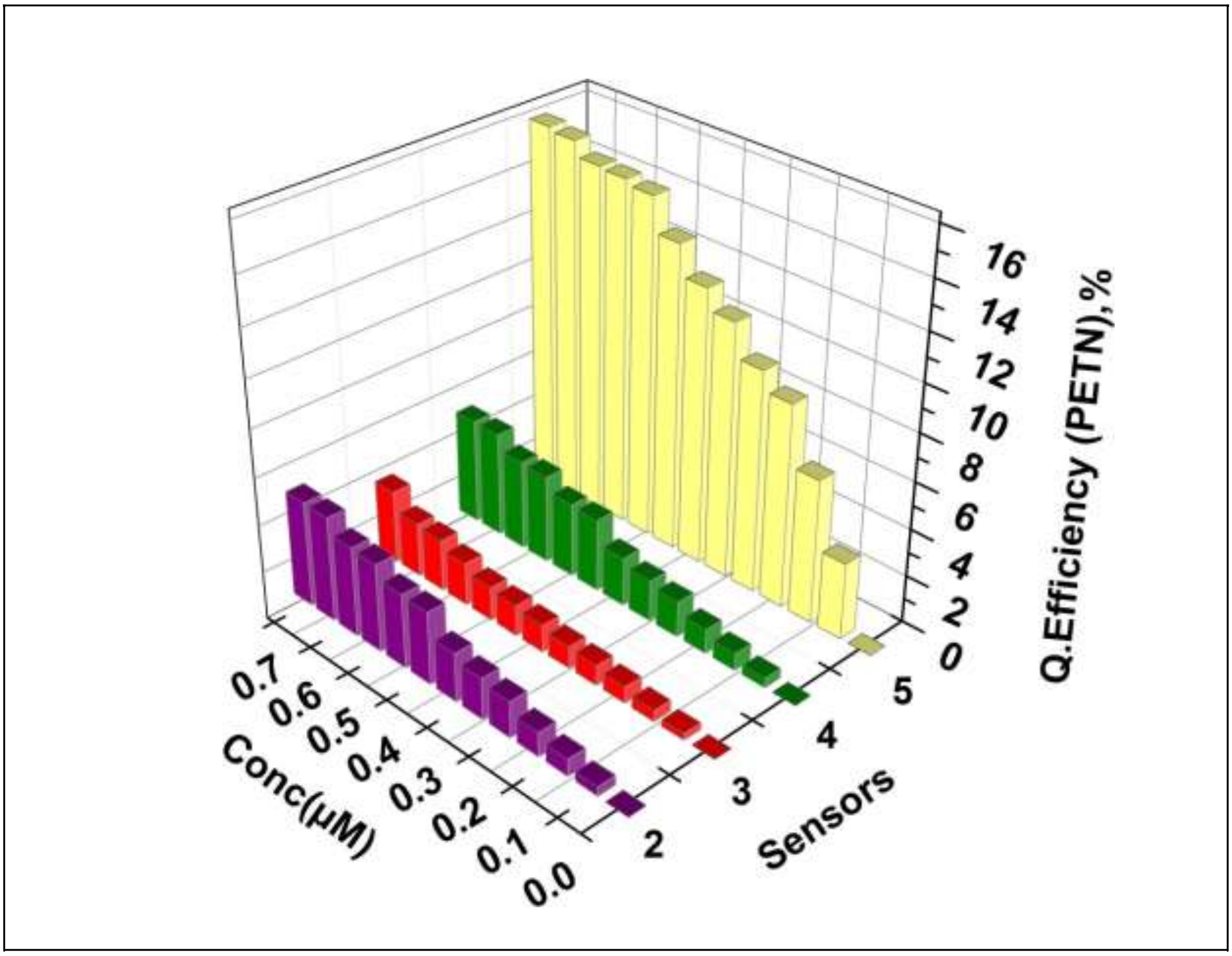

Fig.S81 Quenching efficiency of **2-5** sensors at different concentrations of PETN

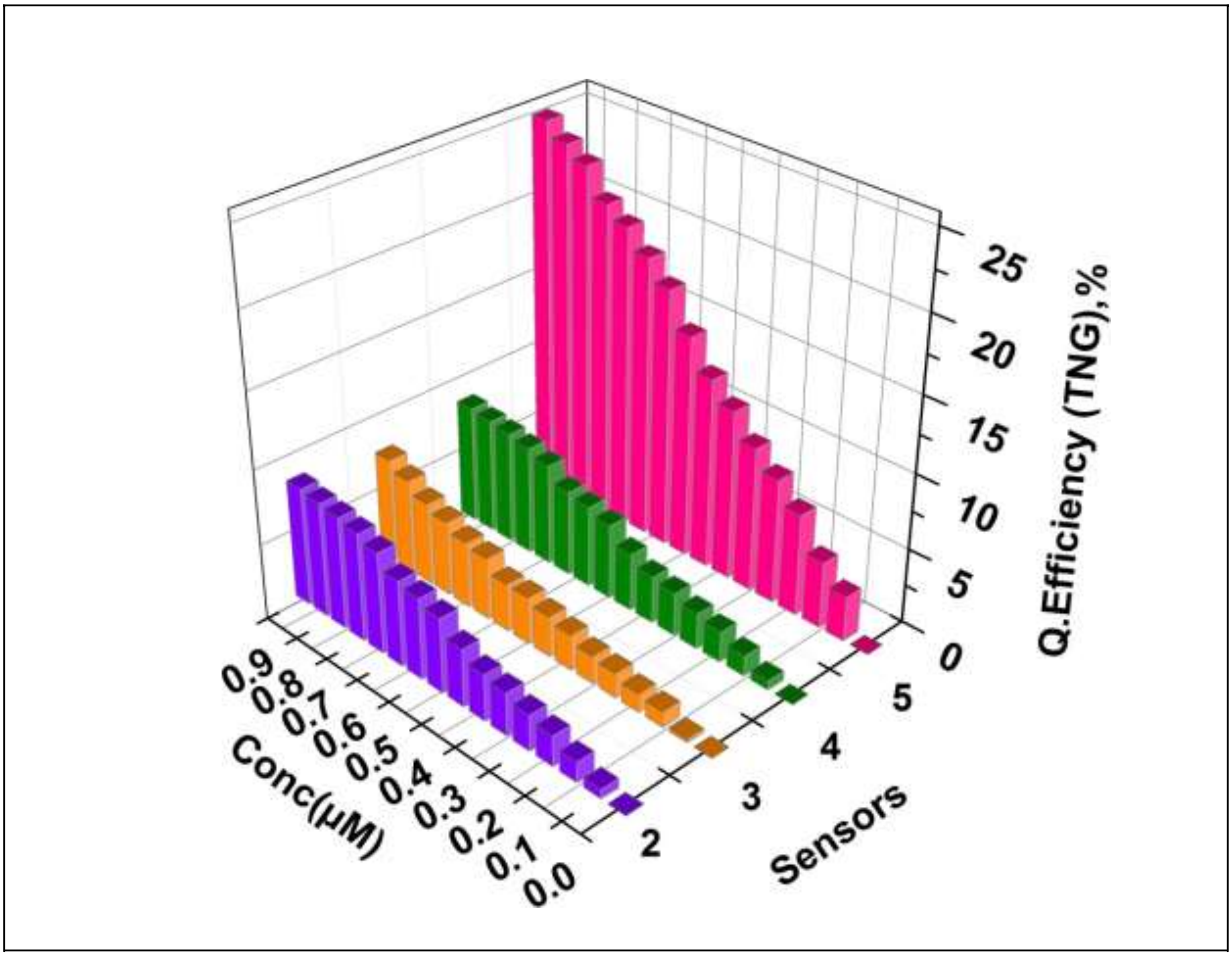

Fig.S82 Quenching efficiency of **2-5** sensors at different concentrations of TNG

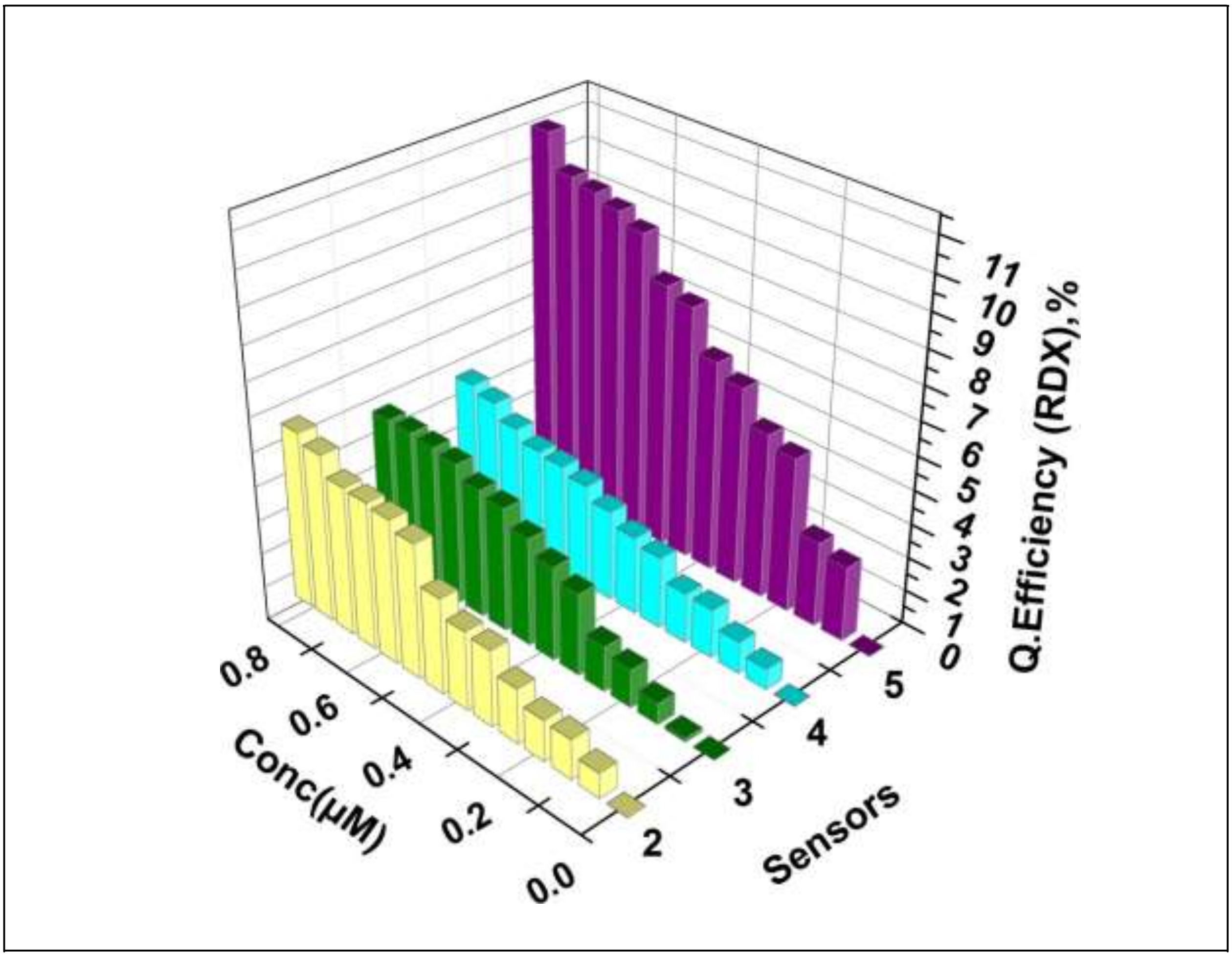

Fig.S83 Quenching efficiency of **2-5** sensors at different concentrations of RDX

11 Density functional theory (DFT)

The density function theory (DFT) studies were carried out with Becke's Three-parameter functional, and Lee-Yang-Parr functional (B3LYP) and 6-31G (d,p) basis set with ultrafine grid and dispersion correction using Gaussian 09 was employed for geometry optimization for the sensors and analytes. The energy of the highest occupied molecular orbital (HOMO) and the lowest unoccupied molecular orbital (LUMO), energy gaps and dipole moments were calculated for the DFT-optimized structures of sensors and analytes (Table S32, S33). The energy level diagram was shown in Figure S63 for sensors **3,5** in comparison with RDX. The possible models of supramolecular complexes between the sensors **2-5** and nitro-analytes (DMNB, TNG, PETN) were suggested as a result of DFT calculations (Table S35).

Table S33 Calculated energy of HOMO/LUMO, energy gaps and dipole moments of analytes based on B3LYP/6-31G (d,p) functional

Compound	HOMO, au (eV)	LUMO, au(eV)	Energy gap, eV	Dipole moment, D
RDX	0.32825 (-8.93214074)	0.1089 (-2.963321)	-5.96882	2.4571
PETN	0.35227 (-9.58575847)	0.10832 (-2.9475384)	-6.63822	0.0033
DMNB	0.31678 (-8.62002602)	0.10517 (-2.8618225)	-5.7582	1.0733
TNG	0.34805 (-9.47092638)	0.11101 (-3.0207371)	-6.45019	1.7342

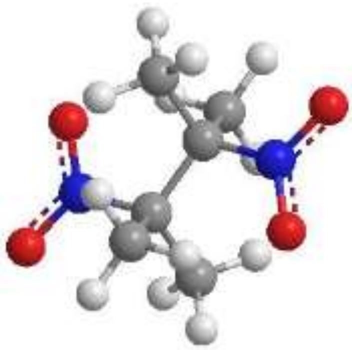

HOMO

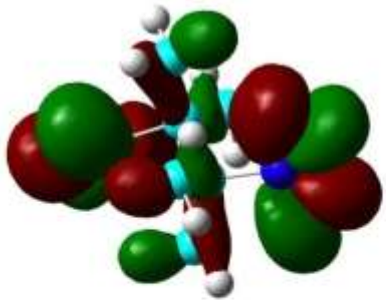

LUMO

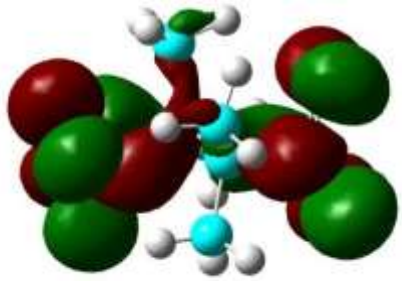

DMNB

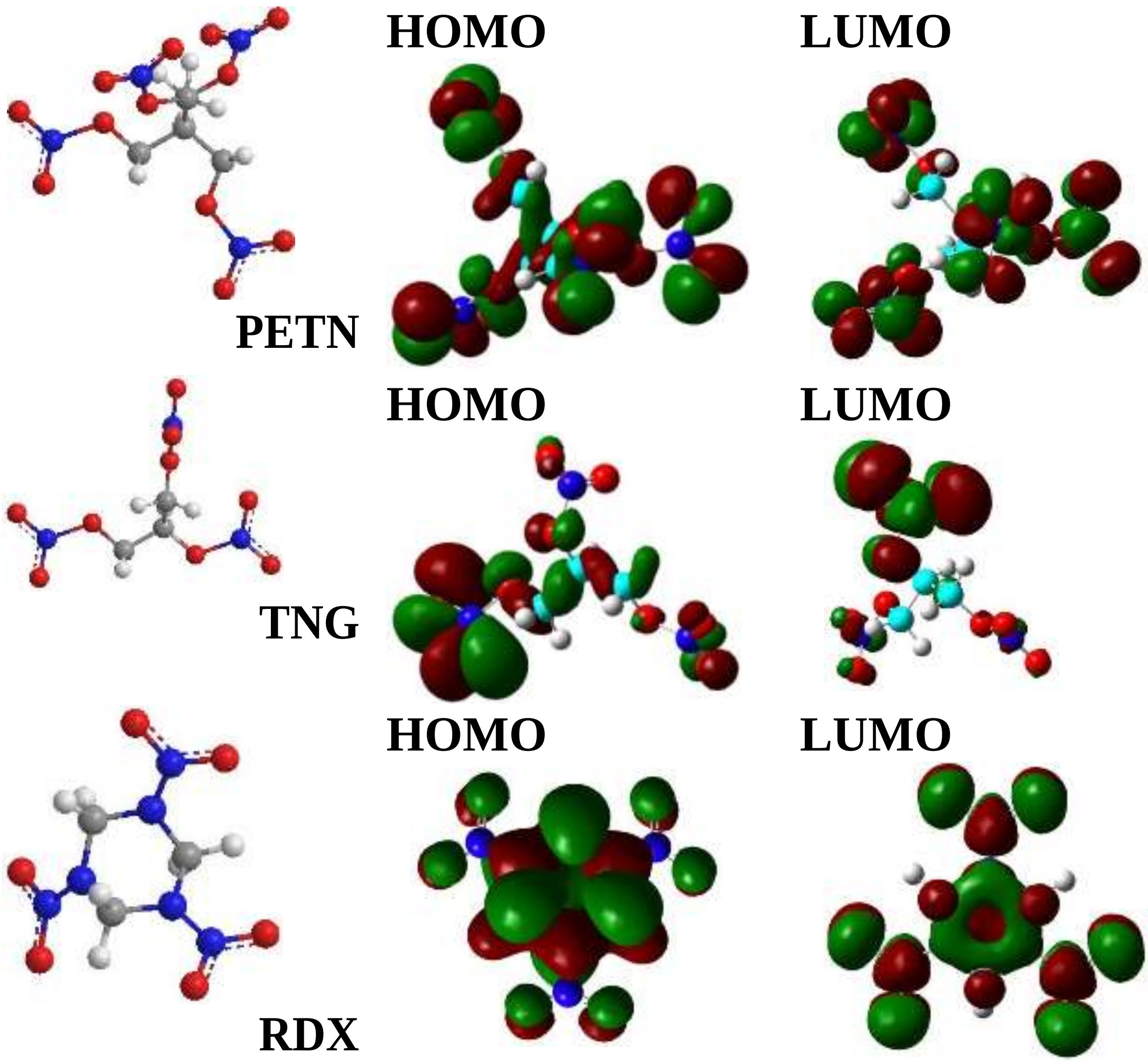

Fig. S84 Geometry optimized structures of explosives based on B3LYP/6-31G (d,p) functional

Table S34 Calculated energy of HOMO/LUMO, energy gaps and dipole moments of sensors based on B3LYP/6-31G (d,p) functional

Compound	HOMO, au (eV)	LUMO,au (eV)	Energy gap, eV	Dipole moment, D
1	**0.19657 (-5.34894411)**	**0.06166 (-1.6778547)**	**-3.67109**	**1.6445**
2	**0.19506 (-5.3078549)**	**0.06116 (-1.664249)**	**-3.64361**	**3.5125**

3	**0.19771 (-5.3799651)**	**0.06359 (-1.7303727)**	**-3.64959**	**2.5918**
4	**0.19273 (-5.24445235)**	**0.05935 (-1.6149964)**	**-3.62946**	**2.7555**
5	**0.19389 (-5.27601757)**	**0.06042 (-1.6441125)**	**-3.63191**	**1.6699**

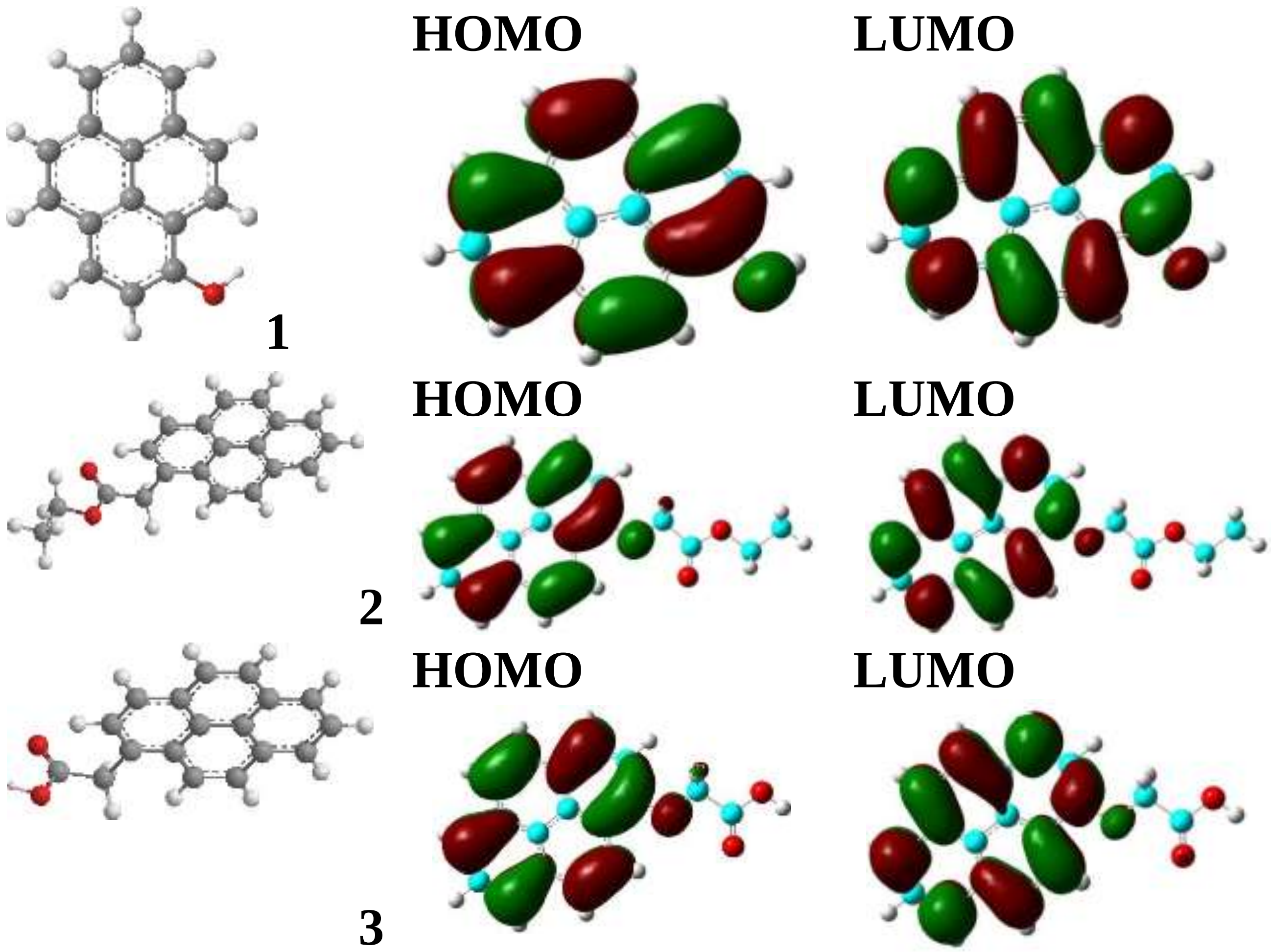

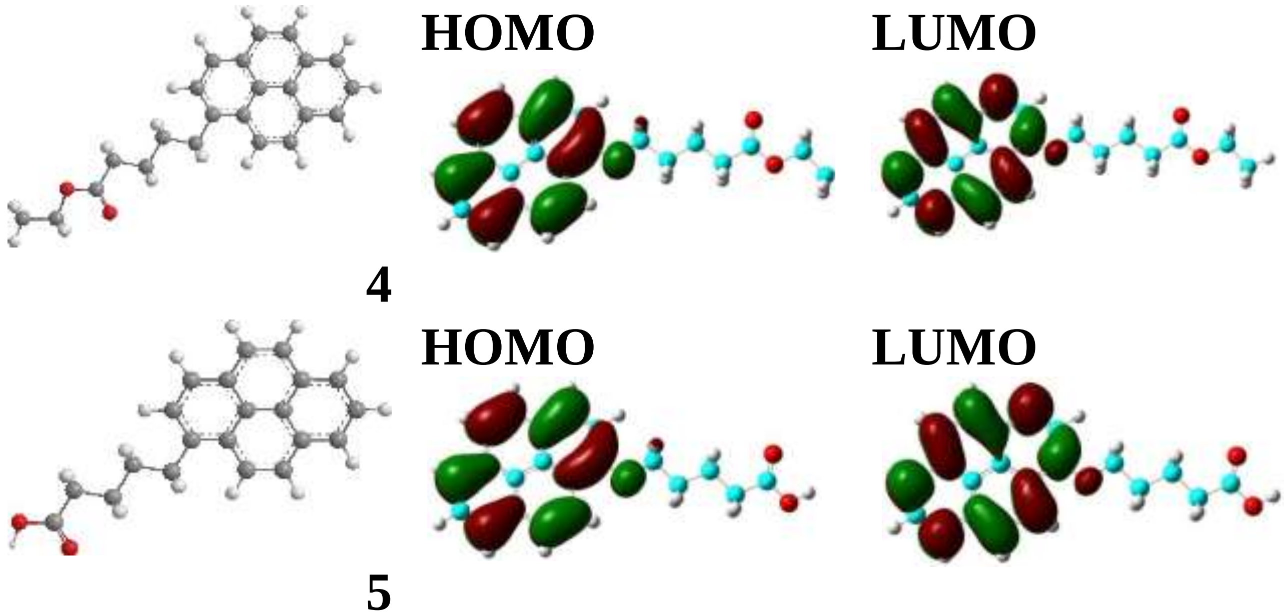

Fig. S85 Geometry optimized structures of sensors based on B3LYP/6-31G (d,p) functional

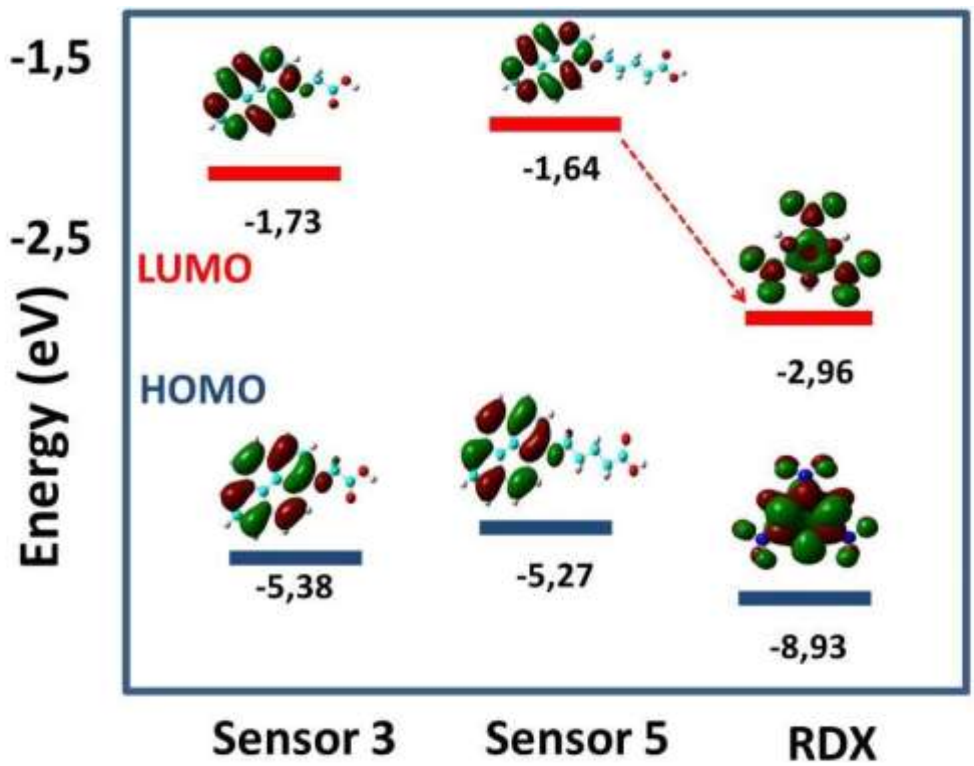

Fig. S86 Energy level diagram of sensors 3, 5 and RDX

Table S35 Quantum calculations of supramolecular complexes of adducts **2-5** with such analytes: DMNB, TNG, PETN

Calculation of Supramolecular Complexes	Composition of Complex
	**Adduct of sensor 2 with DMNB**
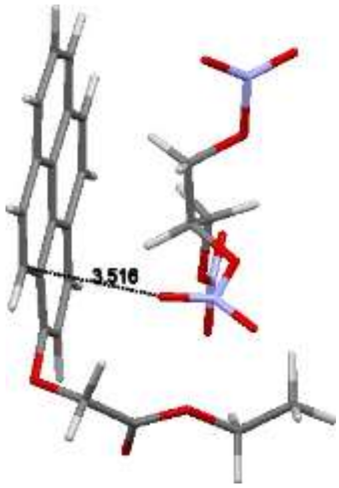	**Adduct of sensor 2 with TNG**

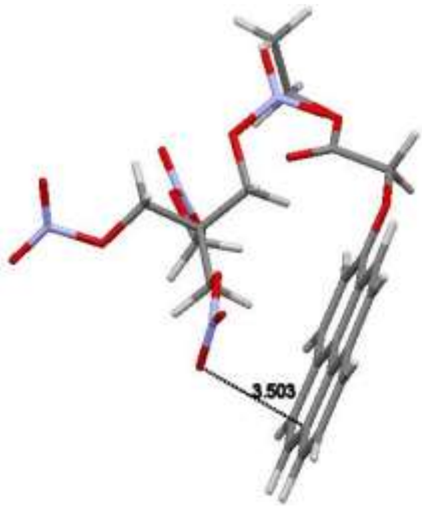	**Adduct of sensor 2 with PETN**
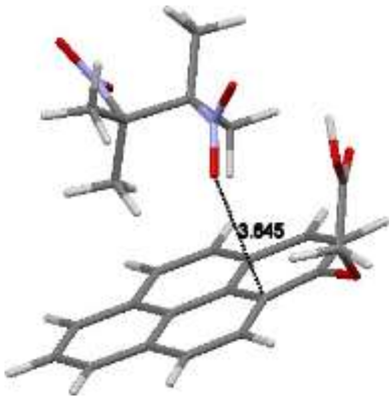	**Adduct of sensor 3 with DMNB**
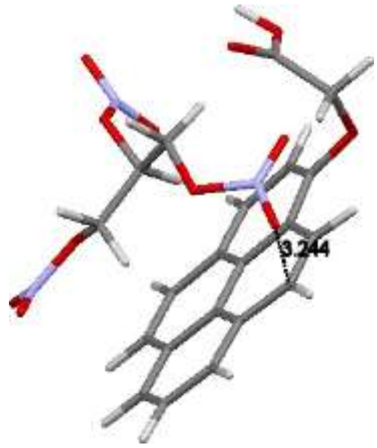	**Adduct of sensor 3 with TNG**

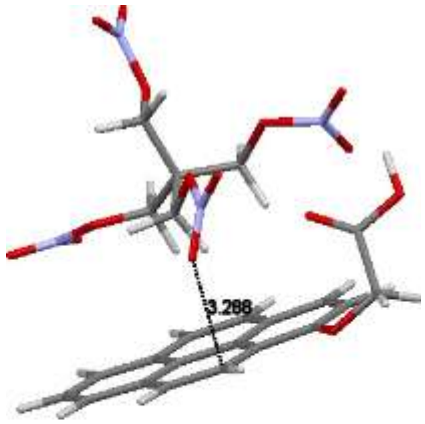	**Adduct of sensor 3 with PETN**
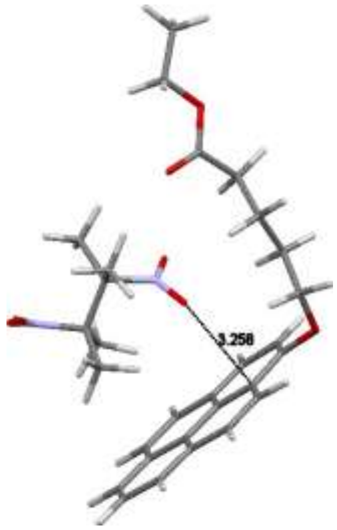	**Adduct of sensor 4 with DMNB**
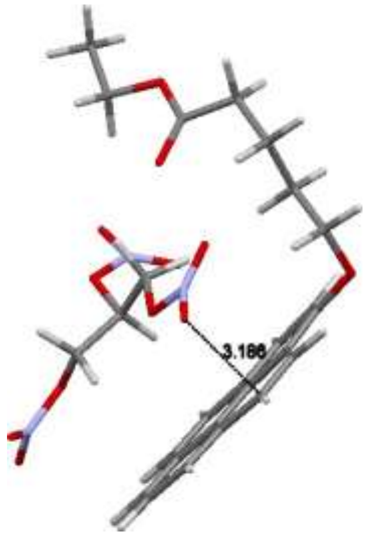	**Adduct of sensor 4 with TNG**

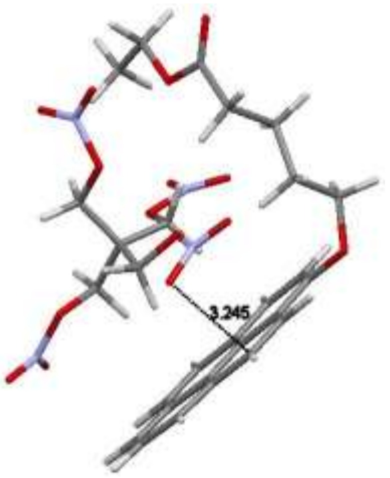	**Adduct of sensor 4 with PETN**
	**Adduct of sensor 5 with DMNB**
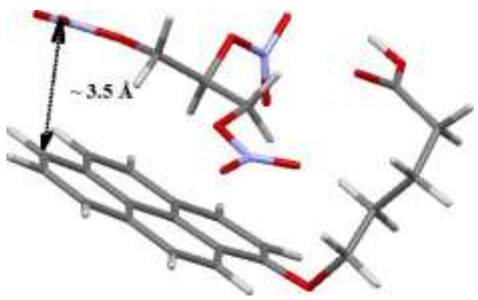	**Adduct of sensor 5 with TNG**
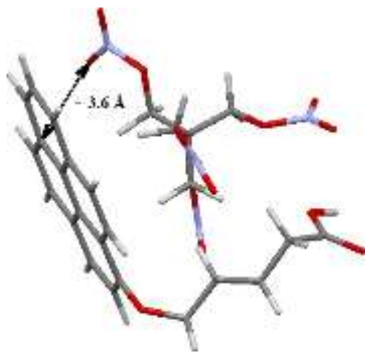	**Adduct of sensor 5 with PETN**

12 Dynamic light scattering (DLS) analysis

DLS analysis was carried out in water solutions of fluorescence probes 3 and 5. The solutions were prepared with the concentration of 10^{-4} M. Periodical DLS measurements had showed that the hydrodynamic radius of the particles of as for probe 3 as for probe 5 increased in time. And the micelle-forming water systems of as for probe 3 as for probe 5 were monodisperse and the aggregation of particles for probe 3 reached to particle radius 500 nm, for probe 5 - particle radius 300 nm.

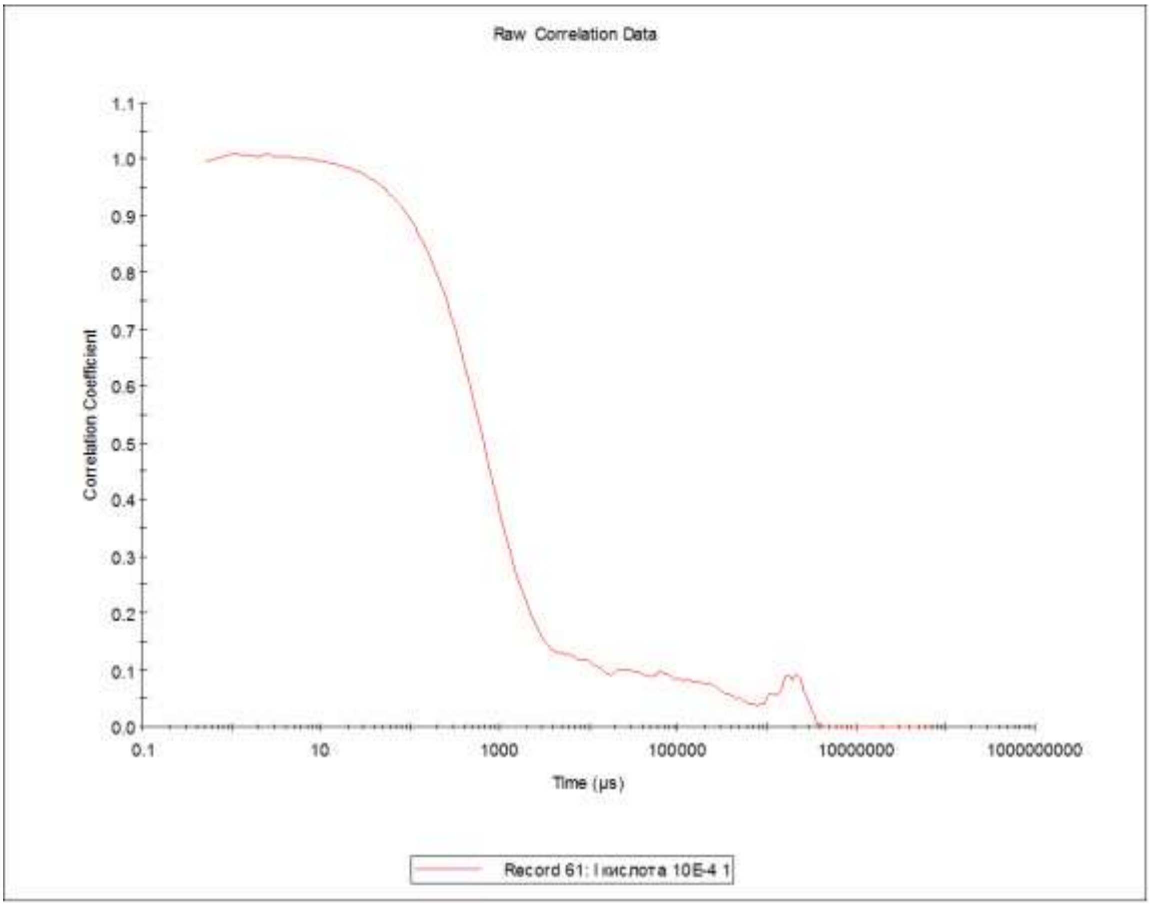

Fig.S87 Autocorrelation function of micelle-forming water solution of sensor **3**

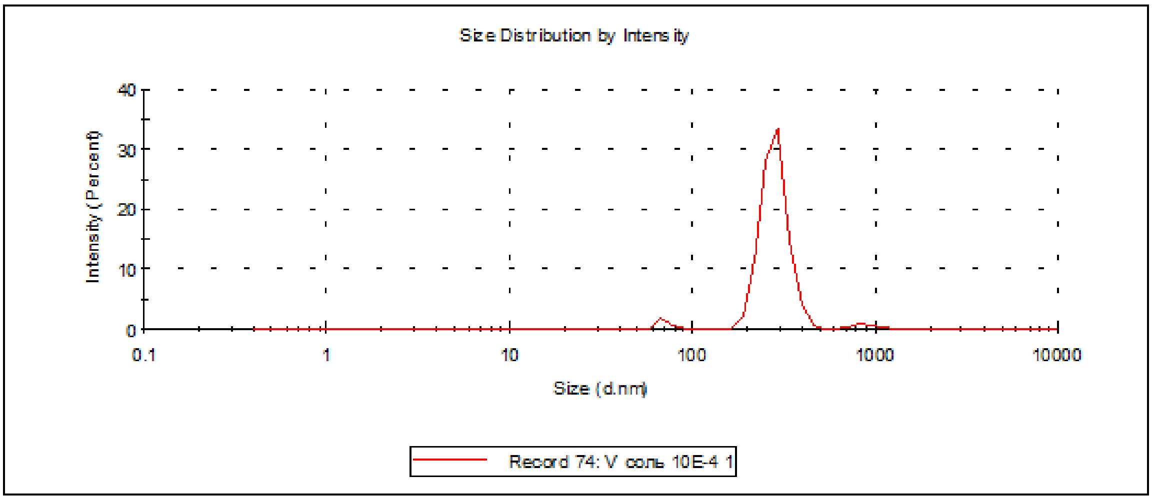

Fig.S88 The aggregation of particles **3** with the largest population of particle radius 500 nm

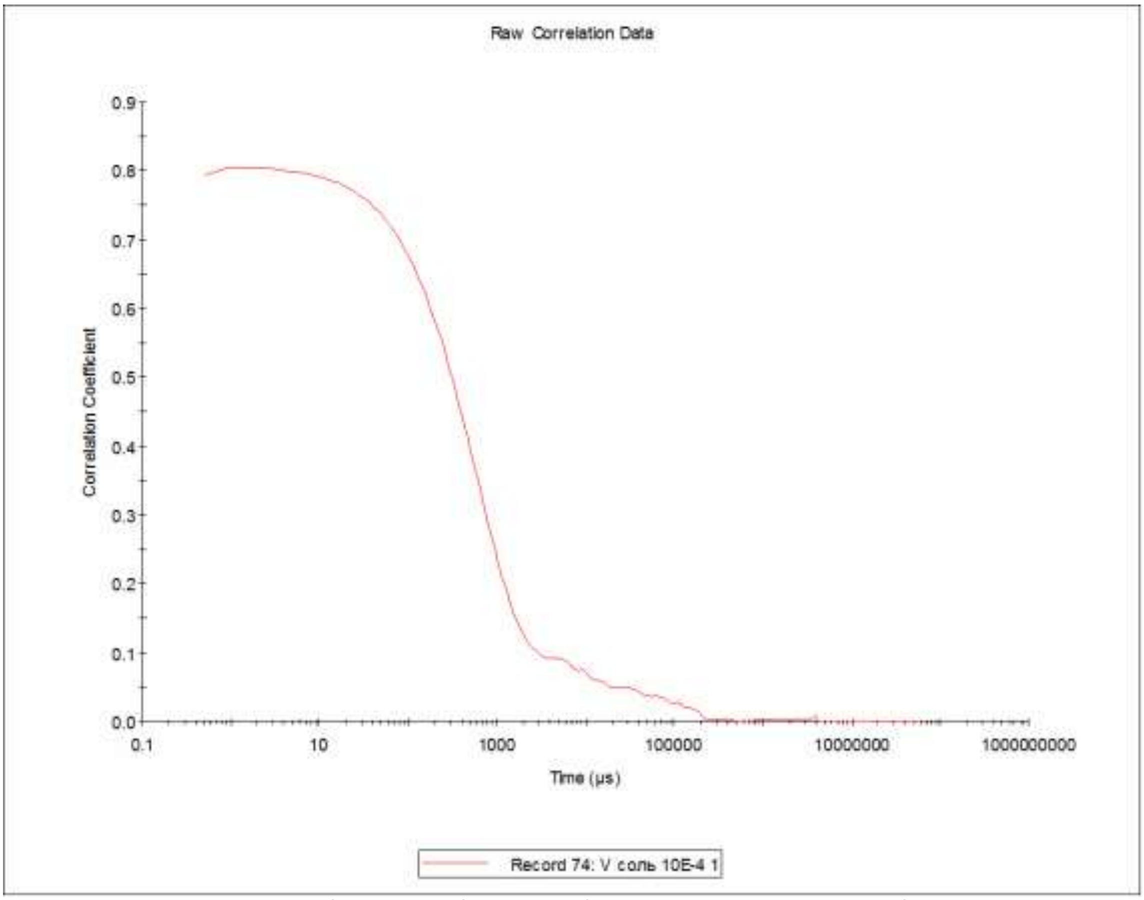

Fig.S89 Autocorrelation function of micelle-forming water solution of sensor **5**

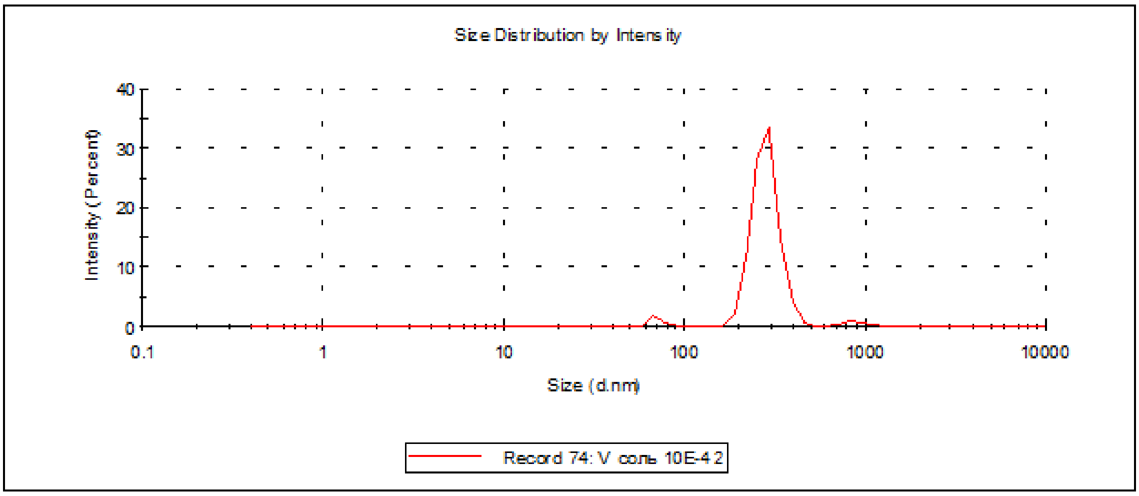

Fig.S90 The aggregation of particles **5** with the largest population of particle radius 300 nm

13 Visualization of micelles

13.1 Tyndall effect

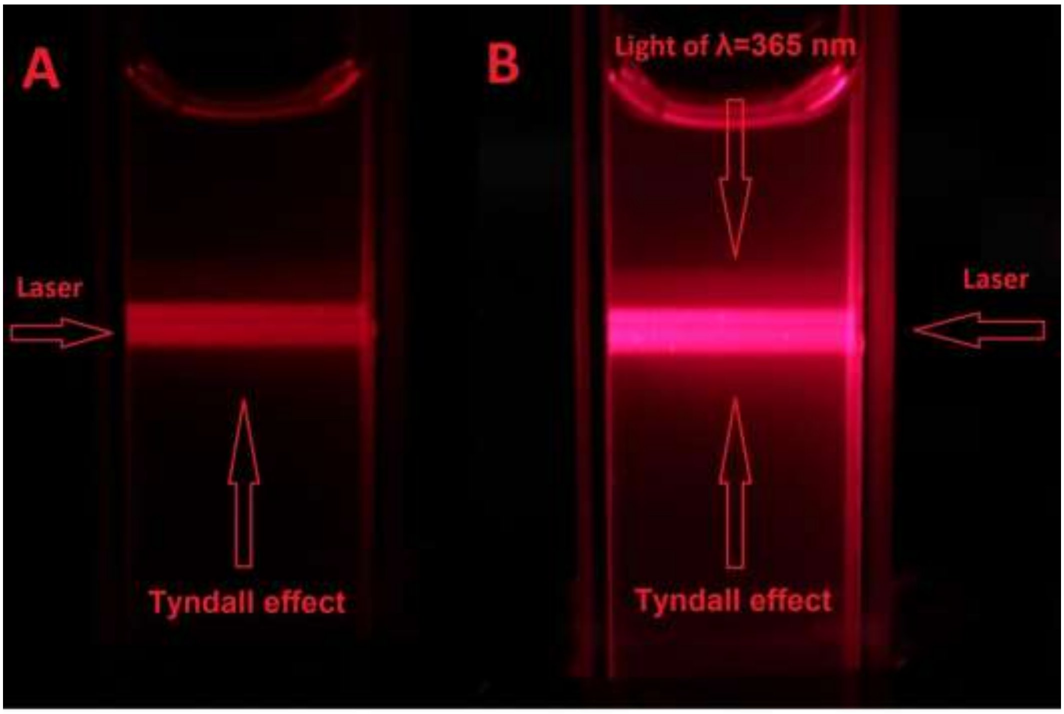

Fig.S91 Tyndall effect of colloidal aqueous solution (10^{-5} M) of **5** in the dark (**A**), **5** under the UV light (**B**)

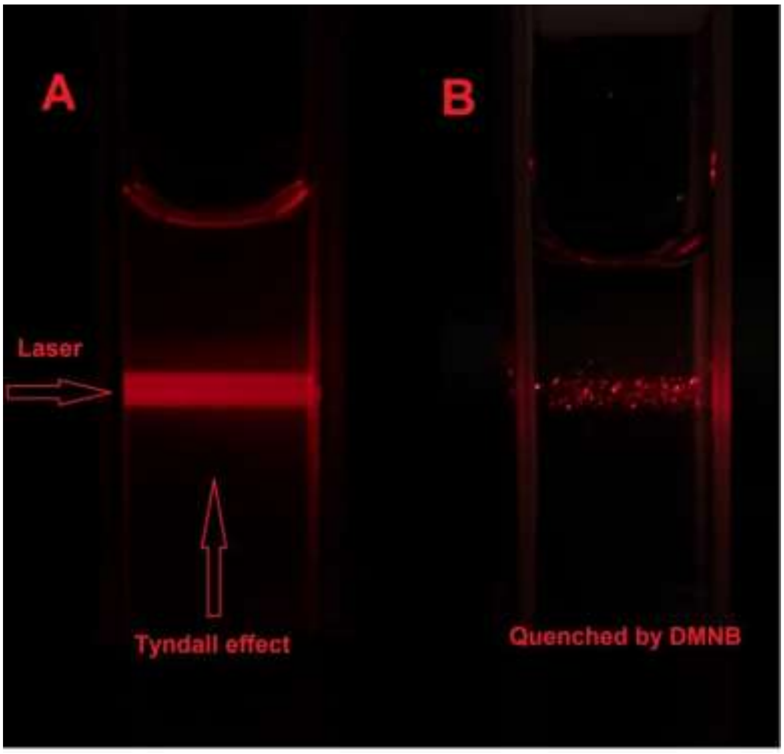

Fig.S92 Tyndall effect of colloidal aqueous solution (10^{-5} M) of **5** (**A**), **5** upon addition of 1 eq. DMNB (**B**)

13.2 The detection of fingerprint contacted with nitro explosives by 5 sensor spraying

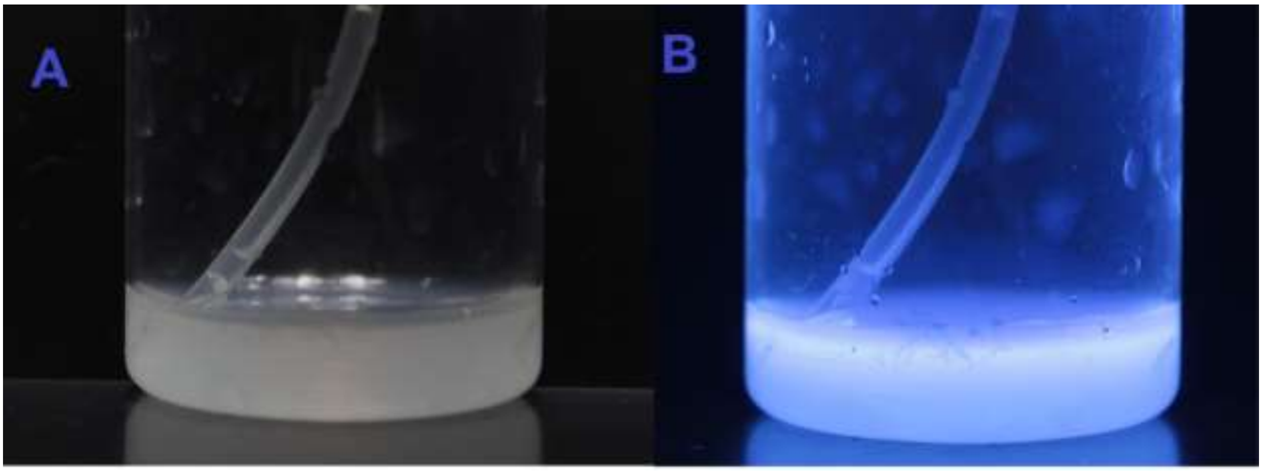

Fig.S93 Spray bottle: (**A)** Colloidal aqueous solution of **5** potassium salt (10^{-4} M), (**B**) under the UV light (λ = 365 nm).

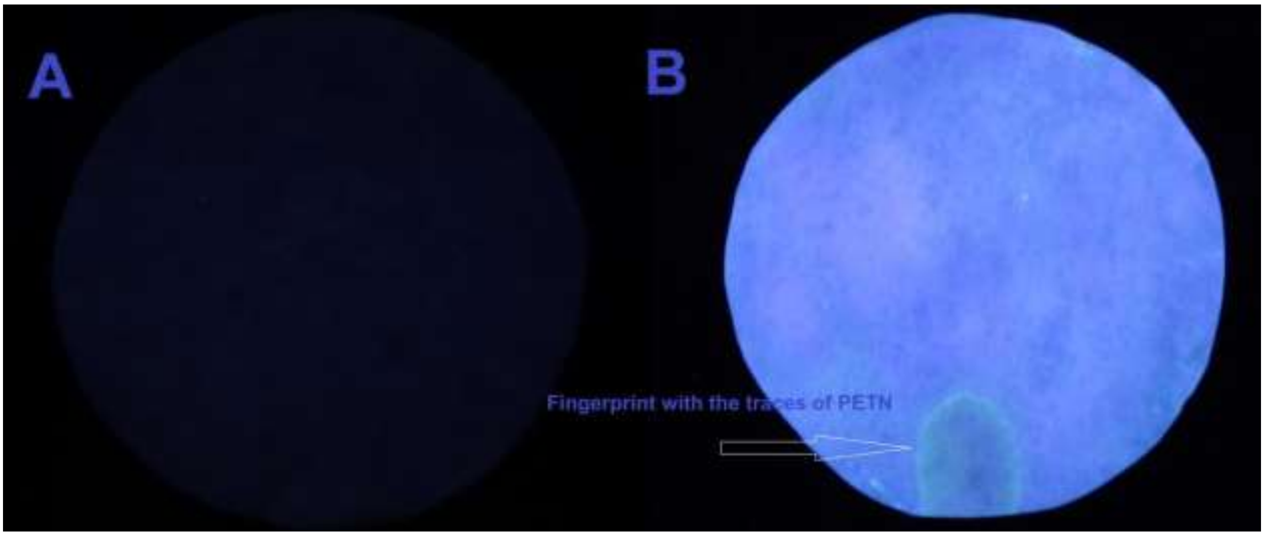

Fig.S94 Filer paper under the UV light (λ = 365 nm) (**A**); filter paper sprayed with aqueous solution of sensor **5** under the UV light (λ = 365 nm) with a fingerprint (a finger was contaminated with PETN).

13.3 Visual quenching experiment of 5 sensor

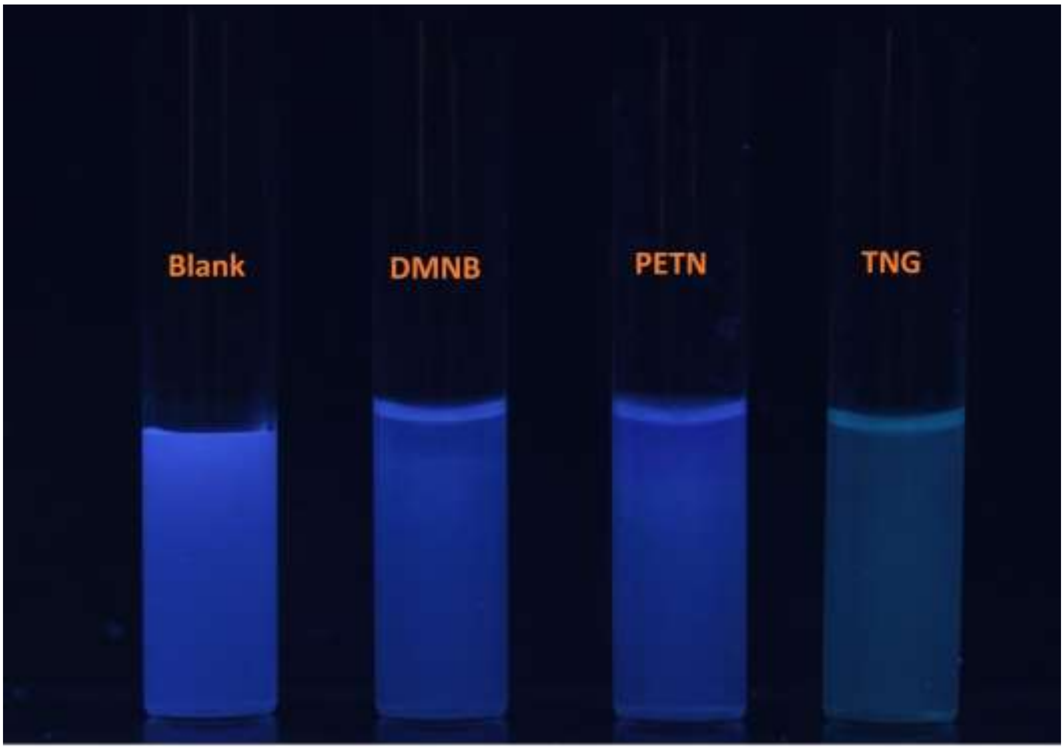

Fig.S95 Aqueous solutions of sensor **5** (10^{-6}M) without (left) and with added nitro explosives (12 ppb)

14 Vapor and solid phase (contact) explosives detection

First of all we have prepared the aqueous solutions of sensors **2-5** (10^{-5}-10^{-7}M). After that the holes of the aluminium chip have been filled with silica gel (Alfa Aesar 60 meshs pore size 60 Å, 230-450 mesh), which was preliminary impregneted with the solutions of the sensors **2-5** and air-dried overnight. This chip was placed to the desiccator and exposed to vapors of DMNB for 15 minutes. The resulted quenching efficiency was calculated for the each sensor. The fluorescence quencing was varied from 72 to 87%, depending on the nature of the chemosenosor (Fig. S96, nm, Table S37)

In the contact experiment the comersially available silica gel glass plate (Sigma-Aldrich, silica gel 60, layer thickness: 210 - 270 µm) of 2.5 x 7.5 sm size has been sprayed with aqueous solution (10^{-5}-10^{-7}M) of sensor **5** for 3-4 times and air dried for ovetnight. After the thus prepared plate was conacted for 2-3 seconds with DMNB contaminated finger of the lab assistant for 1 time. The fluorescence quenching was estimated by the RGB calculations of the phtograph obtained under the UV-light (365 nm). The calculations were done in the software package of Mathcad. The total quenching was found to be up to 62% (Fig. S98-S99).

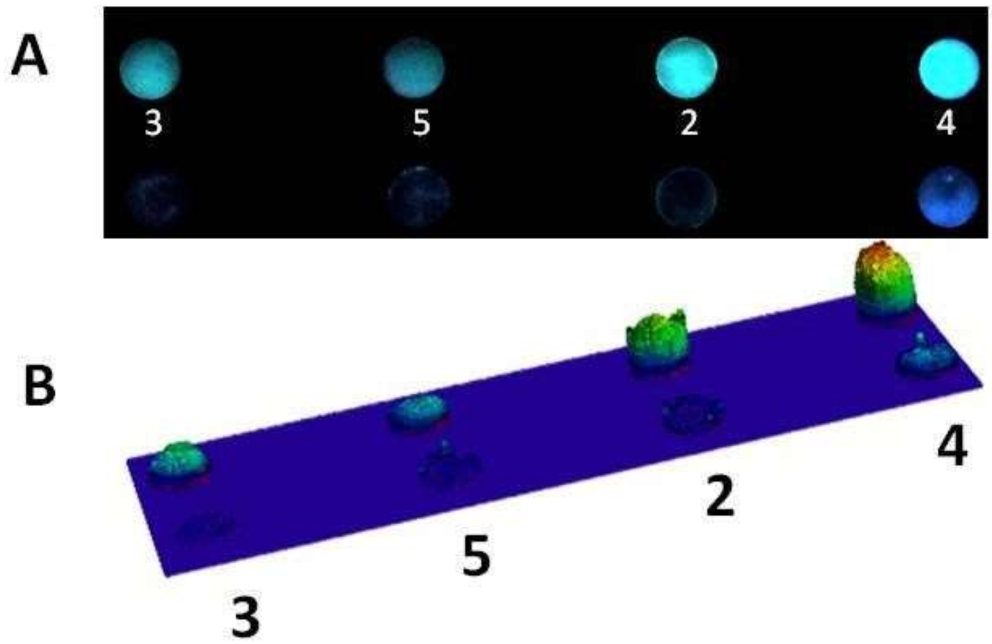

Fig. S96 Fluorescence quenching of holes filled with silica gel impregnated by solutions of sensors 2-5 in the air before (top) and after (bottom) exposure to vapors of DMNB. **B** - The 3D diagram demonstrates the degree of sensor quenching by vapors of DMNB

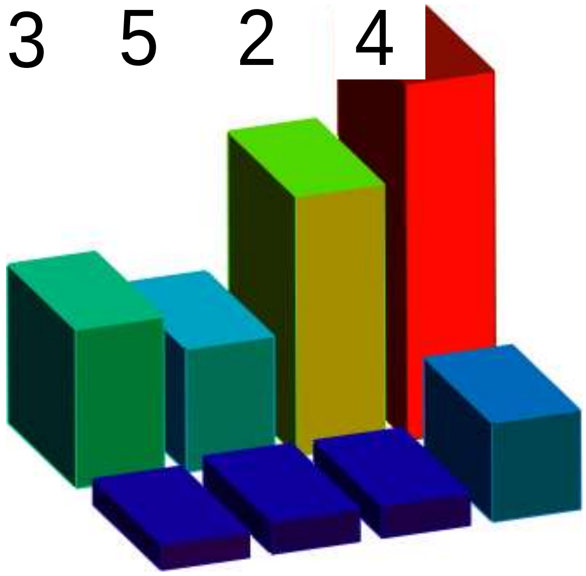

Fig. S97 Quenching efficiency for the sensors **2-5** (DMNB)

Table S37 Quenching efficiency for the sensors **2-5** (DMNB)

#	2	3	4	5
Q.Ef (DMNB), %	87,6	73,6	72,2	83,7

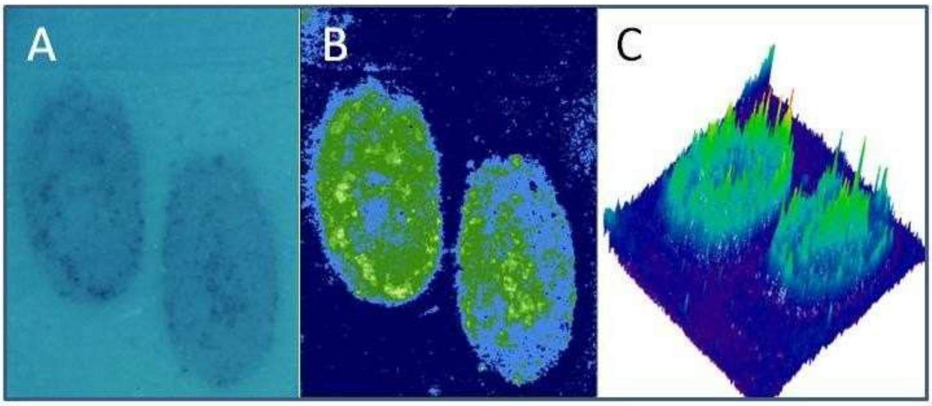

Fig. S98 Silica gel plate sprayed with the solution of sensor **5** with the fingerprints (fingers were contacted with DMNB); **B** –2D imaging of plate based on RGB calculations; **C** - 3D imaging of plate based on RGB calculations (~62% quenching was observed)

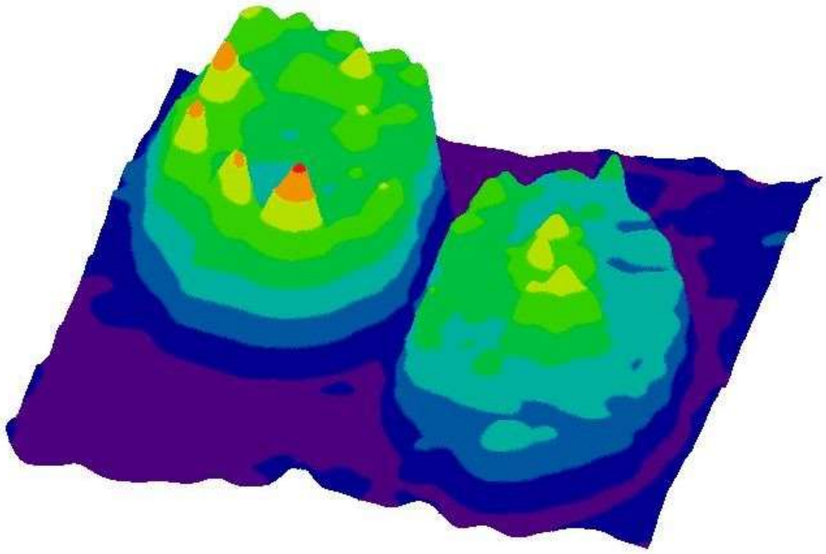

Fig. S99 A 3D graph for the imaging of fingerprints one the silca gel plate (~62% quenching was calculated)

Table S38. Fluorescence quenching titration experiment for the sensor **5** (1.0×10^{-6} M) upon the addition of cyclopentanone in CH_3CN.

Solution of sensor **5**	Concentrate of sensor **5**	Solution of quencher	Concentrate of quencher, M
Potassium salt in water	1.0×10^{-6} M	CH_3CN	2.0×10^{-2} M

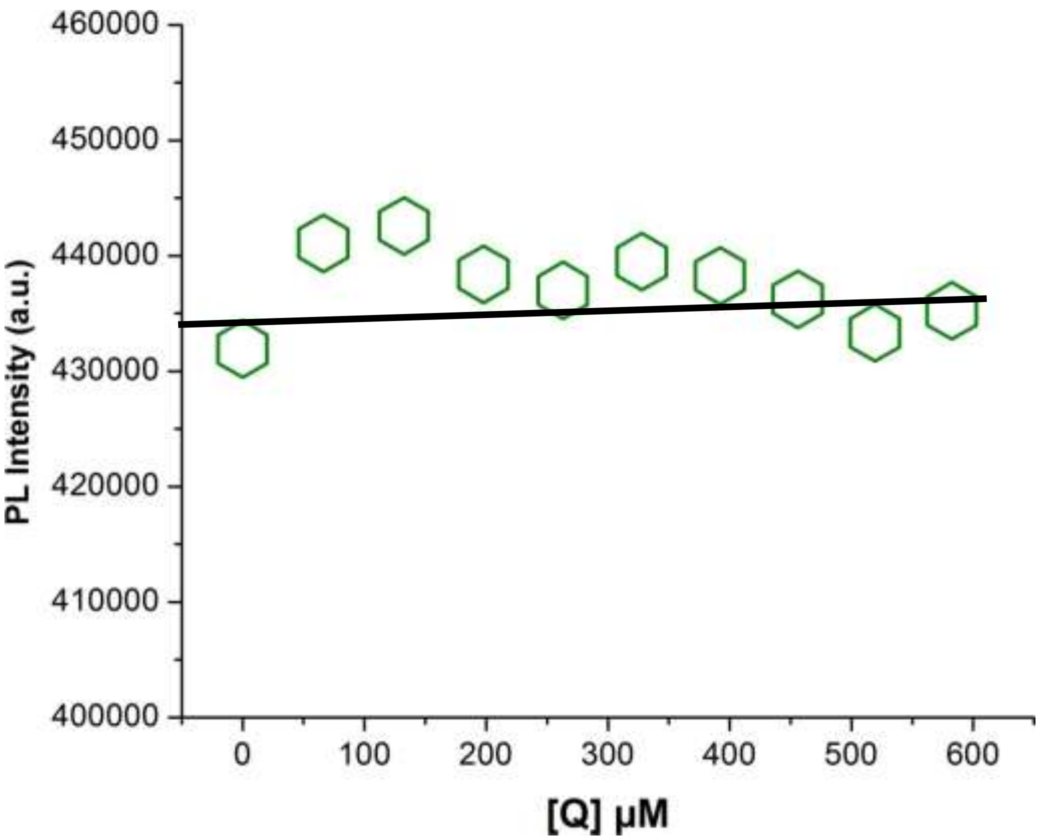

Fig. S100. Stern-Volmer plot

Table S39. Fluorescence quenching titration experiment for the sensor **5** (1.0×10^{-6} M) upon the addition of (1s)-(+)-camphorquinone in CH_3CN.

Solution of sensor **5**	Concentrate of sensor **5**	Solution of quencher	Concentrate of quencher, M
Potassium salt in water	1.0×10^{-6} M	CH_3CN	2.0×10^{-2} M

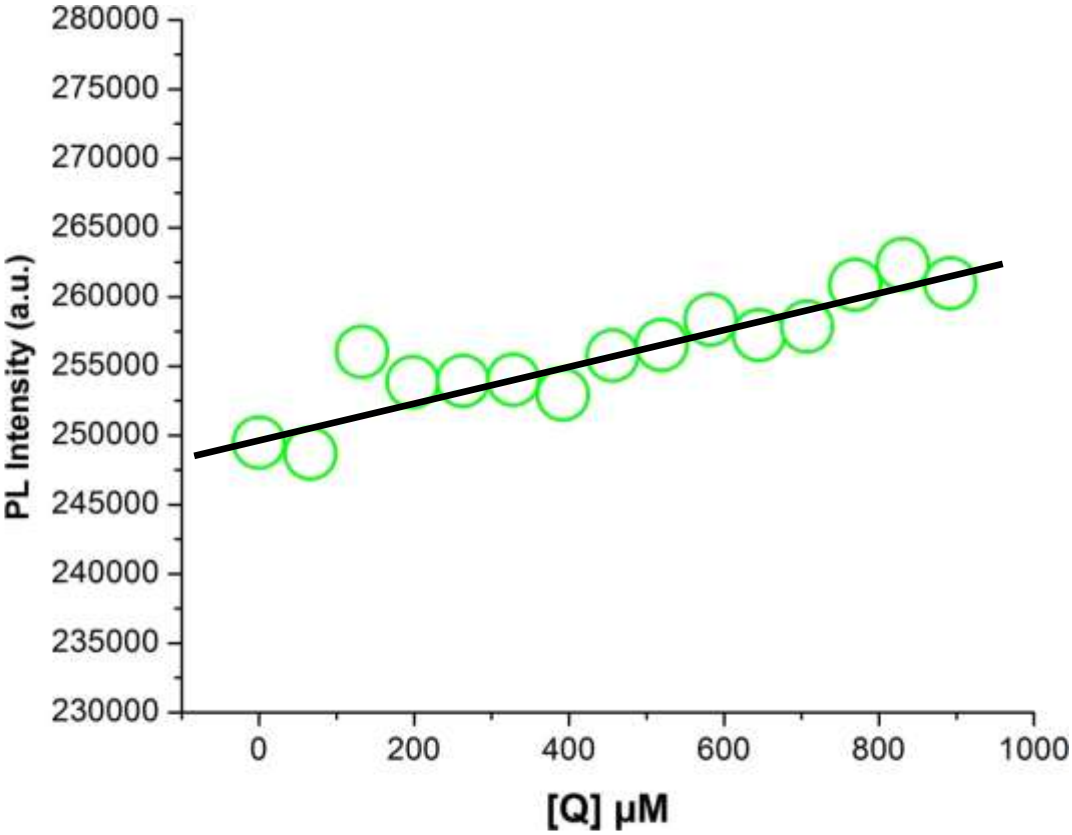

Fig. S101. Stern-Volmer plot

Table S40. Fluorescence quenching experiment of **5** upon addition cyclohexanone

Solution of sensor 3	Concentrate of sensor 3, M	Solution of quencher	Concentrate of quencher, M
Potassium salt in water	1.0×10^{-6} M	CH_3CN	2.0×10^{-2} M

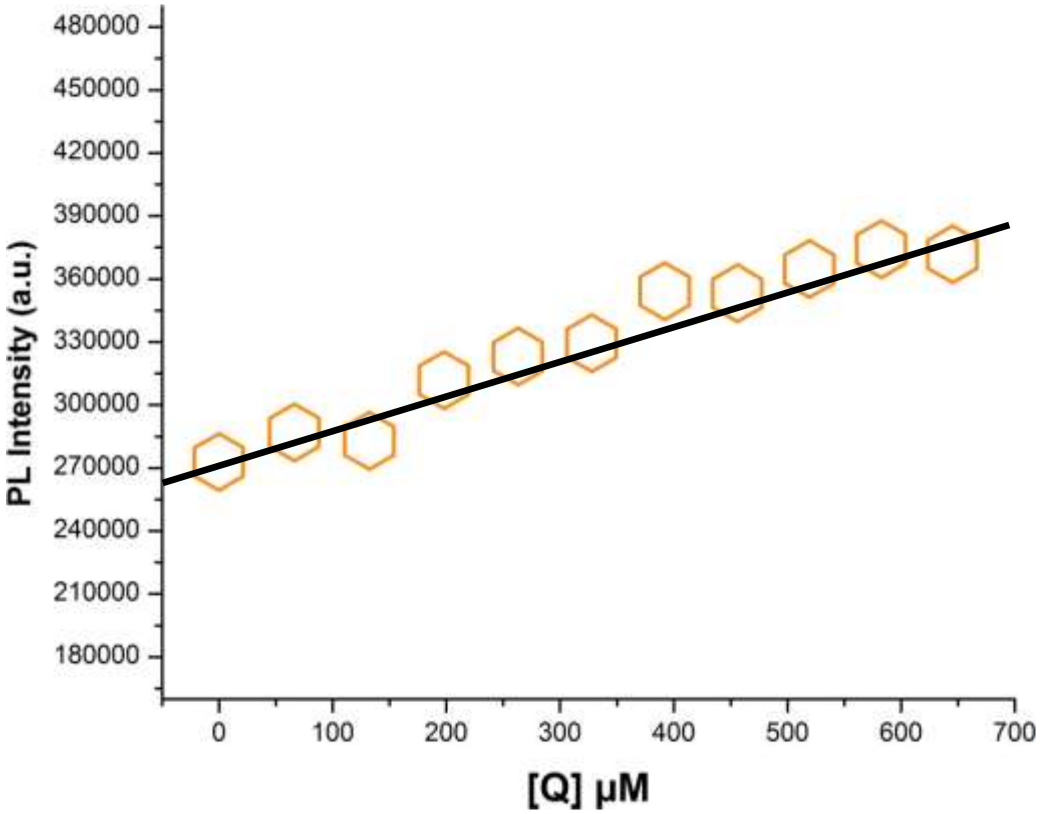

Fig. S102. Stern-Volmer plot

15 ¹H and ¹³C NMR Spectra of sensors 1-5

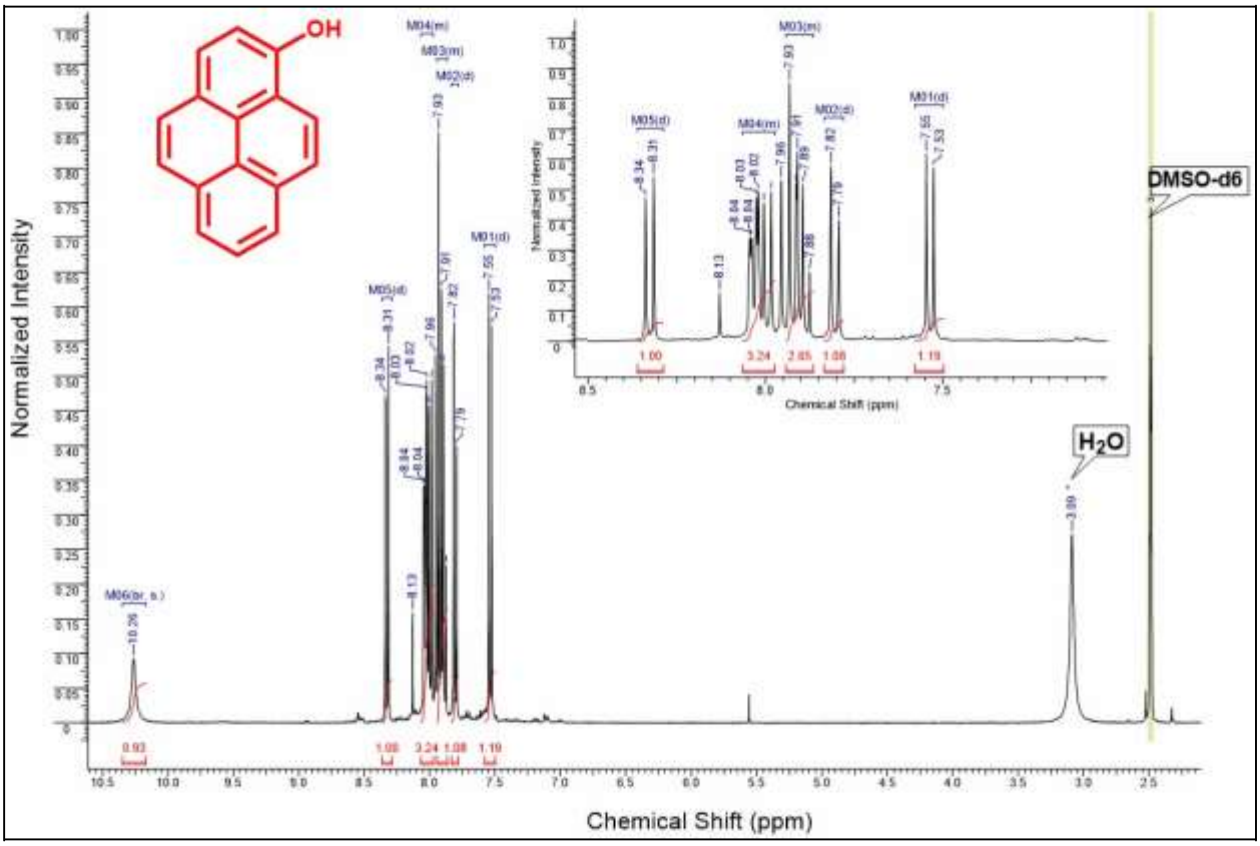

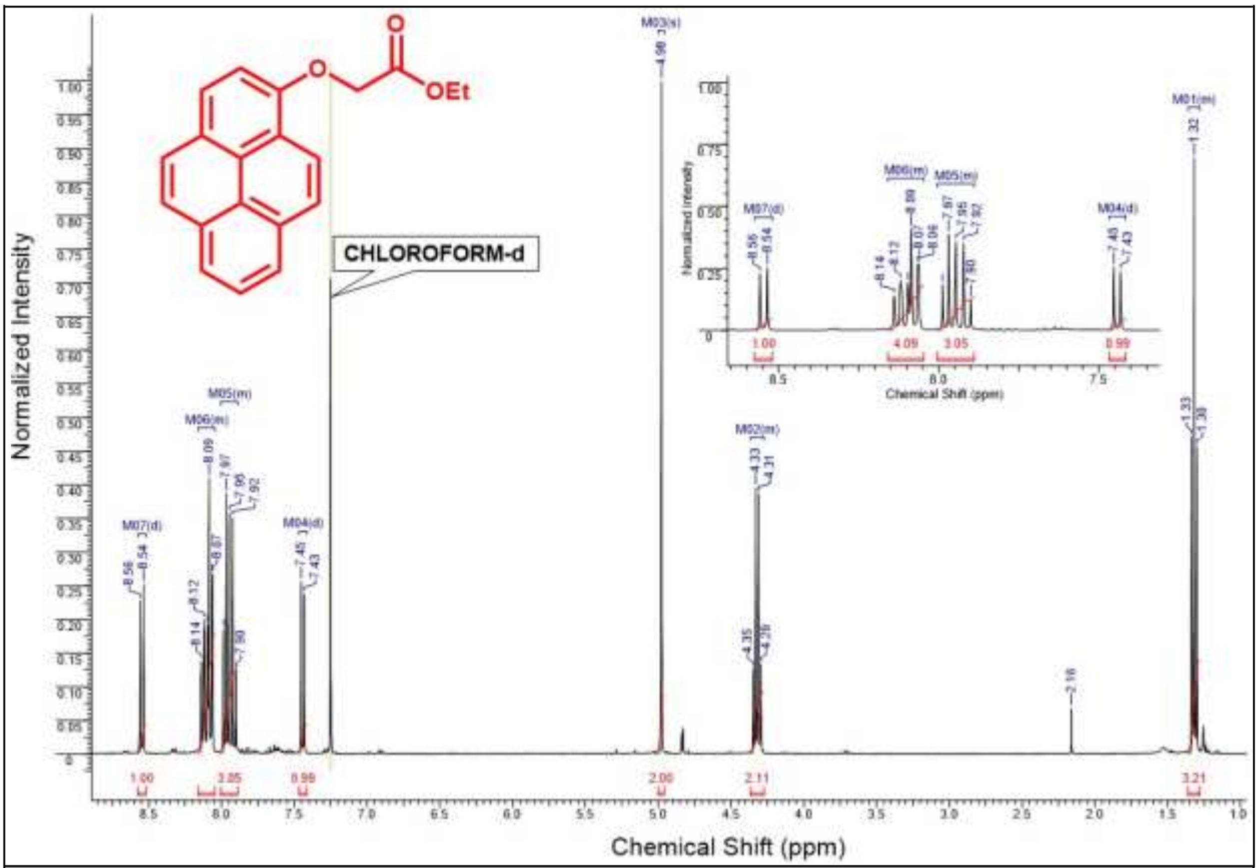
OEt
CHLOROFORM-d
Normalized Intensity
Chemical Shift (ppm)

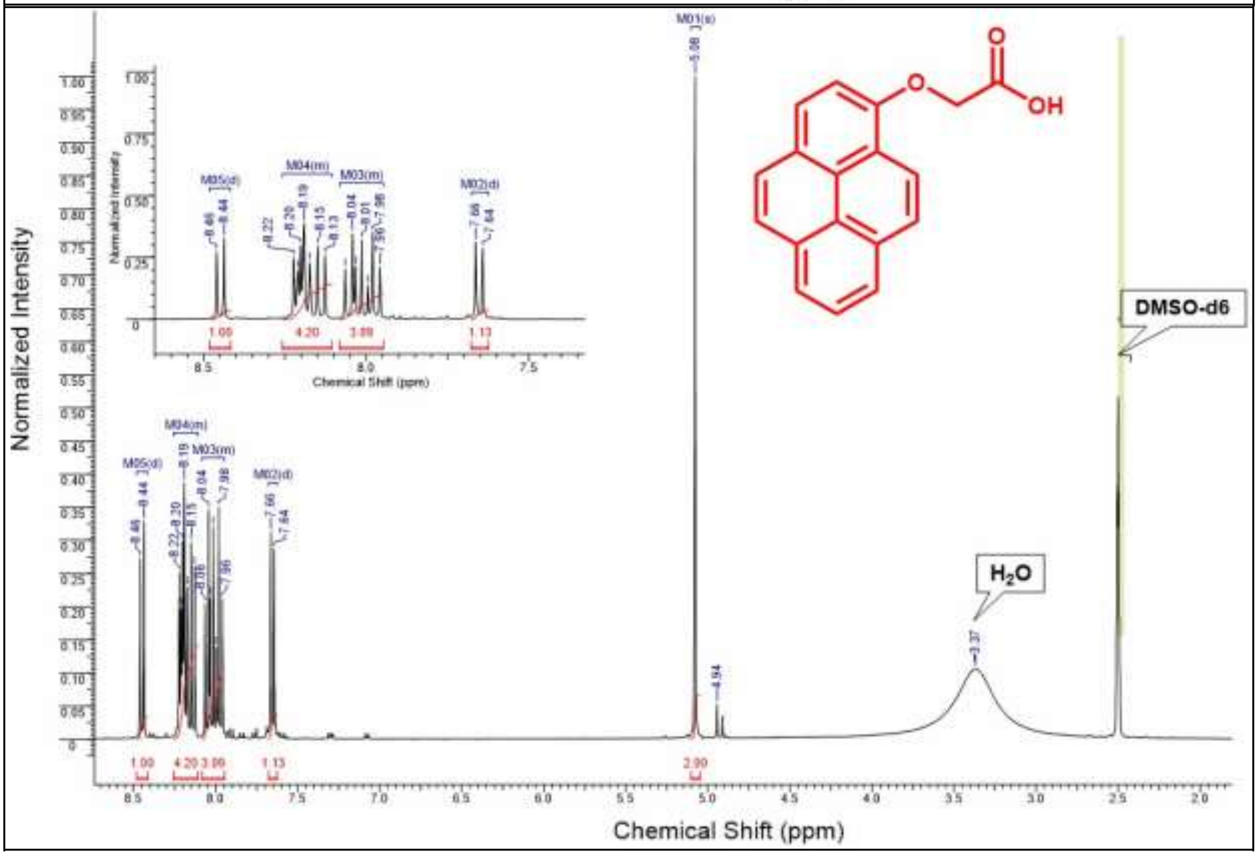
OH
DMSO-d6
H_2O
Normalized Intensity
Chemical Shift (ppm)

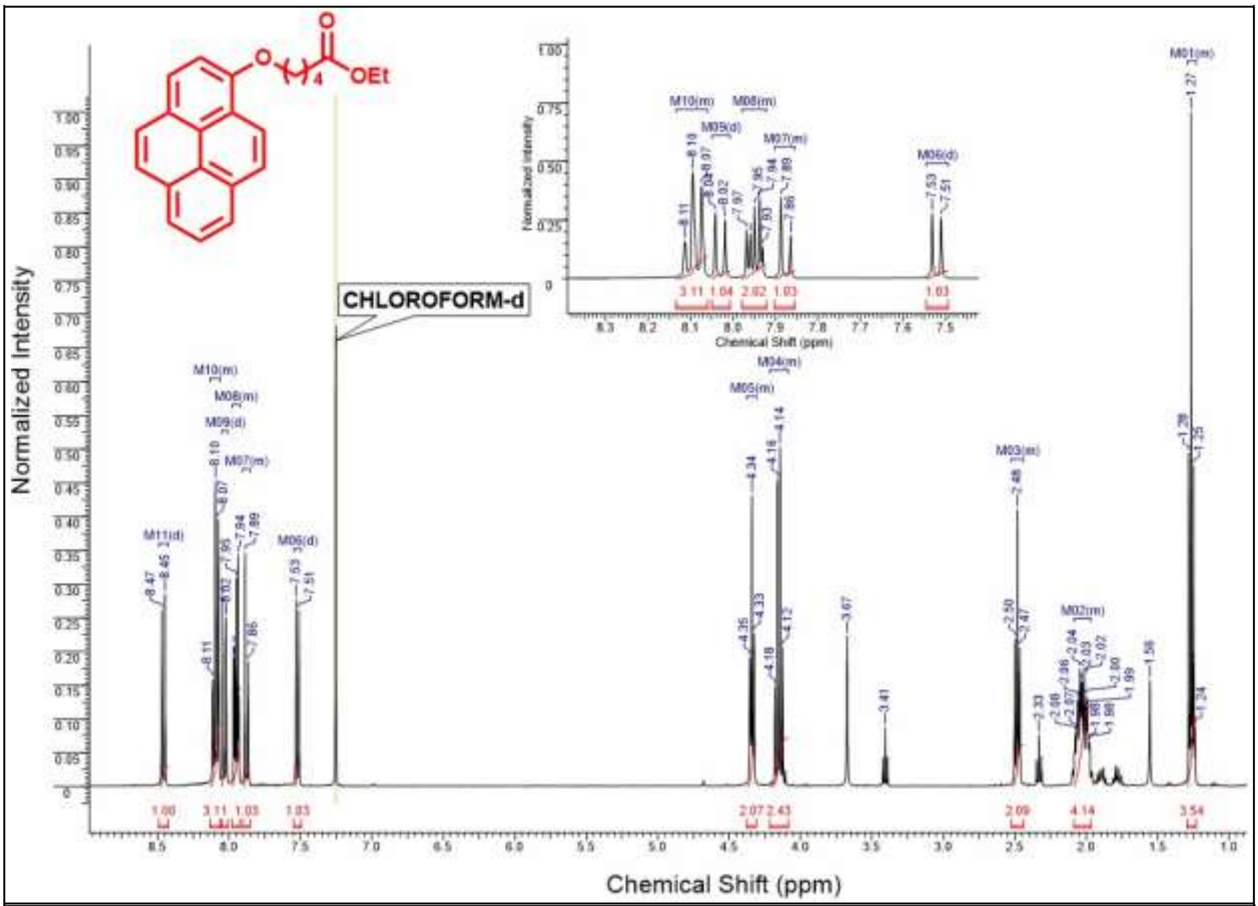

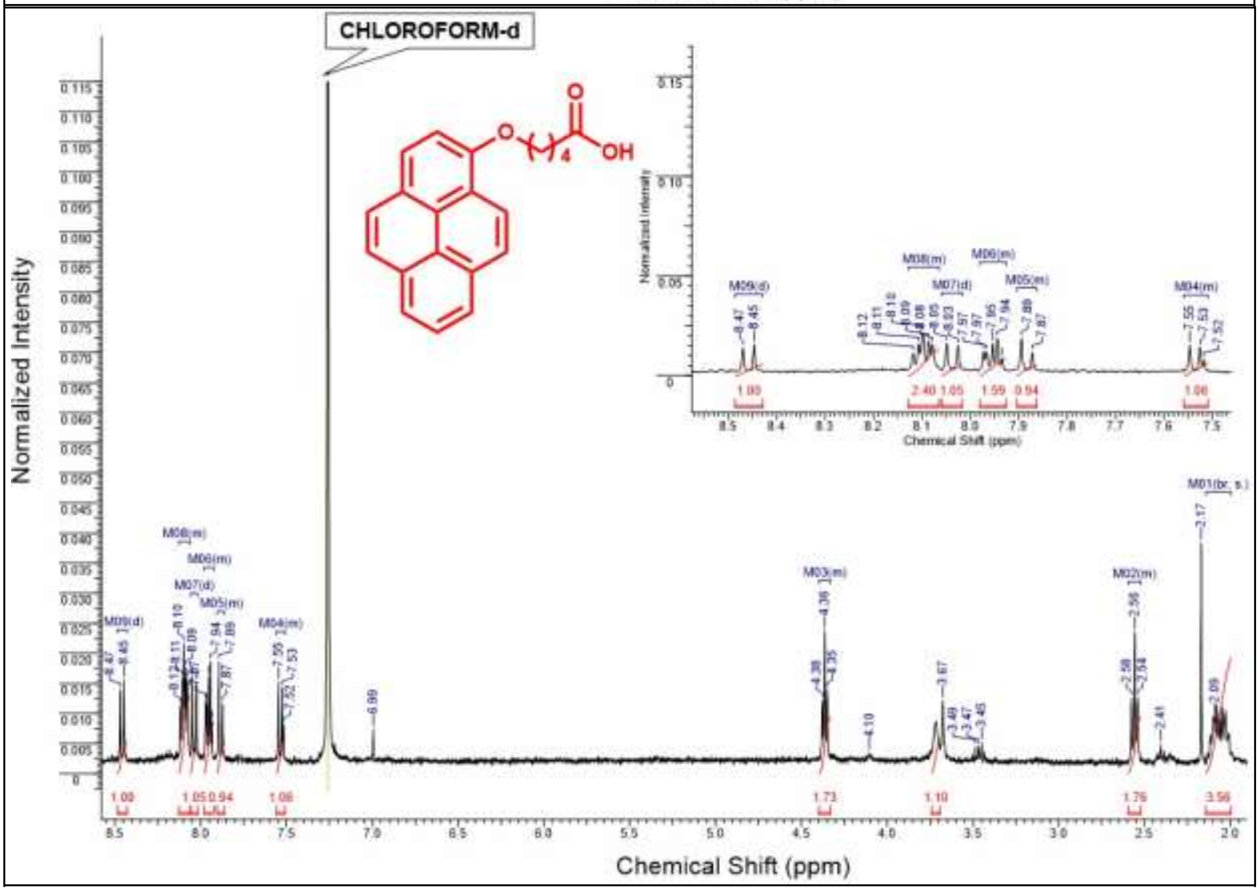

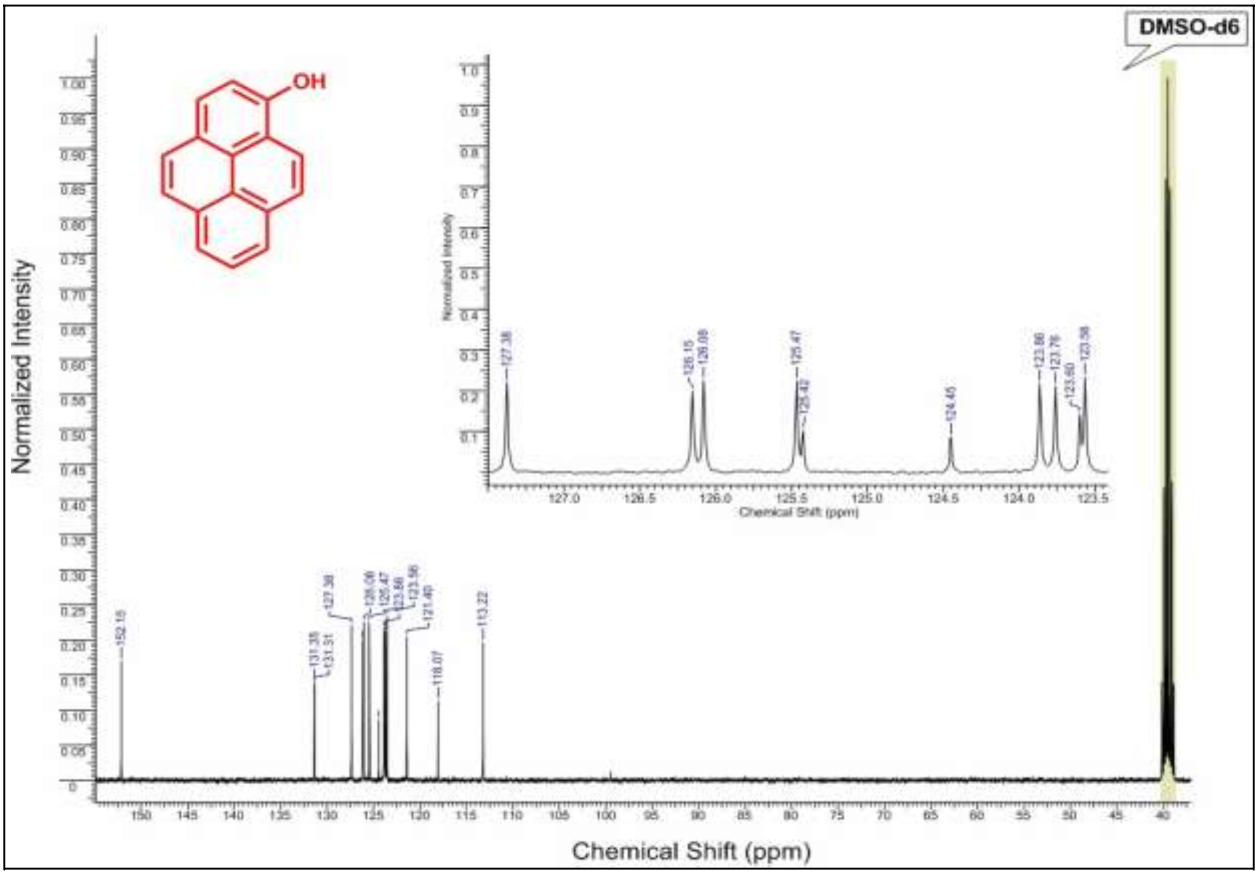
DMSO-d6
OH
Normalized Intensity
Chemical Shift (ppm)
152.15
131.35
131.51
127.38
126.08
125.47
123.86
123.56
121.40
118.07
113.22
126.15
125.42
124.45
123.76
123.60

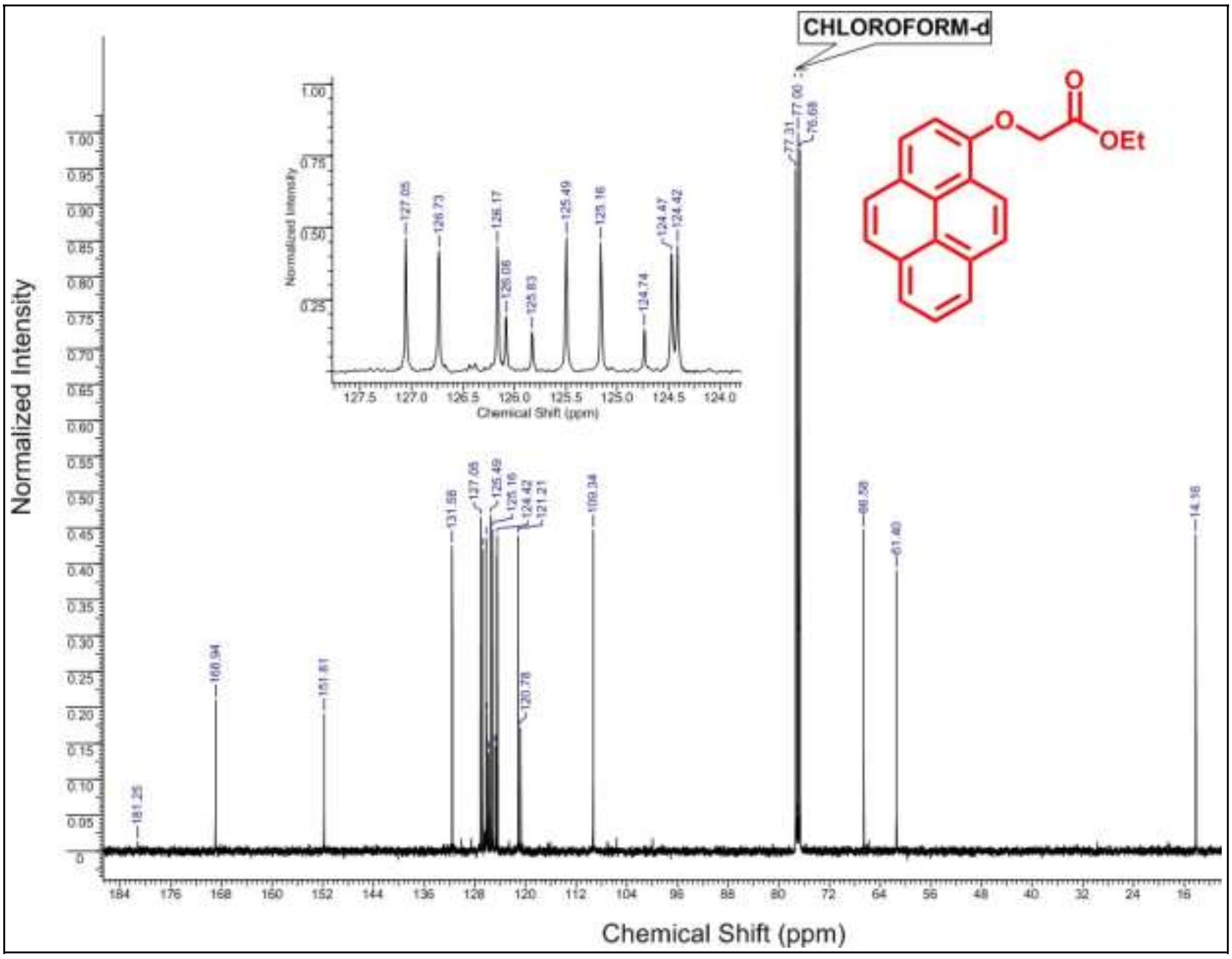
CHLOROFORM-d
OEt
O
Normalized Intensity
Chemical Shift (ppm)
181.25
168.94
151.61
131.58
127.05
125.49
125.16
124.42
121.21
120.78
109.34
77.31
77.00
76.68
66.58
61.40
14.16
126.73
126.17
126.06
125.83
124.74
124.47

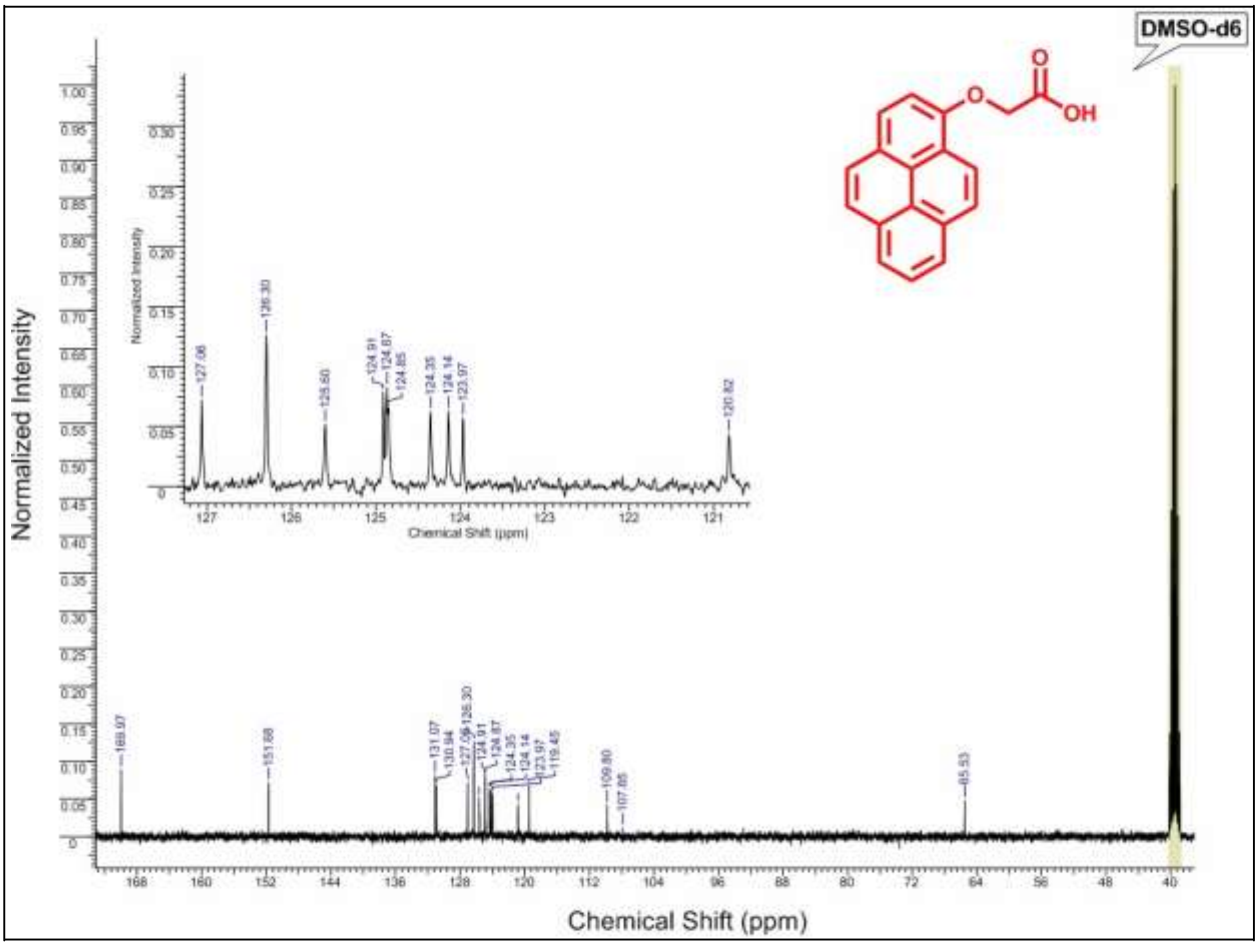
DMSO-d6
OH
O
Normalized Intensity
Chemical Shift (ppm)
169.97
151.88
131.07
130.94
127.06
126.30
124.91
124.87
124.35
124.14
123.97
119.45
109.80
107.65
65.53
125.60
124.85
120.82

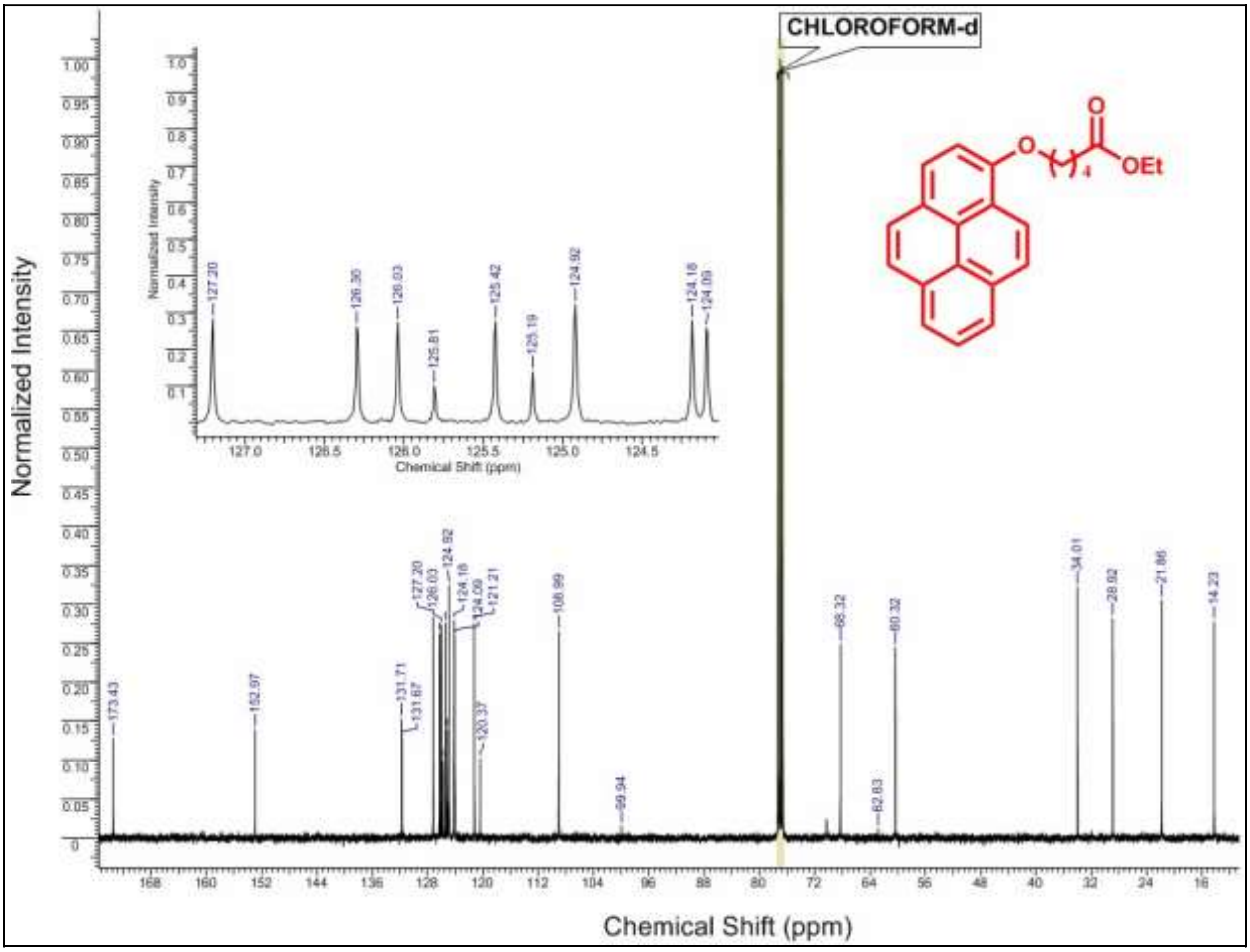

CHLOROFORM-d
Normalized Intensity
Chemical Shift (ppm)
OEt
173.43
152.97
131.71
131.67
127.20
126.03
124.92
124.18
124.09
121.21
120.37
108.99
99.94
68.32
62.83
60.32
34.01
28.92
21.86
14.23
126.30
125.81
125.42
125.19

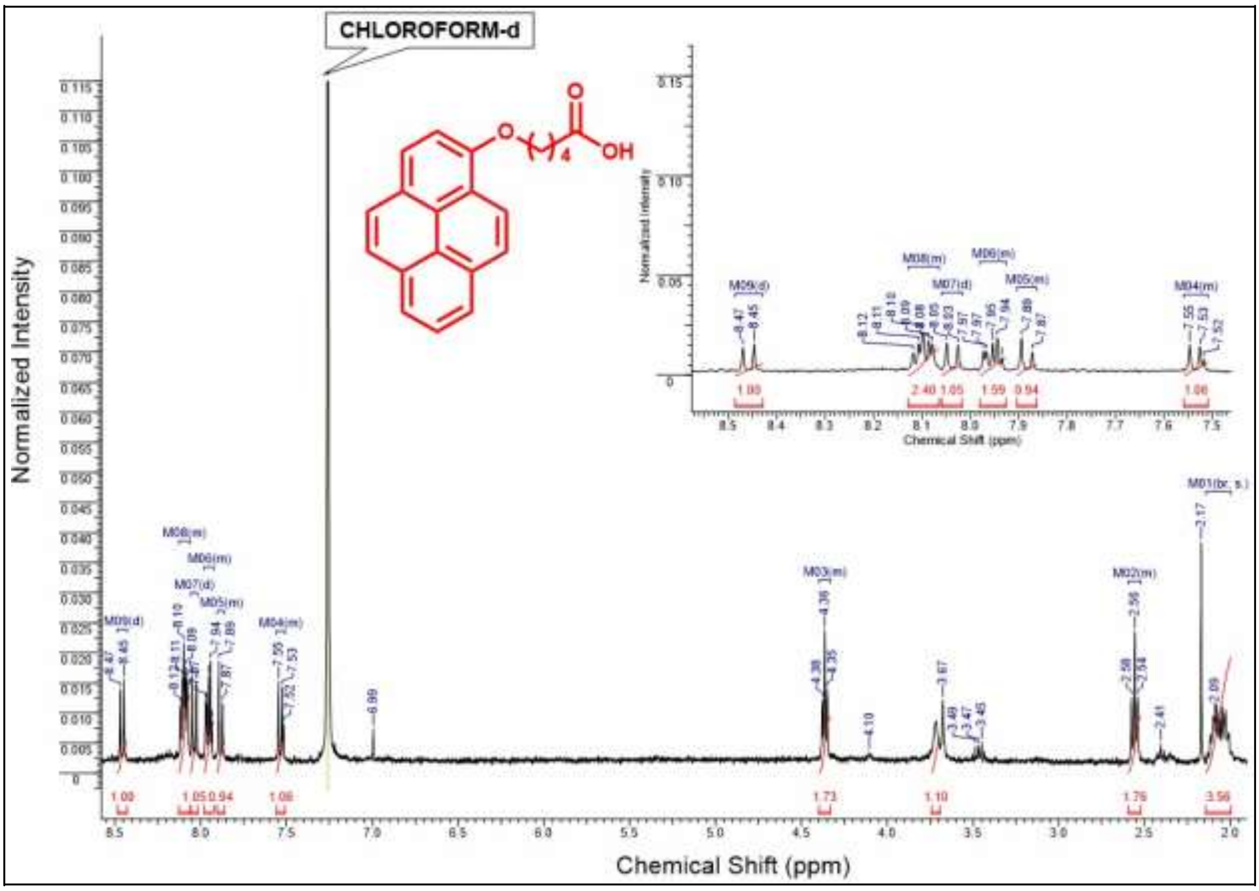
CHLOROFORM-d
Normalized Intensity
Chemical Shift (ppm)
O
OH
4
M09(d)
M08(m)
M07(d)
M06(m)
M05(m)
M04(m)
M03(m)
M02(m)
M01(br. s.)
1.00
1.05
0.94
1.06
1.73
1.10
1.76
3.56
2.40
1.59

References

1. H. Östmark, S. Wallin and H. G. Ang. s.l. : CRC-Press, Boca Raton, 2012,37, Propellants, Explos., Pyrotech., pp. 12-23.

2. *Beiträge zur Kenntnis des Pyrens und seiner Derivate*. Heinrich Vollmann, Hans Becker,Martin Corell,Hans Streeck. 1937, Justus Liebigs Annalen der Chemie, Vol. 531, pp. 1-159.

3. *Fluorescent Detection of 2,4-DNT and 2,4,6-TNT in Aqueous Media*. Igor S. Kovalev, Olga S. Taniya, Nataliya V. Slovesnova, Grigory A. Kim. 2016, Vol. 11, pp. 775 – 781.

4. J. C. Sanchez, A. G. DiPasquale, A. L. Rheingold, W. C. Trogler. 2007,19, Chem. Mat., p. 6459.

5. M. J. Frisch, G. W. Trucks, H. B. Schlegel, G. E. Scuseria,M. A. Robb, J. R. Cheeseman, G. Scalmani, V. Barone,B. Mennucci, G. A. Petersson, H. Nakatsuji, M. Caricato,X. Li, H. P. Hratchian, A. F. Izmaylov, J. Bloino, G. Zheng,J. L. Sonnenberg, M. Hada, M. *Gaussian 09, Revision D.01, Gaussian, Inc*. Wallingford CT : s.n., 2009.

6.